SAPIENZA
UNIVERSITÀ DI ROMA

Renormalization group and critical properties of Long Range models

Scuola di dottorato in Scienze Fisiche

Dottorato di Ricerca in Fisica – XXV Ciclo

Candidate

Maria Chiara Angelini
ID number 1046274

Thesis Advisor

Prof. Federico Ricci-Tersenghi

A thesis submitted in partial fulfillment of the requirements
for the degree of Doctor of Philosophy in Physics

October 2012

Thesis defended on 7 February 2013
in front of a Board of Examiners composed by:

Prof. Claudio Castellani (chairman)

Prof. Sergio Caracciolo

Prof. Maurizio Sasso

Maria Chiara Angelini. *Renormalization group and critical properties of Long Range models.*

Ph.D. thesis. Sapienza – University of Rome

EMAIL: maria.chiara.angelini@roma1.infn.it

A chi in questi anni mi ha fatto capire
che se anche conoscessi tutta la scienza
ma non avessi amore, non sarei nulla.

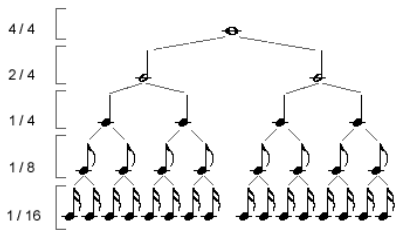

Abstract

We study a Renormalization Group transformation that can be used also for models with quenched disorder, like spin glasses, for which a commonly accepted and predictive Renormalization Group does not exist. We validate our method by applying it to a particular long-range model, the hierarchical one (both the diluted ferromagnetic version and the spin glass version), finding results in agreement with Monte Carlo simulations. In the second part we deeply analyze the connection between long-range and short-range models that still has some unclear aspects even for the ferromagnet. A systematic analysis is very important to understand if the use of long range models is justified to study properties of short range systems like spin-glasses.

Ringraziamenti

Per prima cosa volevo ringraziare Federico, perché mi ha stimolato ad andare avanti, con il suo modo di fare ricerca così pratico, insegnandomi a partire dai problemi semplici, prima di passare a quelli complicati. Nella mia ricerca ho avuto la fortuna di sapere sempre cosa stavo facendo, senza mai perdere di vista l'obiettivo che volevo raggiungere. Grazie ai tuoi mille impegni ho imparato ad andare avanti da sola, anche quando non sapevo come fare. E' stato un insegnamento prezioso per me, soprattutto quando pensavo di non farcela!

Volevo poi ringraziare tutti i membri della saletta dottorandi, Margherita, Luigino, Giacomo, Matteo, Matteo, Niccolò, Andrea e Laura, e tutti quelli che vi orbitavano intorno, perché in questi anni non mi sono mai annoiata (anche se ci sono ancora tante cose da fare: l'anatra da Sonia, il cd ricordo, il trailer di "Io non dormo la notte"...)!

Grazie a Francesco e Ulisse, compagni di gruppo e al mio fianco in questa nuova avventura parigina, è tutto più facile quando si è insieme!

E infine grazie a chi mi ha aiutato a diventare come sono, a chi mi ha insegnato il coraggio, la forza, la determinazione per andare avanti, sempre, stando al mio fianco con pazienza e amore: mamma, papà, Bea e Martino. Non sarei qui se non avessi voi al mio fianco.

Contents

Chapter 1

Introduction

Since their discover, at the end of 60's, spin-glasses received a great attention because they show a very rich and unusual phenomenology. They are disordered magnetic systems that show a specific heat decreasing linearly with temperature at small temperatures, unexplained with conducting electrons, a cusp in the susceptibility at a certain temperature, chaos, memory effects and so on. At the critical temperature T_{SG}, they undergo a phase transition from a paramagnetic phase to a state in which the local spins freeze, but without a regular structure. Many efforts were done to create a theory that could interpret the experimental evidences and characterize the new phase detected. The the Edward-Anderson model [1] was introduced as a simple finite dimensional model for disordered systems, in which important properties as quenched disorder in the Hamiltonian and frustration are the main ingredients. They lead to a great computational complexity and after thirty years there is still not a solution for it, despite all the works that have been done. The Sherrington-Kirkpatrick (SK) model [2] has been introduced as the mean field version of the EA model. After many works, a solution for the SK model was found [3]. It is based on a new kind of spontaneous symmetry breaking, the replica symmetry breaking, and it is a beautiful as far as non-trivial scenario, rich of interesting implications.

We want to point out that the great interest that has received this subject in the last decades is not unjustified. The theoretical work, arising from the study of spin-glasses has now an independent life. In fact concepts and techniques developed in the spin-glass field, have found a wide application in recent years not only in statistical physics, but also in economics, biology, optimization problems, computer science and so on.

The renormalization group (RG) [4] [5] is an important tool to study and characterize phase transitions in different models, allowing to extract critical properties, like universality classes and critical exponents. However when disorder is introduced in the models, it is not obvious how to generalize the concepts and the procedures used in the pure/homogeneous case. Indeed, for disordered systems, like spin glasses, there have been several attempts to find a good renormalization/decimation scheme, but none with satisfactory results. In particular a real space RG has been applied with good results only to disordered models on particular lattices, the hierarchical diamond ones [6], in which the so-called Migdal-Kadanoff (MK) approximation [7] for decimating spins is exact; however it is known that this kind of lattices can not

always reproduce the correct physical behavior of the same models on a regular finite-dimensional lattice. Moreover, for the case of the Edward-Anderson model on a D-dimensional lattice, a (replica) field theory exists, but doing the corresponding ϵ-expansion around the upper critical dimension $D_U = 6$ has proved to be cumbersome, without leading to reasonable values for the critical exponents [8, 9, 10]. Nonetheless, Monte Carlo (MC) simulations provide accurate estimates of critical temperatures and critical exponents for disordered systems [11, 12, 13]. Thus there is a need to find a (semi-)analytical method, able to reproduce and validate these numerical results. This would be of particular importance for those models, like the EA one, for which there is no analytical solution below the upper critical dimension, and for which the existence of a phase transition, and its characterization, has not been proved yet. We think that the failure of previous (real space) renormalization group schemes may be due to the fact the decimation procedure was applied separately on each sample. However, being the important observables those averaged over the disorder (because sample to sample fluctuations are typically largest than thermal ones), it would be more correct to renormalize the whole ensemble into another ensemble of smaller systems. In fact, in the latter case, samples are treated according to their weight in the quenched partition function, while in the former this may not be true. Although the first method is often chosen because it requires a smaller computational effort, we propose a method of the latter type.

In Part I of this Thesis we review the most important RG methods and their applications to SG, and develop a new renormalization group approach that can be generalized without particular difficulties to disordered systems. In principle it can be applied to every disordered system, however the model we study is a particular long range (LR) one dimensional model, the hierarchical model (HM) [14]. It is a fully connected model in which the intensity of the interaction between two spins i and j decays as $r_{ij}^{-(1+\sigma)}$ with their binary distance r_{ij}. We have used this model because the renormalization group equations can be written exactly on it. Moreover, changing the parameter σ, the effective dimension of the system can be changed. In this way, changing only one parameter, we can analyze the behaviour of the model inside and outside the range of validity of the mean-field approximation.

In fact LR models can emulate a short range (SR) model in higher dimension for certain values of the couplings. In particular, for a LR model in dimension $d = 1$, when the couplings decay slowly enough ($\sigma < \sigma_U = 1/2$), the behaviour of the system is mean-field like. It is the analogous of a SR system in dimension $D > D_U$. Above a certain threshold ($\sigma > \sigma_U = 1/2$), the behaviour is non mean field, with critical exponents that change continuously with σ. Increasing σ is thus equivalent to lowering the dimension in a SR model. When the lower critical exponent is reached ($\sigma > \sigma_L = 1$), the couplings decay too slowly and the model recovers the SR behaviour, even if it is still a fully connected one. Different relations between σ and the effective dimension D of a short range model can be written [15, 16, 17], however it is still not clear which is the best one and its range of validity, even for ferromagnetic LR models. In particular a $\sigma - D$ relation for LR models in $d > 1$ dimensions has been never proposed. There is also a debate on the value of the threshold σ_L where the SR behaviour is recovered, especially for $d > 1$ [18]. Moreover the differences between various kinds of LR models are not clear enough. For this reason in Part II of this Thesis, we analyze systematically the connection

between LR and SR ferromagnetic models, for different dimensions and different models, trying to find the answers to all these fundamental questions. These are very important questions if we want to understand how good are LR models to emulate SR models, and if the use of LR models is justified to study properties of SR systems like spin-glasses.

Part I

Renormalization Group and Spin Glasses

Chapter 2

Basic concepts

2.1 Phase transitions

The macroscopic state of a system is determined by some external parameters such as the temperature or the pressure. Sometimes it happens that systems can abruptly change their macroscopic behaviour varying smoothly the external parameters. The point of this change is called a *critical point* and it is often characterized by a phase transition in the state of the system. There are two main type of transition: the first and the second order one. A system approaching a *second order phase transition* is characterized by the range of the correlations between the microscopic variables that grows, until it becomes practically infinite approaching the critical point. This happens even if the interactions between the variables are at finite range. This phenomenon is present in very different systems but maybe the simplest one is the Ising model, that is a simplified model for a uniaxial ferromagnet. The microscopic variables are spins, that are local magnetic moments, taking values $\sigma = \pm 1$, placed at the vertexes of a regular lattice. N is their number, and the Hamiltonian of the system is the following:

$$H = -\sum_{(i,j)} J_{ij}\sigma_i\sigma_j. \tag{2.1}$$

The interactions are ferromagnetic $J_{ij} > 0$, and between pairs of nearest neighbours (i, j), thus at low temperature spins tend to align to each others to minimize the energy. Starting at temperature sufficiently high, the system will be in the so called paramagnetic state, characterized by null magnetization: $M = \sum_i \sigma_i = 0$. Generally, the correlation between the spins decay exponentially fast with the distance. However, lowering the temperature, the range of the correlation between the spins grows. At the critical point T_c, it becomes infinite, and below this temperature, the system changes its state, entering in the ferromagnetic state, characterized by magnetization different from zero $M \neq 0$. The magnetization is the *order parameter* of the transition, that takes different values in the different states. The Hamiltonian in Eq. (2.1) is clearly symmetric under the change of all the spins: $\sigma_i \to -\sigma_i$, however, below the critical temperature, in the thermodynamic limit ($N \to \infty$) the system will have a preferred direction. The spins are mostly positive, or negative, producing $M \neq 0$. This phenomenon is called *spontaneous symmetry breaking*. There are two stable phases in the system, with positive or negative magnetization, and the

system chooses one of them. If a magnetic field h is added in the Hamiltonian, with a term of type $H_h = -h\sum_i \sigma_i$, one can select one of this two states, and the limits $h \to 0^+$ or $h \to 0^-$ are different. This is called a first order phase transition where the controlling parameter is the field.

A very similar behaviour is present also for a liquid. Below the critical point T_c, varying slightly the pressure, (that takes the role of the magnetic field) the system can be in the liquid or in the gas state. Here the role of the magnetization is assumed by the density of the system, that is different in the gas and in the liquid: $\rho_G \neq \rho_L$. When T reaches T_c, the difference $\rho_G \neq \rho_L$ approaches zero, like the magnetization in the Ising model. The density difference is the order parameter of this transition. Above T_c two different states no longer exist.

2.1.1 Critical exponents

Let us now see, more rigorously, how to characterize a second order phase transition. As said, the main characteristic is the divergence of the correlation length ξ. To define it, generally, one can identify a local variable $s(x)$, whose average M is the order parameter, and its local fluctuation $\delta s(x)$ with respect to the mean is analyzed. For ferromagnets $s(x)$ is the local magnetic moment, while for the liquid it is the difference of the density with respect to that at the critical point. ξ is defined looking at the correlation function $G(x)$ as

$$G(x) = \langle \delta s(x) \delta s(0) \rangle = \frac{e^{-x/\xi}}{x^a},$$

where $\langle \cdot \rangle$ indicates the thermal average over all the configurations. The correlation length diverges with a power law approaching the critical point:

$$\xi \propto \begin{cases} (T - T_c)^{-\nu} & T > T_c \\ (T - T_c)^{-\nu'} & T < T_c \end{cases}$$

However various other quantities vanish or diverge at the critical point with power laws, and one can define some characteristic exponents that are called *critical exponents*, ν and ν' are two of them. For example one can define the susceptibility $\chi = \frac{dM}{dh}|_{h=0}$ that is the response of the order parameter to a perturbation in a field h coupled linearly with it. Also the susceptibility diverges at the critical point:

$$\chi \propto \begin{cases} (T - T_c)^{-\gamma} & T > T_c \\ (T - T_c)^{-\gamma'} & T < T_c \end{cases}$$

For the liquid, χ is the compressibility, while in the ferromagnet it is the magnetic susceptibility.

Another critical exponent, called the anomalous dimension η is defined looking at the behaviour of the correlation function at the critical point:

$$G(x) \propto |x|^{-(d-2+\eta)}$$

where d is the dimension of the space.

For the specific heat

$$C \propto \begin{cases} (T - T_c)^{-\alpha} & T > T_c \\ (T - T_c)^{-\alpha'} & T < T_c \end{cases}$$

Sometimes $\alpha = 0$, it means that there is a discontinuity or a logarithmic divergence.

The order parameter, that is different from zero below the critical point, vanishes at the critical point, with a power law:

$$M \propto (T_c - T)^{\beta}$$

As said, for the ferromagnetic case, the order parameter is the averaged magnetization, that is different from zero in the ferromagnetic phase (for $T < T_c$) and it is null in the paramagnetic phase (for $T > T_c$). For the gas-liquid transition, the role of the order parameter is played by the difference between the density of the liquid and the gas $\rho_L - \rho_G$, that disappears above the critical point, where the two phases do not exist.

At the critical point, the order parameter in the presence of an external field $h \neq 0$ is non-null, and vanishes with the field as:

$$M \propto h^{1/\delta}$$

For the gas-liquid transition, the magnetic field is replaced by the variation of the pressure from the critical one: $p - p_c$.

2.1.2 Scaling laws

At the end we can identify nine different critical exponents: $\nu, \nu, \gamma, \gamma', \eta, \alpha, \alpha', \beta, \delta$.

However, under particular assumptions, relations among them can be found. The idea proposed by Widom [19] is to write the asymptotic part of the free energy, or the equation of state, as a homogeneous function of the variables. For example, in general the equation of state describing the relation between magnetization, temperature and magnetic field, can be written as

$$h = M^{\delta} f(M, t)$$

with $t = |T - T_c|$. However one can suppose that f depends only on one variable, obtaining:

$$h = M^{\delta} f(t/M^{1/\beta}).$$

The same thing can be done also for the singular part of the free energy:

$$F(t, h) = t^{2-\alpha} \Phi(t/h^{1/\beta\delta}) \tag{2.2}$$

or for the correlation function at $M = h = 0$:

$$G(r, t) = |r|^{-(d-2+\eta)} g(r/t^{-\nu})$$

This hypothesis has been verified with good accuracy experimentally, and also in some soluble models. In this way relations among the exponents can be found, the so called *scaling laws*:

$$\begin{aligned} 2\beta + \gamma &= 2 - \alpha \\ 2\beta\delta - \gamma &= 2 - \alpha \\ \gamma &= \nu(2 - \eta) \\ \nu d &= 2 - \alpha \end{aligned} \tag{2.3}$$

and also $\alpha = \alpha'$, $\nu = \nu'$, $\gamma = \gamma'$. In this way, it is sufficient to know only two exponents to obtain all the others. The scaling laws will be a consequence of a more general theory that is the renormalization group.

2.1.3 Universality

In second order phase transitions, the variables are strongly correlated, thus it is difficult to study them. However many simplifications appear. In fact for example the critical exponents do not depend on the details of the system. For example the Ising model and a gas-liquid transition at the same spatial dimension d have the same critical exponents and the same happens for the Ising model on a squared lattice or in a triangular lattice with the same d. This property is called *universality*: the critical exponents do not depend on the details of the system, but only on the symmetries of the Hamiltonian, on the spatial dimension and on the dimensionality of the order parameter. The ones that change are the *non universal* quantities like the critical temperatures. The reason of this simplification will be explained by the renormalization group theory.

2.1.4 Mean field theory and critical dimensions

There is a special case, the *mean field* (MF) one, in which the models can be solved analytically. If in the Hamiltonian of Eq. (2.1) the sum runs over all the pairs i, j and not only among nearest neighbors, and the couplings between the spins take the value J, the model is easily soluble, leading to the following self consistent solution for the order parameter at equilibrium:

$$M = \tanh\left[\beta(JM + h)\right] \tag{2.4}$$

and the following critical exponents can be found:

$$\nu = \frac{1}{2}, \quad \beta = \frac{1}{2}, \quad \alpha = 0, \quad \gamma = 1, \quad \delta = 3, \quad \eta = 0. \tag{2.5}$$

The scaling laws are satisfied, except the one involving d. In this *mean field* model there is no spatial dimension or equivalently it corresponds to a model with $d = \infty$. Moreover each spin is connected to all the others, thus each spin is perfectly equivalent to all the others because they see the same things around themselves. This corresponds to a model without fluctuations. The mean field approximation can be applied also to the Hamiltonian of Eq. (2.1) in d dimensions, neglecting the fluctuations. In fact the term $\sigma_i\sigma_j$ can be rewritten with an identity as $\sigma_i\sigma_j = (M + (\sigma_i - M))(M + (\sigma_j - M))$ and expanded in the first order in the fluctuation $\delta\sigma = \sigma - M$: $\sigma_i\sigma_j = M^2 + M\delta\sigma_i + M\delta\sigma_j + O(\delta\sigma^2)$. In this way, also in a regular lattice, the Eq. (2.4) is recovered. The mean field approximation, that is to neglect the fluctuations, can be applied to all the models. The application to the liquid-gas transition model leads to the famous Van der Waals equation of state, that implies the same exponents of Eq. (2.5), confirming universality.

Even if for a d dimensional model the mean field solution is an approximation, the given results are exact if the spatial dimension of the model is higher than the so called *upper critical dimension* d_u that corresponds to $d = 4$ for the Ising model universality class. Above d_u, the fluctuations are not so important because each spin has a "sufficient" number of neighbours. Below d_u, the values of the critical exponents do not correspond to the mean field ones and change with the dimension, until the *lower critical dimension* d_L is reached, and the transition disappears. For the Ising model $d_L = 1$ for discrete variables, while it is $d_L = 2$ if the spins can take continuous values.

2.2 Renormalization Group

2.2.1 The main idea

The renormalization group (RG) is a fundamental tool in theoretical physics [4] [5]. It allows to characterize phase transitions and critical phenomena, by computing critical exponents and universality classes. When a phase transition occurs, the partition function of a system

$$Z = \lim_{N\to\infty} \sum_{\{\sigma\}} \exp(-\beta H(\sigma))$$

becomes singular at the critical point. Thus in the 1970's there was the need to find a theory that could explain how a singularity can emerge, in the thermodynamic limit, from a partition function that is a sum of positive terms. The renormalization group is a non-linear transformation group and the infinitesimal transformations will lead to differential equations. Its advantage is that it allows the singularities at the critical point to occur naturally. Moreover concepts like universality and scaling find an elegant explanation. The concept of universality says that details of the system are not important for the critical properties. This is related with the growing correlation length, that is the important lenghtscale of the system. Then one can think to integrate over the short wave-length degrees of freedom, to simplify the problem without changing its physics. The real space RG can be viewed as a decimation procedure that takes a system made of N dynamical variables and reduces it to a smaller system, in a way which preserves, or scales appropriately, some important physical observables. Such a decimation induces a RG transformation on the system couplings, and the study of such a transformation allows one to identify critical points and critical exponents. The Real Space Renormalization Group (for a review see [20]) is based on the idea to evaluate the partition function by steps. In each step a block of spins, described by the Hamiltonian $H(\sigma)$ with couplings J, is replaced by an equivalent system with fewer spins and Hamiltonian $H(\sigma')$, with new, renormalized couplings J' following the equation:

$$e^{-\beta H'(\sigma')} = \sum_{\sigma} P(\sigma', \sigma) e^{-\beta H(\sigma)} \tag{2.6}$$

and $\sum_{\sigma'} P(\sigma', \sigma) = 1$ in such a way that the partition function of the original and of the renormalized systems are the same.

2.2.2 The one-dimensional Ising model

For example for a one dimensional Ising spin chain with nearest neighbor interactions, one can think to build blocks of b spins and substitute them with a single new spin. Applying Eq. (2.6), the recurrence relation

$$J' = \mathcal{R}_b(J) = \tanh^{-1}[(\tanh J)^b] \tag{2.7}$$

is obtained and the new couplings are again only between nearest neighbours. The form of the Hamiltonian H' is the same as the original one H, a part from a constant term, independent on the spins. The factor β has been included in the couplings, and, calling $x = \tanh(J)$, Eq. (2.7) simply becomes $x' = x^b$. The limit $x \to 0$

corresponds to high temperatures and the limit $x \to 1$ to small temperatures. If we iterate the process many times, starting at $T > 0$, that is $x < 1$, the renormalization flow goes towards $x = 0$, that corresponds to a renormalized system with a high effective temperature. In the RG language, we can say that there are two fixed points of the recursion relation. $x = 1$ is an unstable fixed point: if we start near it, the iteration will lead the coupling far from it. The other fixed point, at $x = 0$, is a stable, attractive one in the whole region $0 \leq x < 1$. Thus the whole region $0 \leq x < 1$ will be in the same phase. $x = 0$ corresponds to an effective temperature $T = \infty$, and thus the phase of the system in whole region will be the paramagnetic one. This corresponds to the well known fact that the Ising model in one dimension does not have a phase transition. With this renormalization procedure we have eliminated the degrees of freedom at small distances, but we have imposed that the large scale physics must remain the same. Thus, near the critical point the renormalized correlation length will remain the same. However the lattice spacing has changed by a factor b. Thus, if we measure the correlation length in units of the lattice spacing, the following relation will hold:

$$\xi(x^b) = b^{-1}\xi(x)$$

that has the solution

$$\xi(x) = \frac{cost}{\ln \tanh(J)}.$$

This is the correct expression of the correlation length for the 1D Ising model, and this is a proof of the usefulness of the RG even when there is no phase transition. The correlation length remains finite, but grows exponentially in the limit $T \to 0$.

2.2.3 The general case

The one-dimensional model is a special case, because usually renormalization in Eq. (2.6) can not be carried out explicitly. In fact the Hamiltonian does not remain of the same form after the reduction of the degrees of freedom, because new couplings terms arise. Moreover, for systems in higher dimensions, where a transition exists, in general, there will be more fixed points. For example for the Ising model in two

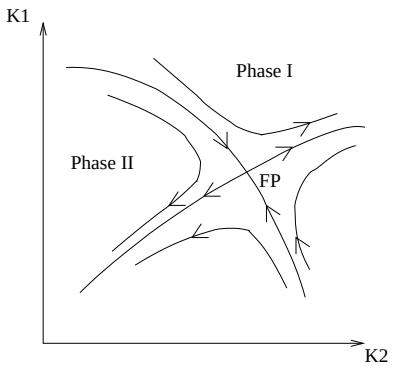

Figure 2.1. RG flows for a two couplings example. There is a critical fixed point, one attractive direction and one unstable direction (the critical surface) that divides the space in two different phases.

dimensions, that has a second order phase transition at $h = 0$ and $T = T_c$, there are three fixed points. Two of them are trivial, and, as in the one-dimensional case, they correspond to the high and low temperature fixed point. Both of them are stable. However there is another fixed point that is called the critical one and is unstable in some directions as we will see in the following. To develop a general theory, we can write the most general Hamiltonian with couplings between any subsets of spins and we will indicate with $\{J\}$ the ensemble of all the couplings. At the beginning only the one between nearest neighbours will be different from zero. We can build blocks of spins and define some new block variables, as the sum of the spins inside a block, properly scaled with a factor to leave the partition function invariant as in Eq. (2.6). We observe how $\{J\}$ evolve, writing recursion relations like that in Eq. (2.7), of the type $\{J'\} = \mathcal{R}_b(\{J\})$. They will depend on the kind of transformation that we choose and on the scale parameter b. In general it will not be simple to solve them, because they are an infinite number and we must do some approximations, depending on the problem (some examples are presented in next chapter). Then we suppose that one or more fixed points of these recursion relations $\{J^*\} = \mathcal{R}_b\{J^*\}$ exist and that the transformation $\mathcal{R}$ is differentiable around them. If it is so, we can linearize the transformation around the fixed point (the non-trivial, critical one is the interesting one):

$$J'_a - J^*_a \propto T_{ab}(J_b - J^*_b)$$

with $T_{ab} = \frac{\partial J'_a}{\partial J_b}\Big|_{J=J^*}$. The matrix $\mathbf{T}$ will have left eigenvectors $\{\phi^i\}$ associated with eigenvalues λ^i:

$$\sum_a \phi^i_a T_{ab} = \lambda^i \phi^i_b$$

(Generally the matrix $\mathbf{T}$ is not symmetric and left eigenvectors will be different from right ones). From these eigenvectors we can construct scaling variables $u_i = \sum_a \phi^i_a (J_a - J^*_a)$ that identify some directions from the fixed points in the space of couplings. The scaling variables will evolve multiplicatively with the transformation:

$$u'_i = \lambda^i u_i.$$

The eigenvalues can be written as a power: $\lambda^i = b^{y_i}$ where y_i are related to the critical exponents. There are three possible cases:

- if $y_i > 0$, u_i is *relevant*: during the renormalization its value will grow, leading it away from the critical point value.
- if $y_i < 0$, u_i is *irrelevant*: starting near the critical point, it will renormalize toward zero
- if $y_i = 0$, u_i is *marginal*: we do not have enough information to predict its behaviour during the renormalization. This is for example the case of the Ising model in four dimensions in which α, the critical exponent of the specific heat is null, and the specific heat has a logarithmic behaviour with temperature.

If we have n couplings, n' relevant variables and $n - n'$ irrelevant ones, if we look at the n-dimensional space of the couplings, we will find $n - n'$ attractive directions, and n' unstable directions. The $n - n'$ irrelevant scaling variable will define a surface called *critical surface*. If the system is on it, during the renormalization it will approach the critical point. The critical surface divides the region of space attracted by the other trivial and stable fixed points. (See Fig. 2.1).

2.2.4 Universality and scaling revisited

How many relevant variables will exist? For example for the Ising model the important parameters for a system to determine which is its phase are two: the temperature and the magnetic field. All the couplings will depend in some way on them. Thus we will expect that also the relevant variables will be only two. Also for the liquid-gas system the important parameters are two: the temperature and the pressure, and we expect two relevant variables.

From this picture universality emerges: the critical properties of a system are determined by the critical fixed points. If the Hamiltonian of two different systems have different couplings, but their fixed points are the same, the critical properties, like critical exponents, of the two systems will be the same, no matter if the original systems were different. We have required the renormalization group transformation to leave invariant the partition function of the system. Thus the free energy density will renormalize as:

$$f(\{J\}) = g(\{J\}) + b^{-d} f(\{J'\}).$$

The factor b^{-d} takes into account the fact that the number of spins of the renormalized system changed from N to Nb^{-d} while $g(\{J\})$ is the contribution to the free energy that comes from the integrated degrees of freedom and the interactions among them. For this reason it does not depend on the new couplings but only on the old ones, thus it is finite and not important when considering the singular part of f. The free energy density will depend only on the relevant variables, in the Ising universality class it will depend on the temperature and magnetic field like variables: u_t and u_h, where t is the deviation from the critical value $t = T - T_c$ (for h it is not necessary because $h_c = 0$). Near to the critical point we can use the linearized transformations to express the n-th renormalization step of the singular part of f:

$$f_s(u_t, u_h) = b^{-nd} f_s(b^{ny_t} u_t, b^{ny_h} u_h).$$

The linearized transformation can not be used too far from the critical point, say until a certain value $u_{t0} = |b^{ny_t} u_t|$. Thus, evaluating the renormalized f up to this final n we find:

$$f_s(u_t, u_h) = (u_t/u_{t0})^{d/y_t} f_s(u_{t0}, u_h (u_t/u_{t0})^{-y_h/y_t}).$$

Note that the scaling factor b has disappeared. If we are able to carry out the renormalization exactly, as we are supposing, the final results will not depend on b. The variables u_t and u_h must vanish at the critical point, thus, taking into account their symmetries, we can write them as:

$$u_t = t/t_0 + O(t^2, h^2), \quad u_h = h/h_0 + O(ht).$$

Rewriting f_s as a function of the physical observables t and h, and incorporating u_{t0} in the scale factor t_0 we obtain:

$$f_s(t, h) = (t/t0)^{d/y_t} \Phi \left[\frac{h/h_0}{(t/t0)^{y_h/y_t}} \right]. \tag{2.8}$$

where Φ is a scaling function. It can not depend on u_{t0} because the left-hand side does not depend on it. From Eq. (2.8) we can obtain the critical exponents in

terms of y_h and y_t, using thermodynamic relations as: $m = \partial f/\partial h|_{h=0}$ or $\chi = \partial^2 f/\partial h^2|_{h=0}$, and obtaining the critical exponents:

$$\beta = \frac{d - y_h}{y_t}, \quad \gamma = \frac{2y_h - d}{y_t}, \quad \alpha = 2 - \frac{d}{y_t}, \quad \delta = \frac{y_h}{d - y_h}. \tag{2.9}$$

Analogous arguments to the scaling of the free energy can be applied also to the renormalization of the correlation length, leading to the determination of the other two exponents as a function of y_t and y_h:

$$\nu = \frac{1}{y_t}, \quad \eta = d + 2 - 2y_h. \tag{2.10}$$

Eq. (2.8) has the same form of Eq. (2.2), and Eq. (2.9) and (2.10) lead to the same scaling laws of Eq. (2.3). Before the introduction of the RG theory, scaling, as universality, was only an hypothesis, supported by experimental validations. However both of them emerge naturally inside the renormalization group theory in a very elegant way. A last remark is required. Not all the scaling laws implied by the RG are valid in the mean field region, as we have seen. This is caused by an irrelevant variable that is *dangerous* and modifies the values of the critical exponents for $d > 4$.

2.2.5 Irrelevant variables and the correction to scaling

Let us analyze the effect of the irrelevant variables in more detail. We consider only the most important one and we call it u, and its exponent will be y_u. It will be a function of the relevant fields: $u = u_0 + at + bh^2 + ...$, however, if we are near enough to the critical point we can keep only the first term u_0. We can rewrite Eq. (2.8) including the irrelevant variable:

$$f_s(t, h) = (t/t0)^{d/y_t} \Phi \left((h/h_0)(t/t0)^{-y_h/y_t}, u_0(t/t0)^{|y_u|/y_t} \right).$$

Near to the critical point we know that $u_0(t/t0)^{|y_u|/y_t}$ is small, thus we can think to expand the free energy in this parameter. Let us put for simplicity $h = 0$. We will obtain:

$$f_s(t, h) = (t/t0)^{d/y_t} \left(a_1 + a_2 u_0 (t/t0)^{|y_u|/y_t} + ... \right)$$

where a_1 and a_2 will be some non universal constants.

Thus the effect of the irrelevant variable will be to add corrections to the scaling. The exponent y_u associated to the most important irrelevant variable defines another universal exponent $\omega = -y_u$. It is very important to consider the effect of the corrections when the critical exponents are extracted from systems of finite size, see for example Appendix A. There are also other correction terms associated with the dependence of u from t and h that we have neglected. However, usually they are not important.

We have expanded the free energy in the variable u_0, assuming that it is analytic in the limit $u \to 0$. However this is not always obvious. When the limit $u \to 0$ is not well defined, the variable u is said *dangerous*, as it happens above the upper critical dimension.

2.2.6 The functional integral formulation and the ϵ-expansion

In the previous sections we have introduced the renormalization group as a decimation of the degrees of freedom in the real space. In particular the number of the spins is reduced in each iteration by forming blocks and introducing new block-spins and new couplings. This procedure is called Real Space Renormalization Group. We have seen that this operation can not be carried out explicitly in more than one dimension, and particular approximations are reviewed in the next chapter. However the RG procedure can be carried out also in the momentum space, performing a Fourier transformation. In this vision, high impulses are integrated out and the important physics is that at small impulses [21]. This particular point of view is very common when the problem is represented with functional integrals, taking the inspiration from quantum field theory where renormalization was firstly introduced. As said before, a phase transition is characterized by an order parameter $\phi(x)$. Once we have identified it (for example the magnetization for the Ising model), we can think to define a statistical weight for a given spatial distribution of the order parameter field to define a measure over the space of these distribution. One possible way is to identify all the possible symmetries of the order parameter, for the Ising model the only symmetry is the $\phi \to -\phi$ invariance. Then, all the possible invariants of the symmetry group are constructed from the field and its derivatives, and a Lagrangian density $\mathcal{L}(\phi)$ is made with the sum of them with arbitrary coefficients. The weight of a certain distribution of the field will be:

$$W(\phi) = \exp\left(-\int dx \mathcal{L}\left[\phi(x)\right]\right).$$

For the Ising model, there will be only even powers of the fields leading to:

$$\mathcal{L}(\phi) = A_0(\nabla\phi)^2 + A_1\phi^2(x) + A_2\phi^4(x) + h\phi(x) \tag{2.11}$$

where h is the magnetic field. We have stopped at the quartic term, because it can be demonstrated that all the terms with higher powers of the fields are irrelevant. If we perform a Fourier transformation, Eq. (2.11) becomes:

$$\begin{aligned}&\int dx\mathcal{L}(\phi) = \\ &\sum_k[(k^2+\mu^2)\phi(k)\phi(-k) + h(k)\phi(-k)] + u\sum_{k_1k_2k_3}\phi(k_1)\phi(k_2)\phi(k_3)\phi(-k_1-k_2-k_3)\end{aligned} \tag{2.12}$$

where the translational invariance in real-space imposes to the sum of the impulses in each term to be null. In field theory the μ coefficient corresponds to the mass of the particle associated to the field. Indeed Eq. (2.12) can be obtained also from the Hamiltonian of Eq. (2.1) with the magnetic field term. To reach this result the Hubbard-Stratonovich transformation:

$$c\exp(s_iV_{ij}s_j) = \int_{-\infty}^{\infty}\prod_{i=1}^{N}dx_i\exp(-\frac{1}{4}x_iV_{ij}^{-1}x_j + s_ix_i). \tag{2.13}$$

is used to eliminate the quadratic term in the spins. Then it is Fourier transformed and an expansion of the couplings for small impulse is performed.

At this point we can perform our renormalization, letting the distance-unit $a \to ba$ and asking how the coefficients must change to leave the Lagrangian $\int dx\mathcal{L}(\phi)$ invariant. There is one trivial fixed point $h = A_1 = A_2 = 0$. Above four dimensions the scaling variable associated to the quartic term is irrelevant, and this fixed point is the important one. This corresponds to the so called *Gaussian* fixed point, because the partition function is a Gaussian integral in the impulse space. At this second order phase transition, in the field theory language, there is a particle with zero mass $\mu = 0$. It can be shown that the coefficient $\mu = \xi^{-1}$, that goes to zero at the critical point. The critical exponents associated to this fixed point are the mean field ones of Eq. (2.5). Indeed the Gaussian solution corresponds to the mean field approximation, where fluctuations are ignored.

Below four dimensions A_2 becomes relevant and a new fixed point arises, different from the Gaussian one. However, if we define a parameter $\epsilon = 4-d$, for small values of ϵ the two fixed points are sufficiently close, and the properties at the non-trivial fixed point can be deduced from the properties at the Gaussian fixed point. For example the critical exponents can be calculated as a power expansion in ϵ around the mean-field value, as it was done for the Ising model in Ref. [22]. The ϵ-expansion can be used only if the non-trivial fixed point can be reached perturbatively from the Gaussian one, as in the case of the Ising model. However if the non-trivial fixed point is of a completely different nature than the Gaussian one, this method can not be used.

Let us mention that an ϵ-expansion can be developed also near the lower critical dimension.

2.3 Spin Glasses

In nature, there exist also magnetic materials, in which the interactions between local magnetic moments are random both positive and negative. Some example of these amorphous magnets are AgMn, CuMn, and AuFe, with the magnetic moments that are vectors (they are called Heisenberg spins). There are also Ising-like materials, like $Fe_xMn_{1-x}TiO_3$, with uniaxial spins. All these materials are called spin-glasses. The simplest model to describe them is the Edward-Anderson (EA) model [1]. The Hamiltonian is the same as in Eq. (2.1), but the couplings J_{ij} can be positive or negative. We can assume them to be independent identically distributed random variables extracted from a distribution $P(J)$, that can be for example a Gaussian with zero mean. In this case it is not possible to find a spin configuration that is able to satisfy all the interactions. The system is *frustrated*. One would like to calculate the free energy density of the system for a given coupling realization,

$$f_J = \frac{1}{\beta N} \log Z_J = \frac{1}{\beta N} \log \sum_{\{\sigma\}} \exp(-\beta H_J[\sigma])$$

and also its average over the disorder, indicated by the overbar:

$$f = \overline{f_J} = \sum_J P(J) f_J.$$

This is the so called *quenched* average. It is different from the *annealed* one:

$$f_A = \frac{1}{\beta N} \log \overline{Z_J},$$

that is simpler to solve. In the annealed mean, the couplings can change at the same level of the spins in order to minimize the free energy. However, this is not what happens in real spin glasses where the couplings are fixed for each sample. We may ask if it is a good idea to calculate the quenched free energy to understand the properties of a given sample. For a model with short range interactions it is easy to demonstrate that the free energy is *self-averaging*, namely in the thermodynamic limit it assumes the same values for all the realizations of the couplings that have non null probability. When a spin interacts with all the others, in the so called Sherringhton Kirkpatrick (SK) model [2], that is a mean field model, the property of self-averageness is not rigorously demonstrated, but it has many numerical validations.

2.3.1 The replica symmetric solution

There is not a solution for the EA model, however there is a solution for the SK model (for a complete review see Ref. [23]). To calculate the quenched mean, one uses the mathematical property:

$$\log(x) = \lim_{n\to 0} \frac{x^n - 1}{n}.$$

Instead to calculate $\overline{\log Z_J}$, one can calculate $\overline{(Z_J)^n}$. In practice, for integer n the mean of n uncoupled replicas of the original system with the same distribution of the disorder is calculated:

$$(Z_J)^n = \sum_{\{\sigma^1\}} \sum_{\{\sigma^2\}} ... \sum_{\{\sigma^n\}} \exp\{-\sum_{a=1}^{n} \beta H_J[\sigma^a]\}$$

and the average of f is obtained with an analytical continuation at $n = 0$ done only at the end of the calculation. The equation for the free energy is thus:

$$f = \lim_{N\to\infty} -\frac{1}{\beta N} \lim_{n\to 0} \frac{\sum_{\{\sigma^1 ... \sigma^n\}} \int dP[J] e^{\sum_{ij}(\beta J_{ij} \sum_{\alpha=1}^{n} \sigma_i^\alpha \sigma_j^\alpha)} - 1}{n}$$

and the main steps of the calculation are the following. After that the average over the disorder is performed, the quadratic term in the spins is eliminated using a generalization of Eq. (2.13). In this way the quadratic term disappears, but we have introduced some new auxiliary fields, that will be called Q_{ab}. It is a nxn matrix. Thanks to the limit $N \to \infty$, a saddle point is performed and, at the end of the calculation, the result is:

$$f_n = -1/(\beta n) \min_Q A[Q] \quad \text{with} \quad A[Q] = -n\beta^2/4 + \beta^2/2 \sum_{a\le b=1}^{n} (Q_{ab})^2 - \log Z[Q]$$

$$\text{and } Z[Q] = \sum_\sigma \exp\{-\beta H[Q,S]\}$$

$$H[Q,S] = -\beta \sum_{a\le b=1}^{n} Q_{ab} S_a S_b - h \sum_{a=1}^{n} S_a$$

where $H[Q,S]$ is a single site Hamiltonian. In the original formula, the thermodynamic limit was preceded by the the limit in the number of replicas going to zero. Here the two limits are inverted. However this can be done without causing problems. The minimization of A can also be written as a self-consistent equation: $Q_{ab} = \langle S_a S_b \rangle_{H[S,Q]}$. The replica indices have been introduced as a pure mathematical trick, and the previous equations are symmetrical for the exchange of the replica indices, thus naively the right form for the matrix Q_{ab} seems to be the symmetric one:

$$Q_{a\neq b} = q, \quad Q_{aa} = 0.$$

This is called the replica symmetric (RS) ansatz. Once inserted in the previous equation, it is found that for $T > T_c$ the solution is at $q = 0$, while for $T < T_c$, the solution is at $q \neq 0$. There is a transition. However, for this solution, the entropy results to be negative (that is impossible for a system with discrete degrees of freedom), and a more careful analysis shows that the solution for $T < T_c$ is not stable [24] (the Hessian $\partial^2 A/\partial Q \partial Q$ calculated at the replica symmetric solution has negative eigenvalues and its square root, that is imaginary, enters in the proportionality coefficient and in the $O(1/N)$ corrections of the leading result of the saddle point approximation). In fact in the region $0 \leq n < 1$, the minimum of A becomes a maximum. Thus a different solution must be found for the low temperature phase. The new solution must satisfy the equation $\partial A/\partial Q = 0$ and $\lim_{n\to 0} \partial^2 A/\partial Q \partial Q > 0$. The new solution is not necessarily a minimum of the free energy, indeed it will be a maximum.

2.3.2 The replica symmetry breaking

The correct solution is the Replica Symmetry Breaking (RSB) one that has been proposed in Ref. [3]. $k+1$ integer numbers are introduced: m_i with $i = 0, 1, ..., k$. The n replicas are divided in n/m_1 groups of m_1 replicas, each of these groups is divided in m_1/m_2 groups of m_2 replicas and so on. $Q_{ab} = q_i$ if the replicas a and b are in the same group at level i but not at level $i+1$. This ansatz for the matrix is introduced in the Eq. $\partial A/\partial Q_{ab} = 0$ and the q_i are determined. Then the free energy is calculated. At the end the limit $n \to 0$ is taken. When $k \to \infty$, the q_i's become a continuous function $q(x)$. The fact that Q is a nxn matrix, and m_i are integer numbers smaller than n can look strange in the $n \to 0$ limit. However there are no particular difficulties in the application of the prescription, that is to perform the limit $n \to 0$ at the end of the calculation, even if the analytical continuation is not rigorous. Naturally, this matrix breaks the symmetry of the replicas, even if the free energy is symmetric under the replicas exchange. It is a spontaneous symmetry breaking.

2.3.3 The overlap as order parameter

What is the meaning of this particular matrix? Under the critical temperature T_c the phase space is divided in many different equilibrium pure states, separated by extensive barriers. Different replicas of the system will fall in different states. Each pure state α has a certain weight w_α in the partition function and it is characterized by certain magnetizations $\{m_i^\alpha\}$. In fact, while above T_c the state is paramagnetic and $\langle \sigma_i \rangle = 0$, below T_c the spins of the system will freeze in their position, but

there will be no preferential orientation, and $M = 0$. The *overlap* parameter $q_{\alpha\beta}$ measures how much two different states are similar:

$$q_{\alpha\beta} = \frac{1}{N}\sum_i m_i^\alpha m_i^\beta, \quad -1 \leq q_{\alpha\beta} \leq 1.$$

To characterize a phase of a system, one can use the overlap distribution, that measures if the system has different states and how much they are similar:

$$P(q) = \overline{\sum_{\alpha\beta} w_\alpha w_\beta \delta(q_{\alpha\beta} - q)}.$$

The moments of this distribution can be obtained as:

$$q_k = \int_{-1}^{1} P(q) q^k dq.$$

It is easy to show that

$$P(q) = \lim_{n\to 0} 1/[n(n-1)/2] \sum_{a,b} \delta(Q_{ab} - q) \tag{2.14}$$

$$q_k = \lim_{n\to 0} 1/[n(n-1)/2] \sum_{a,b} Q_{ab}^k$$

In these equations the physical meaning of the Q matrix is enclosed.

In the ferromagnet, there are only two states of equilibrium, with opposite magnetization. Thus the $P(q)$ is trivial; it has two peaks, at m^2 and $-m^2$, related by the obvious Z_2 symmetry. For the spin glass the order parameter is no more the magnetization but the overlap distribution that is not trivial [25]. In fact, when the saddle-point solution Q_{ab} is inserted in Eq. (2.14), the $P(q)$ is obtained. It has a continuous support $q \in [0, q_{EA}]$, where $q_{EA} = \frac{1}{N}\sum_i m_i^\alpha m_i^\alpha$ is the self-overlap inside a state. Looking at this function we can learn that there are many states, with different distances. Moreover the block structure of the RSB ansatz for Q_{ab} implies the ultrametricity property: if we take three states, and we identify the mutual overlap as the distance between them, it can be demonstrated that the property

$$q_{\alpha\beta} = \max(q_{\alpha\gamma}, q_{\gamma\beta})$$

holds. This naturally leads to a hierarchical organization of the states: in fact some states are grouped in a family with a certain overlap, then families are grouped in bigger families with a smaller overlap and so on. The practical consequence of such a complicated free-energy landscape is that in the low temperature phase there is a strong non-ergodicity and it is quite impossible to equilibrate large systems. In practice numerical simulation of spin-glasses for large sizes and low temperature, are out of equilibrium. This mean field theory is called the Replica Symmetry Breaking (RSB) theory, and it predicts a thermodynamic transition also in magnetic field h at a finite temperature [3]. In this framework, a transition line, called *deAlmeida-Thouless* (AT) [24] line, can be identified in the $T-h$ plane between a paramagnetic and a spin glass phase. It starts at $(T, h) = (T_c, 0)$ and it ends at $(T, h) = (0, h_c)$. $h_c = \infty$ for the SK model while it is finite when the dimension of the space is finite.

2.3.4 SG in finite dimensions

For the EA model in finite dimension (below the upper critical one $D = 6$), there is no analytical solution. Two main scenario are supposed: the first one is that the mean field solution remains valid also in finite dimension. The critical exponents will change below the upper critical dimension but the qualitative landscape of the free energy will remain the same. At sufficiently low dimensions (i.e. below the lower critical dimension, D_L) the transition disappears. The value of D_L is not known, but it is quite possible that in a field D_L is higher than for $h = 0$ (as it happens for a ferromagnet in a random field). There are some numerical evidences [26] (and analytic results[27]) supporting $D_L = 2.5$ at zero field. Indeed a non-integer lower critical dimension is a strange, unique thing. For $h > 0$, some recent works, revised in the next section, argued that the AT line can be continued below $D = 6$.

The second scenario is the *droplet* one [28]. In this theory, instead, no transition is predicted to remain as soon as an infinitesimal field is switched on, independently from the value of D. At null field, there are only two stable states, linked by the reversal symmetry, and the $P(q)$ is delta-shaped.

Extensive numerical works on the Edwards-Anderson model in 4D and 3D yielded evidence both in favor of a transition in field [29] [30] [31] and against it [32] [33] [34]. Unfortunately, finite size corrections are very strong in the presence of an external field and it is hard to say whether these simulations were really testing the thermodynamic limit.

For what concerns real materials, in the most common Heisenberg-like amorphous magnets, e.g., AgMn, CuMn, and AuFe, a SG phase has been detected also in presence of an external field [35]. In Ising-like materials, instead, it is still a matter of debate whether or not a SG phase occurs when the system is embedded in a magnetic field [35], [36].

2.4 Attempts to renormalize Spin Glasses

To solve the important problem of the spin-glass phase in finite dimensions, a useful instrument can be the RG. Unfortunately, while RG transformations have been studied in great detail for homogeneous models, much less is known for disordered models, that contain quenched randomness in the Hamiltonian (either random fields and/or random couplings). This is specially true for frustrated models, like SG, for which a satisfying RG transformation is still lacking. For example, for the Edwards-Anderson SG model on a D-dimensional lattice all the attempts to develop a field theory by performing an ϵ-expansion around the upper critical dimension $D_u = 6$ have proved to be very complicated [37, 8]. These studies have led to the discovery of fixed points different from the mean-field (MF) ones, however the implications of that are not completely clear.

We have seen how the mean field free energy can be expressed as a function of uniform replica fields $Q^{\alpha\beta}$, in a $n(n-1)/2$ dimensional replica space. If we are in finite dimension, we can not forget spatial fluctuations. For this reason, if we want to construct a perturbation expansion around the mean field critical value, we can consider a replica field for each site, that can be divided into the mean-field value,

and the fluctuations around it:

$$Q_i^{\alpha\beta} = Q^{\alpha\beta} + \phi_i^{\alpha\beta}.$$

Ising spin glass transition in an external magnetic field can be studied with the generic replica symmetric field theory developed in [8], with a Lagrangian $\mathcal{L} = \mathcal{L}^{(2)} + \mathcal{L}_{\mathcal{I}}$. The quadratic term has three different masses:

$$\mathcal{L}^{(2)} = \frac{1}{2}\sum_p \left[(\frac{1}{2}p^2 + m_1) \sum_{\alpha\beta} \phi_p^{\alpha\beta}\phi_{-p}^{\alpha\beta} + m_2 \sum_{\alpha\beta\gamma} \phi_p^{\alpha\gamma}\phi_{-p}^{\beta\gamma} + m_3 \sum_{\alpha\beta\gamma\delta} \phi_p^{\alpha\beta}\phi_{-p}^{\gamma\delta} \right]$$

while the interaction term has eight different cubic terms and the interaction with the magnetic field. The Lagrangian can be rewritten in the basis of the eigenvector of the mass part, that are called replicon, anomalous and longitudinal. In the mean field region, above $D = 6$ the fixed points are well identified: the fixed point at zero external field is characterized by the three masses becoming null together, while if a small external field is present, the AT line is identified when only the replicon mass becomes critical. The existence of replica symmetry breaking (RSB) fixed points in the non-mean field region $D < D_u$ is more difficult to demonstrate, and it has been shown only very recently [9]. In this work the AT line is obtained with an ϵ-expansion below 6 dimensions, reviewing and confirming the results in Ref. [10]. However the range of validity of this expansion is very limited, and nothing is said about the lower critical dimension. It is possible that the lower critical dimension in field is higher than $D = 3$. Thus much is still missing, like for example estimates of critical exponents are still not reliable.

In this framework the development of a (semi-)analytical real space RG for disordered models would be very welcome. The outcome of such a RG transformation could be well compared with Monte Carlo (MC) simulations, that provide accurate estimates of critical temperatures and critical exponents for disordered models. A new kind of real space RG for disordered models will be proposed in next chapters.

Chapter 3

Real Space Renormalization Group and Hierarchical Model

We have seen that the real-space renormalization group (RSRG) transformation consists in integrating out the degrees of freedom at small distances creating blocks of spins, defining block variables and looking at the flow of the new couplings among them, that leave the partition function invariant. The beautiful aspect of RSRG is that the physical meaning of the steps is clear, and there is not the risk to forget the point that we want to reach. This is not so obvious when other methods like field theoretical analysis, or ϵ-expansion are used, especially when disorder is present because the replica action averaged over the disorder contains all the physical information but in a somehow implicit form. This is one of the reasons under our choice to apply a RSRG to disordered systems. However we have seen that RSRG can not be carried out exactly in more than one dimension because couplings between any subset of spins are created. For this reason many approximations have been developed. These approximations do not leave the partition function invariant, as in Eq. (2.6), however they can give good results.

3.1 The Migdal-Kadanoff approximation

Among these approximations, there are the lower bound transformations, invented by Kadanoff [38]. The Hamiltonian of the system that we want to renormalize is $H(\sigma)$ but we replace it by $H(\sigma) + V(\sigma)$ where $V(\sigma)$ is chosen so that the sum over the spins configurations can be evaluated explicitly and the new renormalization

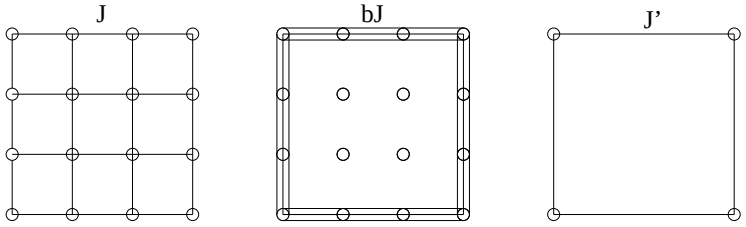

Figure 3.1. MK renormalization for a block of size $b = 3$.

equation becomes

$$e^{H'(\sigma')} = \sum_{\sigma} P(\sigma', \sigma) e^{H(\sigma)+V(\sigma)} \tag{3.1}$$

For the partition function one obtains

$$\begin{aligned} \sum_{\sigma'} e^{H(\sigma')} = \sum_{\sigma} e^{H(\sigma)+V(\sigma)} \geq \sum_{\sigma} e^{H(\sigma)}[1+V(\sigma)] \\ Z[H'] = Z[H+V] \geq Z[H](1+ < V >_H) \end{aligned} \tag{3.2}$$

If we choose a potential with $< V >_H = 0$, the free energy of the renormalized system is a lower bound to the free energy of the original system. For the nearest neighbor Ising model, one good choice for $V(\sigma)$ is the bond moving potential. One example is $V(\sigma) = J(\sigma_3\sigma_4 - \sigma_1\sigma_2)$. The property $< V >_H = 0$ is satisfied thanks to the translational invariance. The effect of this kind of potential is to move some couplings between two spins to other spins, and in this way some of the spins can be decoupled. When a spin has only interactions in one direction it can be renormalized exactly as shown in Section 2.2.2.

Let us see how the Migdal-Kadanoff renormalization [39] works on a nearest neighbour Ising model on a 2-dimensional lattice, as explained in Fig. 3.1. The spins are divided in blocks of size b. Then all the couplings are moved to the spins at the edges of the blocks, their sum being bJ. At this point a decimation of the spins at the edges except that on the corners is performed obtaining $J' = \mathcal{R}_b(bJ)$, where the function $\mathcal{R}_b$ has been defined in Eq. (2.7). The recursion relation is easily generalized to $J' = \mathcal{R}_b(b^{d-1}J)$ in d-dimensions. The final result will depend of our choice of b, because we are not taking an exact RG. For this reason the best choice is to take the infinitesimal transformation. The limit $b \to 1$ can be analyzed setting $b = 1 + \delta l$ and obtaining

$$\frac{dJ}{dl} = (d-1)J + \sinh J \cosh J \ln \tanh J.$$

For $d = 2$, the fixed point of the infinitesimal transformation is the correct one $J^* = \frac{\ln(1+\sqrt{2})}{2}$, thanks to the fact that the 2D square lattice is self dual. The same good results are not found for the critical exponents for which, in the limit $b \to 1$, one finds $1/\nu = 0.754$ [39] instead of $1/\nu = 1$.

3.2 The Hierarchical diamond lattices

There are some particular lattices, the hierarchical diamond lattices, for which the Migdal-Kadanoff renormalization procedure is exact, as pointed out by Berker and Ostlund [6]. They can be generated iteratively as in Fig. 3.2. The procedure starts at the step $G = 0$ with two spins connected by a single link. At each step G the

Figure 3.2. Construction of a Hierarchical Lattice with $b = 3$ and $s = 2$.

construction in Fig. 3.2 is applied to each link of step $G-1$. For each link, b parallel branches, made of s bonds in series each, are added, with $b\cdot(s-1)$ new spins. The effective dimension of this model is $d = 1 + \ln(b)/\ln(s)$. In fact in a standard d dimensional lattice, if the length grows of a factor L, the number of links grows with a factor L^d. If in the hierarchical lattice the length grows of a factor s, the number of links grows of a factor $b\cdot s$. However for example if $b = s$, it corresponds to $d = 2$. But for various values of $b = s$, the results are different. It means that d is not sufficient to identify the lattice. Starting from a lattice at the G generation, summing over the spin introduced in the last generation, one can obtain a lattice of the $G-1$ generation with renormalized couplings. In fact each s-tuple of couplings in series produces an effective coupling $\tilde{J} = R_s(J) = \tanh^{-1}[(\tanh J)^s]$. Then each b-tuple of effective couplings in parallel linking the same pair of variables is summed together, giving the renormalized coupling $J' = b\cdot\tilde{J}$. Repeating this renormalization procedure, one can exactly renormalize the whole lattice. For this property, the hierarchical lattices have been widely used, also recently, to analyze RG flows of the systems, even when the disorder is included [41, 40, 42, 43]. Unfortunately, the hierarchical lattices do not always have the same characteristics as the usual short range lattices. In particular, as shown rigorously in Ref. [44], spin glasses on hierarchical lattices are replica symmetric. The low temperature phase is thus different from that in usual lattices.

3.3 The Hierarchical model

3.3.1 Definition of the model and general properties

Another particular model for which the renormalization group equations can be written in a closed form is the hierarchical model (HM). It is a particular one-dimensional long range model, firstly introduced by Dyson [14] (for a review see [15]). It is a *fully connected* model, where each spin is connected to all the others with interactions decaying as a power with a special distance. For short range models we have seen that the lower critical dimension is $D = 1$. For long range models however it is possible to have a transition even in $D = 1$ as in this case. The Hamiltonian of the HM for $N = 2^n$ spins can be constructed iteratively in the following way:

$$H_n(s_1,...,s_{2^n}) = H_{n-1}(s_1,...,s_{2^{n-1}}) + \\ + H_{n-1}(s_{2^{n-1}+1},...,s_{2^n}) - c^n \sum_{i<j=1}^{2^n} J_{ij}\, s_i\, s_j\ . \quad (3.3)$$

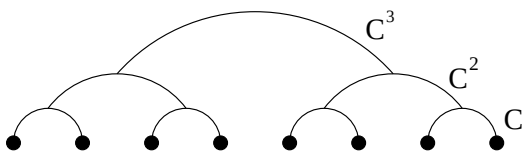

Figure 3.3. The HM with three levels

In practice H_n is the sum of interactions at n different levels, of intensity $c^k = 2^{-k(1+\sigma)}$, where k is the index of the level, see Fig. 3.3. If the system is decimated by a standard block-spin transformation, the new Hamiltonian does not contain any new term (at variance to what happens on finite dimensional lattices). So, considering only pairwise interactions of the same type of the original ones in the RG is not an approximation for the HM. Moreover the ferromagnetic (FM) version, with $J_{ij} = 1$, can be exactly solved in a time growing only polynomially with N, since the probability distribution of the magnetization satisfies the equation

$$p_n(m) \propto e^{\beta c^n m^2} \sum_{m_L, m_R} p_{n-1}(m_L)\, p_{n-1}(m_R)\, \delta_{m_L+m_R,m}$$

where m_L and m_R are the magnetizations of the half systems.

By properly tuning the topological factor c that controls how fast the couplings intensity decays with distance, the HM can emulate a D-dimensional short range (SR) model: $c \simeq 2^{-1-\frac{2}{D}}$ (see next section). This relation is exact at the upper critical dimension because the long range HM and the SR D-dimensional model have the same field theory at leading order.

In order to have a phase transition from a paramagnetic to a ferromagnetic phase at a finite temperature, the c parameter must satisfy $\frac{1}{4} < c < \frac{1}{2}$. The lower bound value of c corresponds to the lower critical dimension (and thus $T_c = 0$), while if c reaches the upper bound the energy is no longer extensive (thus $T_c = \infty$). For $c > 2^{-\frac{3}{2}} = c_U$, the model shows mean field critical properties (like for $D > D_U$ in SR models). So, tuning a single parameter in the HM, we can move from the MF region to a non-MF one.

3.3.2 Gaussian fixed point and c-D relation

The HM has been constructed in such a way that we can write exact, analytical RG equations on it. In fact, the procedure to blockspin is very simple. The blocks will be made of two neighbouring spins,

$$s'_i = \sqrt{c}(s_{2i-1} + s_{2i}) \tag{3.4}$$

where the rescaling factor $\sqrt{c}$ is introduced to leave the partition function unchanged in the thermodynamic limit. The energy of the total system is rewritten as

$$H_n(s) = H'_{n-1}(s') - \frac{1}{2}\sum_{i=1}^{2^{n-1}} (s'_i)^2. \tag{3.5}$$

In other words we can blockspin without thinking about H and then include the second term of Eq. (3.5) to take into account the contribution of the integrated spins in the partition function. The problem is identical to the original one, except from the fact that we pass from n to $n-1$ levels and we use a different weight for the distribution of the field (that we will call ϕ from now on). The change in the weight can be expressed through the recursion relation:

$$W_{n+1}(\phi') = e^{(\beta/2)\phi'^2} \int_{-\infty}^{\infty} d\xi W_n(\frac{\phi'}{2\sqrt{c}} - \xi) W_n(\frac{\phi'}{2\sqrt{c}} + \xi) \tag{3.6}$$

where ϕ' is the rescaled field. If we start with a Gaussian measure:

$$W_0(\phi) \propto e^{-A\phi^2} \tag{3.7}$$

the renormalized measure will always be Gaussian:

$$W_n(\phi') \propto e^{-A_n\phi'^2}$$

with $A_{n+1} = -\frac{\beta}{2} + \frac{1}{2c}A_n$. The fixed point of this recursion relation is $A^* = \frac{\beta c}{1-2c}$ that leads to $A_n = (\frac{1}{2c})^n(A - A^*) + A^*$. Thus the local measure for the original field after n_{max} iterations can be expressed as $W_{n_{max}} \propto e^{-[(A-A^*)+(2c)^{n_{max}}A^*]\phi^2}$. When $A = A^*$, we are at the critical point in the infinite volume limit. At finite volume and $A = A^*$ the mass (that is, the coefficient of the quadratic term in the field) is $m^2 = (2c)^{n_{max}}$. If we compare this result with a short range Gaussian theory for a D-dimensional system, at finite size L, at the critical point the mass is $m^2 = (\xi^{-1})^2 = L^{-2}$. Equating the two masses and comparing the volume: $\Omega = L^D = 2^{n_{max}}$, the $c - D$ relation is obtained:

$$c = 2^{-1-2/D}. \tag{3.8}$$

The upper critical $c_U = 2^{-\frac{3}{2}}$ corresponds to $D_U = 4$, as expected. This relation has been obtained from the Gaussian fixed point, thus it can be inexact below the upper critical dimension. This point will be discussed in Part II. Usually the field scales during the renormalization with a factor $b^{\frac{D+2-\eta}{2}}$. On the other hand, in Eq. (3.4) the rescaling factor is $1/\sqrt{c}$, and $b = 2$. Recalling that $c = 2^{-(1-\sigma)}$ and the dimension of the system is $D = 1$, the relation

$$\eta = 2 - \sigma \tag{3.9}$$

is obtained. This equation for η is thus valid in the mean-field region. However, for long-range systems, it is commonly believed that it remains valid also in the non-mean field region [45]. Again this point will be discussed in Part II.

3.3.3 The non trivial fixed point in high temperature expansion

Below c_U the Gaussian fixed point is no longer stable and a new fixed point arises. There are various methods to calculate it numerically, here we will review the one based on polynomial truncation. The recursion relation in Eq. (3.6) for $W(\phi)$, can be rewritten for its Fourier transform $R(k)$ as:

$$R_{n+1}(k) \propto e^{-\frac{1}{2}\beta\frac{\partial^2}{\partial k^2}} \left(R_n(\sqrt{c}k)\right)^2. \tag{3.10}$$

A good approximation for $R_n(k)$ in the symmetric phase is:

$$R_n(k) = 1 + a_{n,1}k^2 + a_{n,2}k^4 + ... + a_{n,l_{max}}k^{2l_{max}},$$

that can be viewed as a high temperature expansion. When introduced in Eq. (3.10), the recursion formula becomes a l_{max}-dimensional map with variables $a_{n,i}, i \in \{1, ..., l_{max}\}$. The fixed points will be determined by coefficients $\{a_i^*\}$, and critical exponents are extracted from the linearized transformation around the fixed point, taking the first eigenvalue Λ of the matrix $M_{l,m} = \frac{\partial a_{n+1,l}}{\partial a_{n,m}}\big|_{\{a_i^*\}}$. In fact $\nu = \frac{\log 2}{\log \Lambda}$, where the factor 2 is our scaling factor b. Knowing the exact value of η from 3.9, in Ref. [46] the value $\gamma = 1.299140730159$ is obtained for a value of c corresponding to $D = 3$ following the relation 3.8. Also the critical temperature can be extracted, leading to $\beta_c = 1.179030170$ in $D = 3$ [47].

3.3.4 The ϵ-expansion around c_U

The fixed points for $c < c_U$ can be obtained also with an ϵ-expansion around c_U as explained in Sec. 2.2.6. We will briefly sketch here the important passages of the calculation. Let us add to the local measure a quartic term, that is the next term that can be added, invariant for the symmetry $\phi \to -\phi$ of the system:

$$W_0(\phi) \propto e^{-A\phi^2 - w\phi^4}. \tag{3.11}$$

This new measure is inserted in Eq. (3.6). Now, if we suppose that for c sufficiently near to c_U the new fixed point will be near enough to the Gaussian one, we can suppose that w is small and will remain small during the iteration. For this reason we can perform an expansion around $w = 0$ and find the recursion relations for the parameters A_{n+1}, w_{n+1} as a function of A_n, w_n.

If we call $\epsilon = \sigma - \frac{1}{2}$, from these relations one can note that for $\epsilon < 0$ the parameter w becomes smaller at each iteration. In this region it is an irrelevant variable, in fact the Gaussian measure is the stable one. If $\epsilon > 0$, w_k grows at each iteration, thus it is a relevant variable. From the recursion relations one can also find the fixed point $(A_k^*, w_k^*) = (A_{k+1}^*, w_{k+1}^*)$, that differs from the Gaussian one to order ϵ: $w^* = O(\epsilon)$. At this point the critical exponent ν can be extracted from the first eigenvalue Λ of the 2x2 matrix $M = \frac{\partial(A_{n+1}, w_{n+1})}{\partial(A_n, w_n)}\big|_{(A^*, w^*)}$ as $\nu = \frac{\log 2}{\log \Lambda}$. For the Gaussian fixed point the calculation is exact and leads to the result:

$$\nu = \frac{1}{\sigma}. \tag{3.12}$$

For the non trivial fixed point, the critical exponent will be a series expansion in ϵ. In Ref. [48] this series is showed to be not convergent. However the application of the Borel resummation method yields to a convergent series for ν. At the end the value $\gamma = 1.2986$ is obtained for c equivalent to $D = 3$. The quality of the result is tested comparing the results with those obtained with other methods, for example the one in the previous section. The agreement is very good, confirming the applicability of the ϵ-expansion, that is the possibility to go perturbatively from the Gaussian fixed point to the non-trivial one.

3.4 Disordered HM

The spin-glass version of the Hierarchical Model was firstly introduced in Ref. [49]. The Hamiltonian is always the one in Eq. (3.3), and the couplings at level k are independent identical distributed random variables, distributed with a Gaussian law of zero mean and variance $\sigma_k^2 = 1$. This time we will define $c = 2^{-\frac{1+\sigma}{2}}$. The sum of the squares of the interactions at the last level is $2^{-n(1+\sigma)} \sum_{i<j=1}^{2^n} J_{ij}^2 \propto 2^{n(1-\sigma)}$. This is of the order of the volume for $\sigma = 0$, thus this case corresponds to the infinite range Sherrington-Kirkpatrick model. The SG HM model has a finite temperature spin-glass transition for $\sigma \in [0, 1)$, and the $c - D$ relation is the same of Eq. (3.8). When the disorder is introduced, a recursion relation like the one in Eq. (3.3.1) for the magnetization can be written for the distribution of the new order parameter of the system, that is the overlap matrix Q:

$$\mathcal{Z}_k[Q] = \exp\left(\frac{\beta^2}{4}\mathrm{Tr}[Q^2]\right) \cdot \int [dP] \mathcal{Z}_{k-1}\left[\frac{Q+P}{2^{(1-\sigma)/2}}\right] \cdot \mathcal{Z}_{k-1}\left[\frac{Q-P}{2^{(1-\sigma)/2}}\right]. \tag{3.13}$$

$\int[dP]$ indicates the functional integral over the matrices Q_{ab}. As in the ferromagnetic case, the recursion relation can be solved exactly in the mean field region and perturbatively in the non-classical one. This has been done in Ref. [50]. First of all one can assume that the overlap distribution is Gaussian: $\mathcal{Z}_k[Q] = \exp(-r_k \mathrm{Tr}[Q^2])$. Inserting it into Eq. (3.13) the recursion relation is obtained: $r_k = \frac{2r_{k-1}}{2^{1-\sigma}} - \frac{\beta^2}{4}$. This is the mean field solution of the model characterized by the Gaussian fixed point $r^* = \frac{\beta^2 2^{1-\sigma}}{4(2-2^{1-\sigma})}$.

Non Gaussian solutions can be constructed perturbatively introducing an extra-term in the overlap distribution, consistent with the symmetries of the model: $\mathcal{Z}_k[Q] = \exp(-r_k \mathrm{Tr}[Q^2] - \frac{w_k}{3}\mathrm{Tr}[Q^3])$.

At this point recursion relations can be obtained for the parameters of the function r_k and w_k, performing an expansion around the new term w_k, supposing it to be small. At the end of the calculation the limit $n \to 0$ has to be taken. For $\sigma < 1/3$ the Gaussian solution is the stable one. In fact the new term w_k will flow to zero during the renormalization. Instead for $\sigma > 1/3$ a new fixed point arises with w_k different from zero. Thus $c_U = 2^{-\frac{2}{3}}$ and it corresponds, using Eq. (3.8), to $D_U = 6$ as expected. The ν critical exponent can be computed in the standard way from the first eigenvalue of the matrix that linearizes the transformation near to the critical fixed point. For the Gaussian FP the solution is exact:

$$\nu = \frac{1}{\sigma} \tag{3.14}$$

while for the non-trivial fixed point it is obtained as an ϵ-expansion, leading to the result:

$$\nu = 3 + 36\epsilon + \left[432 - 27(50 + 55 \cdot 2^{1/3} + 53 \cdot 2^{2/3}) \log 2\right] \epsilon^2 + O(\epsilon^3) \tag{3.15}$$

with $\epsilon = \frac{3}{2}(\sigma - 1/3)$. The exactness of the result has been verified with a different method based on a field theoretical approach. Analysing the coefficient of the $O(\epsilon^2)$ term, that is quite big, we can think that probably the series is non-convergent, thus it is not predictive without the use of some resummation technique. However, looking at the first order in the expansion, in the vicinity of the critical c, the exponent grows lowering c. If higher orders of the series are computed, and a resummation scheme yields to a convergent series for the ν exponent we can say that the spin-glass fixed point beyond mean-field region is qualitatively similar to the Gaussian one, confirming thus a scenario mean-field like. If the series is not convergent, neither after resummation, it means that the ϵ-expansion is not a good instrument, probably due to a different nature of the non-trivial fixed point, for example due to a finite dimension scenario droplet-like.

Chapter 4

A new Renormalization Group scheme

In this chapter, we want to introduce a new RG scheme, that can be applied also to disordered systems. The model that we use is the Hierarchical one. In particular, we have studied three versions of this model: the ferromagnet (FM), where $J_{ij} = 1$; the diluted ferromagnet (DFM), where a random fraction $1-p$ of FM couplings are set to zero; and the SG version, with Gaussian couplings $P(J) \propto e^{-J^2/2}$.

4.1 RSRG for the ferromagnetic version

We describe now in detail how to apply a new RS-RG scheme to the HM. The FM version, that has been solved analytically, is a benchmark for our numerical implementation of this new approach. We want to find the new parameters of the Hamiltonian, the new couplings that make a smaller system equivalent to a bigger one. In particular we want the physics of the two systems to be the same. For this reason we require the value of some chosen observables in the two systems to be the same.

We allow couplings to assume different values at each level: in the original HM all couplings are equal to 1, but we have seen that the RG iteration produces different couplings at different levels. We start from a system with n levels that we want to reduce to an "equivalent" smaller system of $n-1$ levels.

1. First we compute $(n-1)$ observables $\langle O_k \rangle$ in the larger system.

2. Then we identify the values of couplings in the smaller system by requiring that $\langle O_k \rangle = \langle O'_{k-1} \rangle$ for any $k \in \{1, 2, ..., (n-1)\}$.

3. Finally we join two smaller systems with couplings of the original intensity, to obtain again a system of the original size.

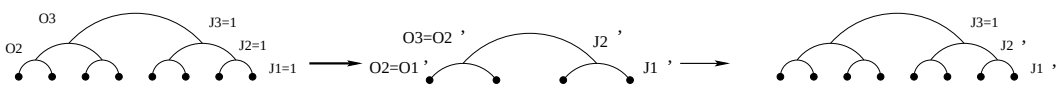

Figure 4.1. The three steps of the renormalization procedure

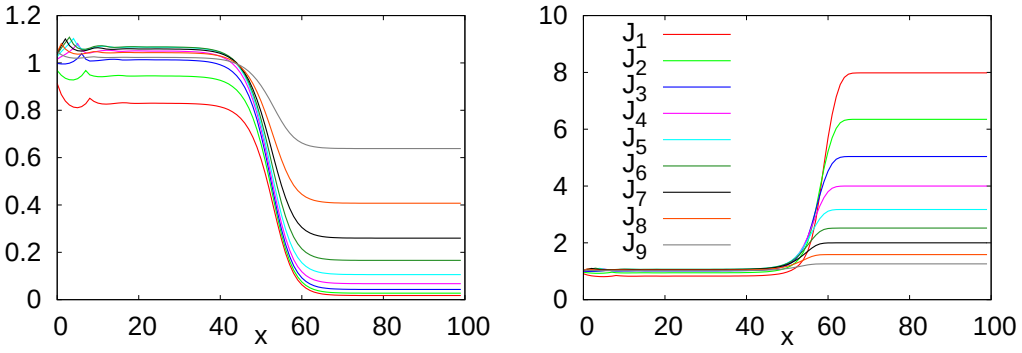

Figure 4.2. Renormalized couplings J' in a FM system with $n = 10$ levels versus the number of RG steps, for temperatures slightly bigger (left) and smaller (right) than T_c.

In the previous steps, angular brackets are thermal averages with respect to the Gibbs-Boltzmann distribution and primed quantities refer to the smaller system. The first two steps are the true renormalization steps, while the latter is required to obtain a final system size, that will allow us to iterate the method, until convergence. A graphical representation of the three steps is in Fig. 4.1. Thermal averages are computed exactly: this is easy to do in the FM, as explained in Sec. 3.3.1.

The observables O_k that we use in the RG equations are the correlation of the magnetization at level $k+1$, normalized by those at level k, with $k \in \{1, \dots, n-1\}$:

$$\langle O_k \rangle = \frac{\langle m_{L_k} m_{R_k} \rangle}{\langle m_{L_k} m_{L_k} \rangle} \, .$$

m_L and m_R are the magnetization in the left and right sub-systems. The denominator is necessary to reduce finite size effects and to ensure that a solution to the RG equations always exists. This is not true in general for other observables. For example if we use the magnetization as observable it is not possible to find a solution for all the $n-1$ equations at the same time.

Applying the previously described procedure, the flux of couplings and correlations can be followed, see Fig. 4.2. If $T \simeq T_c$, renormalized couplings stay for a while close to the critical fixed point (FP), and then go towards the high temperature (HT) FP if $T > T_c$ or the low temperature (LT) FP if $T < T_c$. We estimate the critical temperature as the temperature dividing the flows towards the two different FP. Please note that the HT and LT fixed points are not characterized by the usual $J = 0$ and $J = \infty$ coupling values: the reason is that in step 3 of our procedure we put new couplings of original intensity. Nonetheless couplings flows clearly differentiate HT and LT behaviors.

In order to extract critical exponents from the RG equations, we focus on the early regime, when the coupling flows leave the critical FP. From the Wilson relation an equation relating renormalized coupling after x RG steps can be obtained:

$$\frac{J(x)}{T} - \frac{1}{T_c} = \left(\frac{1}{T} - \frac{1}{T_c} \right) b^{\frac{x}{\nu}} \, ,$$

where $b = 2^{\frac{1}{D}}$ is the scaling factor in our case. To eliminate the dependence from

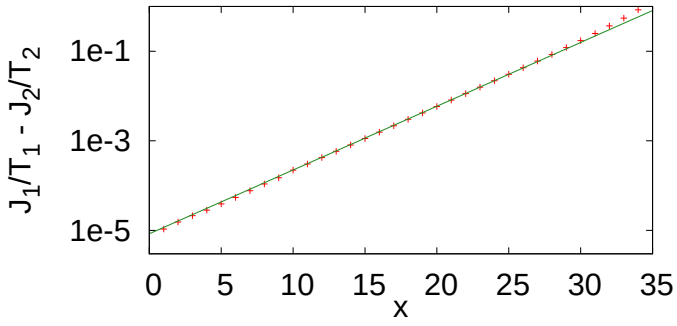

Figure 4.3. Difference between the renormalized couplings at $T_1 = 0.84571$ and $T_2 = 0.845716$ versus the renormalization step in the FM HM with $n = 13$ levels and $c = 2^{-\frac{5}{3}}$. The fit estimates the ν exponent.

the unknown critical temperature, the renormalized couplings at two different temperatures can be compared, leading to a slightly different equation:

$$\frac{J_1(x)}{T_1} - \frac{J_2(x)}{T_2} = \left(\frac{1}{T_1} - \frac{1}{T_2}\right) b^{\frac{x}{\nu}} .$$

Thus, the ν exponent can be estimated from a fit like the one in Fig. 4.3. The values obtained for the critical temperature and the critical exponents for $c = 2^{-\frac{5}{3}}$ (in the non-classical region) are the following: T_c extrapolates to 0.8478(1) in the large n limit and the measured ν exponent is 2.076(6) for $n = 13$ (although the extrapolation of ν to the $n \to \infty$ limit is much harder due to strong finite size effects). They can be compared with those in the literature finding a good agreement: the critical temperature is $T_c = 0.848154717$ [15], and the critical exponents are $\eta = \frac{4}{3}$, $\gamma = 1.299140730159(1)$ [46], leading to $\nu = 1.948711095$ using the scaling relations.

Moreover we have checked that our numerical RG recovers the right bounds on c, namely $T_c \to 0$ for $c \to c_L = 1/4$ and $T_c \to \infty$ for $c \to 1/2$. In particular these limits are recovered for each number of levels n. This happens for the choice of the observables in Eq. (4.1). If we used as observable the magnetization, or the correlation without the normalization, the right bounds on c would be recovered only in the limit $n \to \infty$. Our choice does not suffer of these finite size effects.

4.2 RSRG on disordered HM

When the disorder is introduced, the couplings become independent random variables extracted from a given distribution $P(J)$ and the important observables became those averaged over the disorder. Previous attempts of developing such a real space RG for disordered systems, and in particular on the HM [51], focused on transformations mapping a single sample of size N to a smaller system. In formulae, we can write the mapping $\{J_{ij}\} \to \{J'_{ij}\}$ as the one solving a set of equations like

$$\langle O_k(\{J_{ij}\})\rangle = \langle O'_k(\{J'_{ij}\})\rangle , \tag{4.1}$$

where the number of observables O_k are enough to determine the new couplings $\{J'_{ij}\}$. Given an ensemble of systems of size N, the above transformation can be

applied to each of them in order to obtain an ensemble of systems of size $N/2$. In this way the renormalized distribution of the couplings can be deduced. However we believe that such a mapping is suboptimal for models with quenched disorder and a better RG transformation should consider explicitly the average over the quenched disorder (as was done in Ref. [52]). What we are proposing is a mapping between probability distributions of couplings $P(J_{ij}) \to P'(J'_{ij})$ such that the following equations hold

$$\overline{\langle O_k(\{J_{ij}\})\rangle} = \overline{\langle O'_k(\{J'_{ij}\})\rangle} \,. \tag{4.2}$$

The overbar represents the average over the quenched disorder (i.e. the couplings in the present case). The rationale beyond this choice is that in models with strong disorder (like SG) sample-to-sample fluctuations may dominate thermal ones.

Two simple examples may help elucidating the limits of the RG transformation working sample by sample, Eq.(4.1), and thus justify the use of the one in Eq.(4.2), that we will call Ensemble RG (ERG). In a diluted ferromagnet, where couplings are positive with probability p and null with probability $1-p$, a single step of the decimation procedure induced by Eq.(4.1) typically generates all non-zero couplings (i.e. $p = 1$). And this is clearly not very useful if one is willing to follow the RG flow in the $p-T$ plane. Moreover, in frustrated models the decimated system is typically much less frustrated than the original one if open boundary conditions are present: the extreme case is the transformation of a 4-spins system in a 2-spins system, being the latter unfrustrated for any coupling choice! This tendency to reduce frustration makes the RG using Eq.(4.1) clearly unfit to describe SG fixed points.

In principle, our ERG scheme can be applied to any disordered system, however we choose to apply it to the HM with disorder.

Each coupling distribution is parametrized by $K \in \{1, 2\}$ few numbers (that is the mean for FM, the variance for SG and the fraction of non-zero couplings and the mean for DFM), otherwise the search for a solution to Eq.(4.2) would become too difficult. The renormalization of Section 4.1 revisited for disordered systems is the following:

1. First we compute $(n-1)K$ observables $\overline{\langle O_k\rangle}$ in the larger system.

2. Then we identify the parameters of the renormalized couplings distributions $P'(J'_{ij})$ in the smaller system by requiring that $\overline{\langle O_k\rangle} = \overline{\langle O'_k\rangle}$ for any $k \in \{1, 2, ..., (n-1)K\}$.

3. Finally we construct a new ensemble of systems, building two smaller systems with couplings extracted from the renormalized distribution $P'(J'_{ij})$, and joining them with random couplings extracted from the original distribution, to obtain again an ensemble of systems of the original size.

Again, we allow the parameters of the distribution to be different at each level, but for simplicity we assume couplings at different levels to remain independent during the RG. Correlations between couplings will be considered in a future work.

Thermal averages are again computed exactly. However because the disorder is present, there are no recursive relation to compute them in a fast way. In the DFM and in the SG we do it by exhaustive enumeration, thus limiting us to a

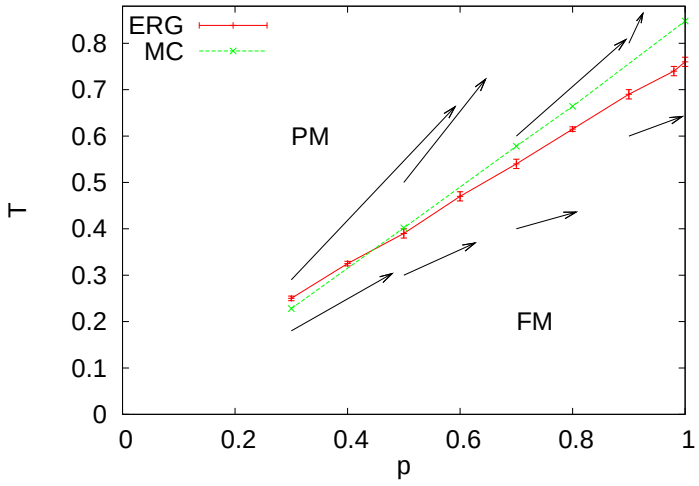

Figure 4.4. Phase diagram in the $p - T$ plane for the $3D$ DFM as obtained by the ERG and by MC simulations. Arrows represent the first iteration of the ERG.

small number of levels. The average over the disorder is not exact, but taken over $\sim 10^5$ samples. Step 2 is actually accomplished by minimizing $\sum_k (\overline{\langle O_k \rangle} - \overline{\langle O'_k \rangle})^2$, and we have checked that the minimum reached is always very close to zero. Since couplings distributions are different at each level, we do not see any better option than extracting the new couplings in step 3 from the original distribution.

4.2.1 RSRG on diluted HM

We consider now the DFM. At our knowledge, nobody has previously introduced and studied this kind of HM. The Hamiltonian of the model is always the one in Eq. (3.3), but the couplings at level k are independent random variables extracted from the distribution

$$P_k(J) = p_k\, \delta(J - J_k) + (1 - p_k)\, \delta(J) \; .$$

At the beginning $p_k = p$ and $J_k = 1$ for any k, while under the RG they will differentiate. The number of parameters to be determined in the ERG is $2(n-1)$, and we use the following observables, with $k \in \{1, \ldots, n-1\}$, to fix them:

$$\overline{\left(\frac{\langle m_{L_k} m_{R_k} \rangle}{\langle \sqrt{m_{L_k}^2 m_{R_k}^2} \rangle} \right)} \quad , \quad \overline{\left(\frac{\langle m_{L_k} m_{R_k} \rangle}{\langle \sqrt{m_{L_k}^2 m_{R_k}^2} \rangle} \right)^2} \; .$$

Applying the same procedure as for the pure model, we are able to draw a flow diagram in the $p - T$ plane for $c = 2^{-\frac{5}{3}}$ (that corresponds to $D = 3$ following Eq. (3.8)) and to determine the critical line dividing the ferromagnetic and the paramagnetic region (see Fig. 4.4). The validity of the phase diagram found with the ERG is confirmed by a set of MC simulations [56] whose T_c estimates are also shown in Fig. 4.4. The differences between the two estimates of T_c are due to finite size effects. In fact, for the ERG we can not go to n bigger than 4, because we

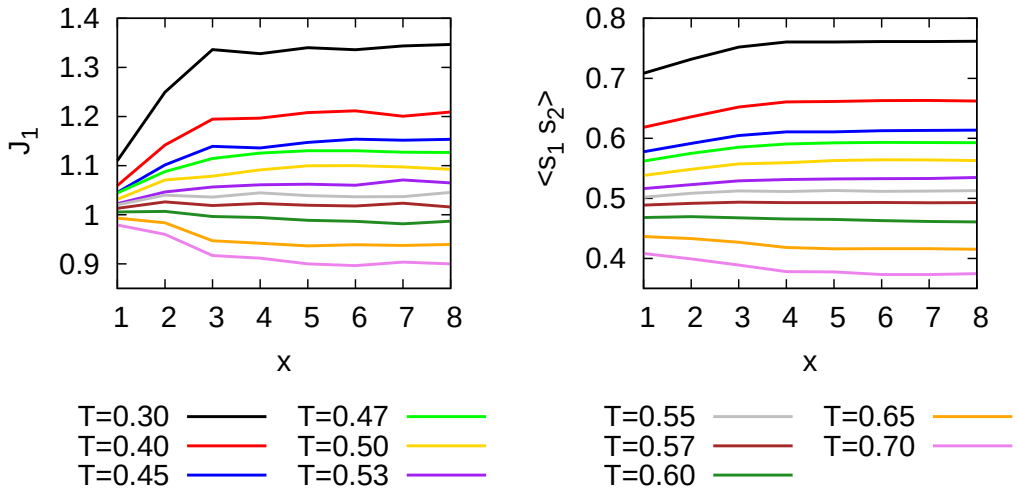

Figure 4.5. Variances of renormalized couplings (left) and of SG correlations (right) at the lower level ($k = 1$) in a SG system with $n = 4$ levels and $D \simeq 3$ versus the number of renormalization steps x, for many temperatures. We locate the critical temperature at $T_{SG} = 0.58(1)$.

compute thermal averages exhaustively. Instead for the MC estimate we analyze systems of sizes up to $n = 10$.

The only disappointment about this phase diagram is that we do not find an unstable FP along the critical line. This fixed point is expected because, for the Harris criterion [54], if the α exponent for the pure model is positive, the introduction of a small amount of disorder will change the universality class of the system. In $D = 3$ SR model, the new fixed point is placed at $p \simeq 0.8$, looking at the point where scaling corrections are smaller [55]. However this can be explained by noticing that the α exponent of this model is very small, $\alpha = 0.051288905$, and so the crossover from the pure behavior can be extremely long.

4.2.2 RSRG on spin-glass HM

Finally we study the SG version. The Hamiltonian is always the one in Eq. (3.3), and the couplings at level k are distributed with a Gaussian law of zero mean and variance σ_k^2 (at the beginning $\sigma_k^2 = 1$ for any k). The assumptions that the renormalized couplings are independent and normally distributed can be released by adding extra terms in the coupling distributions [52], but we leave these generalizations for future works. In the SG case the observables used to fix the $n - 1$ variances are SG correlations at different levels, normalized with the correlations within the two sub-blocks:

$$\overline{\langle O_k \rangle} = \frac{\overline{\sum_{i \in L_k,\, j \in R_k} \langle s_i s_j \rangle^2}}{\sqrt{\sum_{i,j \in L_k} \langle s_i s_j \rangle^2 \sum_{i,j \in R_k} \langle s_i s_j \rangle^2}} \,.$$

Again the normalization is very important. It takes into account the change of frustration changing the size of the system. If we use as observables the non-normalized correlations, no spin glass phase can be found. Indeed we think that the useful

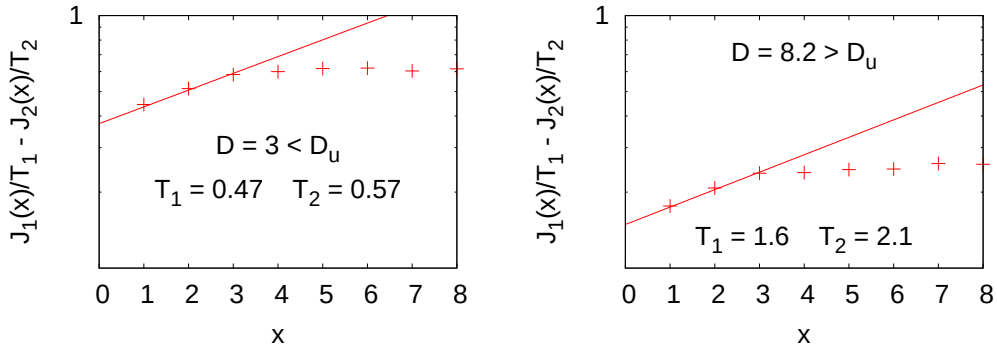

Figure 4.6. Difference between the renormalization flux of the couplings at two different temperatures in a semi-log scale for $D \simeq 3 < D_u$ (left) and $D \simeq 8.22 > D_u$ (right). The first part, not affected by finite size effects, has been used to extract the ν exponent, through a power law fit.

observables are the dimensionless one (like in numerical simulations, where Binder-like observables are used). Because of the computational costs we use $n \leq 4$, so the early regime leaving the critical FP is rather short, and the stationary regime is soon reached (with respect to the FM case). This effect is also enhanced by the disorder: indeed, even exactly at criticality, the SG ensemble contains many samples which are not critical, and the couplings of these samples flow away from critical values very fast. So, it seems unavoidable that disorder increases the instability of critical FP and consequently the uncertainty on the estimates of critical exponents. Nonetheless we can distinguish two temperature regions separated by a critical temperature T_{SG} (see Fig. 4.5 for $c = 2^{-\frac{5}{6}}$ that corresponds to an effective dimension $D \simeq 3$ using Eq. (3.8), with $T_{SG} = 0.58(1)$), such that above T_{SG} correlations and couplings decay towards zero, while below T_{SG} correlations and couplings variances grow, suggesting that the system is in a SG phase. In Fig. 4.5 we have plotted only couplings and correlations variances measured at the lowest level $k = 1$, but (as in the FM, see Fig. 4.2) the renormalized variances at the other levels are related to those at $k = 1$: for example, $\sigma_2 > \sigma_1$ if $T > T_{SG}$ and $\sigma_2 < \sigma_1$ if $T < T_{SG}$ (remember that parameters at the lowest level are those which are less influenced by the choice to put original couplings at the highest level, and for this reason they are more free to grow or to lower under renormalization). Also in the SG case we are able to estimate the ν exponent from the flux of the couplings at early times. The procedure used is the same of that in the FM case and typical fits are shown in Fig. 4.6 for $c = 0.65$ ($D \simeq 8.22$) in the mean-field region and for $c = 2^{-\frac{5}{6}}$ ($D \simeq 3$) below the upper critical dimension. We obtain $\nu = 4.34(6)$ in $c = 2^{-\frac{5}{6}}$ and $\nu = 4.15(10)$ for $c = 0.65$. The mean field value is known analytically from Eq. (3.14) ($\nu_T(0.65) = 4.11562$), in good agreement with our result.

4.3 Algorithmic implementation

To implement the renormalization procedure previously described, we have written a C code, we report here the pseudo code.

Define $P(J)$ with variances $\sigma_i = 1$, $i = 1, ..., n$
for $x = 1, ..., steps$ **do**
  $O_j = 0$ $j = 1, ..., K(n-1)$
  for $i = 1, ..., N$ **do**
    create a random sample with n levels from $P(J)$
    for $j = 1, ..., n-1$ **do**
      $O_j +=$ exact thermal average of the j-th observable of this sample
    end for
  end for
  while the minimum is not found **do**
    change $\{\sigma'\}$ following the Nelder-Mead method
    Initialize $P'(J)$ with $\{\sigma'\}$
    $O'_j = 0$, $j = 1, ..., n-1$
    for $i = 1, ..., N$ **do**
      create a random sample with $n-1$ levels from $P'(J)$
      for $j = 1, ..., n-1$ **do**
        $O'_j +=$ exact thermal average of the j-th observable of this sample
      end for
    end for
    calculate the function to minimize $f = \sum_k (\overline{\langle O_k \rangle} - \overline{\langle O'_k \rangle})^2$
    verify if it is at the minimum
  end while
  Print correlations and variances of the x-th step
  Redefine $P(J)$ with $\sigma_i = \sigma'_i$, $i = 1, ..., n-1$ and $\sigma_n = 1$
end for

To search for the minimum, the Nelder-Mead downhill simplex method has been used, with the support of the Gnu Scientific Libraries. The algorithm stops when the gradient of the function is smaller than the threshold 10^{-7}.

4.4 Comparison with earlier results

In Fig. 4.7 we report the estimates of ν for several effective dimensions D: we see that in the mean-field region results are compatible with linear behavior $\nu = D/2$ that is obtained using Eq. (3.14) and Eq. (3.8). More interestingly, the critical exponent ν have a minimum around the upper critical dimension $D_u = 6$. This minimum was not observed in previous RG studies [51], while it is present in SR models, although nobody has never highlighted it until now: in Fig. 4.7 we report the νD estimates for the EA model in $D = 4$ as found from numerical simulations [13] and in $D = 5$ as found from high temperature expansion series [57] (We did not succeed to find numerical estimates in the literature). The EA values of the exponents are close to the ERG estimates for the hierarchical model. The same cusp-like behavior for the ν exponent has been also seen numerically in a $1D$ SG

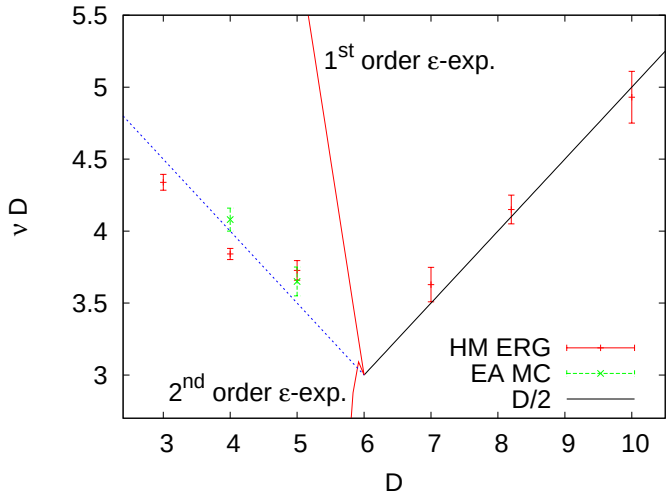

Figure 4.7. The estimation of the ν exponent from the ERG at different effective dimensions D. The line for $D \geq 6$ is the MF prediction, while the one for $D < 6$ is just a guide for the eyes. Also results from the ε-expansion and νD values for the EA model in $D = 4, 5$ are added for comparison.

model with power law decaying interactions [59]. The relation between the critical exponents in hierarchical model, SR models and power law long range models will be studied deeply in the second part of this work.

In Fig. 4.7 we have added also the ϵ-expansion of Eq. (3.15) [50]. As can be seen, the first order term makes a cusp at the upper critical dimension. The second order term is in the opposite direction, however the coefficient is great, thus probably the series is non convergent and needs a resummation to be predictive. This work solves an apparent inconsistency problem between the ϵ - expansion and the other real space RG approach recently proposed in Ref.[51], where the νD exponent was found to decrease linearly with D, with no minimum at all around the upper critical dimension. In this work we have shown that such a minimum in νD, predicted by the ϵ-expansion and present in all the other SG models, exists if a better RG transformation is used.

4.5 Comparison with Monte Carlo results

For the diluted ferromagnetic version there are no previous results in the literature since the model has been introduced in this Thesis. For the SG version of the HM, results of Monte Carlo simulations in Ref. [49], but they refers to a slightly different model, a diluted version of the one analyzed in this work (for details see Sec. 5.3). However we expect it to be in the same universality class. For $c = 2^{-0.707}$, in the non-classical region the authors of Ref. [49] measure $\nu = 3.09$, confirming the non monotonic behaviour of ν at the upper critical c.

In order to check critical temperatures and the critical exponent ν in the non-mean-field region, we have run MC simulations for the fully connected SG version of the HM at different values of c, for couplings extracted from a Gaussian and

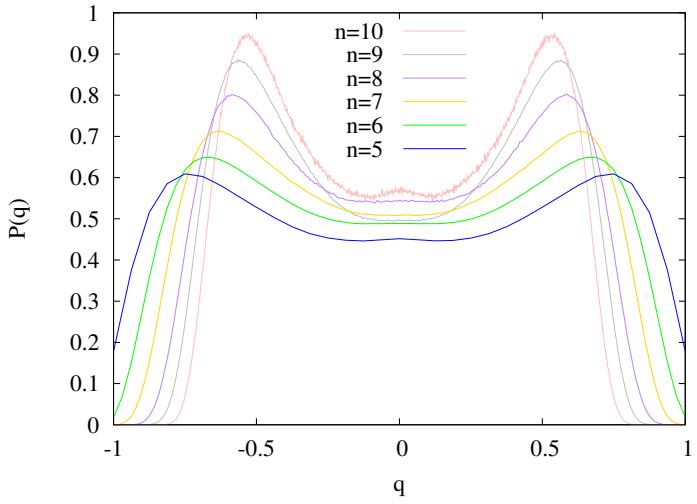

Figure 4.8. Overlap distribution $P(q)$ for different sizes 2^n of a SG HM with $c = 2^{-\frac{5}{6}}$ (in the non mean field region) and a Gaussian distribution of the couplings at $T = 0.43 < T_c$

from a binary $\pm J$ distributions. We have used the parallel tempering algorithm [58], running simultaneously at 20 different temperatures. Two replicas have been simulated in parallel, to measure the overlap distribution $P(q)$ between them. We have checked the equilibration dividing the first measurements into bins with a logarithmically growing size, and we have assumed that the system has reached the equilibrium when the average of the energy and of the second moment of the overlap are the same in two neighbouring bins within the error. We have found that the equilibration time is $\tau \simeq 10^5 - 10^6$ MC steps for the largest sizes at smaller temperatures and we have acquired data for $5 \cdot \tau$ MC steps. For the model with Gaussian couplings we have used $n = 6, 7, 8, 9, 10$, while for the one with $\pm J$ couplings, that is easier to simulate, $n = 6, 7, 8, 9, 10, 11$. Averages were performed over 400 samples for the larger systems up to 2000 samples for the smaller ones.

First of all we have verified that below the critical temperature determined with the ERG method the system is in a SG phase. In Fig. 4.8 the overlap distribution $P(q)$ for different sizes 2^n is plotted for a HM with $c = 2^{-\frac{5}{6}}$ (in the non mean field region) and a Gaussian distribution of the couplings at a temperature $T = 0.43$ (for this system the ERG method gives $T_c = 0.58(1)$). It has the typical shape of systems with RSB. In fact it has a finite support, with two symmetric peaks and it is different from zero at $q \simeq 0$. From Fig. 4.8 it seems that data for $n = 10$ are still too noisy and we have to increase the number of samples.

To verify the exactness of the critical temperatures extracted from the ERG method we look at some scale-invariant observables that have the property to cross at different sizes $L = 2^n$ at the critical temperature as explained in Appendix A. In particular we analyze the dimensionless Binder parameter $B = \frac{1}{2}\left[3 - \frac{\overline{\langle q^4 \rangle}}{\overline{\langle q^2 \rangle}^2}\right]$. We can construct also another scale-invariant observable from the SG susceptibility $\chi_{SG} = q_2 L$ [1] because we know analytically its dimension $2-\eta$. Thus if we divide χ_{SG}

[1] with q_k we indicate the k-th moment $\overline{\langle q^k \rangle}$

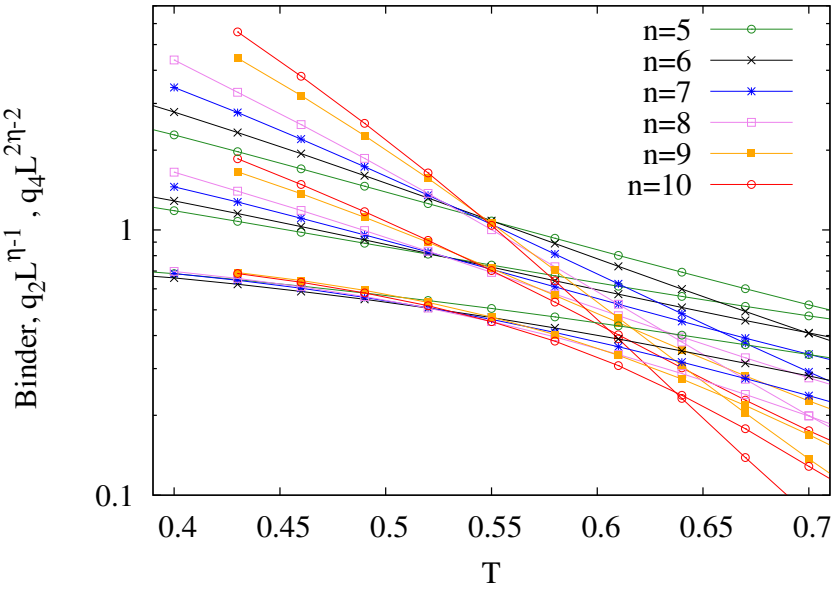

Figure 4.9. Scale-invariant observables, B, $q_2L^{-1+\eta}$ and $q_4L^{-2+2\eta}$ for different sizes $L = 2^n$ as a function of the temperature for a HM with $c = 2^{-\frac{5}{6}}$ and a Gaussian distribution of the couplings. The crossing points locate the critical temperature $T_c = 0.55(1)$

by its dimension the result $q_2L^{-1+\eta}$ should remain finite at the critical temperature. We can apply the same argument to the fourth moment susceptibility, obtaining another scale-invariant observable $q_4L^{-2+2\eta}$.

In Fig. 4.9, we plot the three scale-invariant observables, B, $q_2L^{-1+\eta}$ and $q_4L^{-2+2\eta}$ for different sizes $L = 2^n$ as a function of the temperature for a HM with $c = 2^{-\frac{5}{6}}$ and a Gaussian distribution of the couplings. The crosses of the curves should approach the critical temperature that we estimate to be $T_c = 0.55(1)$. The data are not so accurate to permit the estimate of the correction to scaling effects and to measure the critical exponent ω. However we can see that the Binder parameter is the observable that has greater finite size effects. The critical temperature can be compared with the one obtained from the ERG $T_c = 0.58(1)$. The two estimates are in good agreement, considering that the one from ERG is obtained with a small number of levels $n = 4$. However the ERG estimate has been obtained in a time much much faster.

To measure the critical exponent ν we have used the more accurate data for the model with $\pm J$ interactions. However, despite critical temperatures can be different for models with Gaussian and $\pm J$ interactions (they are non-universal quantities), the critical exponents should be the same, because the two models are in the same universality class. We use the same observables previously described to determine the critical temperature that we estimate $T_c = 0.545(10)$ for $c = 2^{-\frac{5}{6}}$. Then we look at the values of $d(q_2L^{-1+\eta})/dT$ at this critical temperature. The dimension of this observable is $1/\nu$ and its finite size scaling form at leading order around T_c is described by the Eq.:

$$d(q_2L^{-1+\eta})/dT = L^{1/\nu}F(L^{1/\nu}(T - T_c)).$$

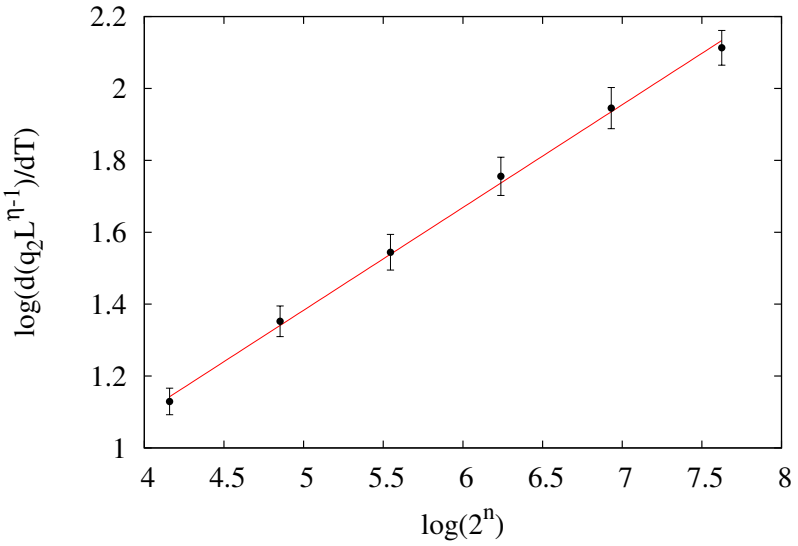

Figure 4.10. $d(q_2 L^{-1+\eta})/dT$ at $T_c = 0.545$ for different sizes as a function of the size of the system in a log-log scale. The straight line is the best fit to extract the exponent ν. The system has $\pm J$ interactions and $c = 2^{-\frac{5}{6}}$.

In Fig. 4.10 the values for $d(q_2 L^{-1+\eta})/dT$ at $T_c = 0.545$ for different sizes are plotted as a function of the size of the system in a log-log scale. We have chosen this particular observable because we have seen that it has the smallest finite size effects. In this scale $1/\nu$ can be extracted via a linear fit as the angular coefficient. The straight line is the best fit that leads to $\nu = 3.50 \pm 0.02$. This result should be compared with the ERG estimate $\nu = 4.34(6)$. They are different. However we know that for the estimate of ν exponent with the ERG method we have very large finite size effects (we have them already for the ferromagnetic case). Nevertheless the important thing is that the non monotonic behaviour of ν with c is confirmed.

In Fig. 4.11 we have plotted the three scale-invariant observables B, $q_2 L^{-1+\eta}$ and $q_4 L^{-2+2\eta}$ for different sizes as a function of $L^{1/\nu}(T - T_c)$, with $\nu = 3.5$ and $T_c = 0.545$. We can see that curves at different sizes collapse quite well.

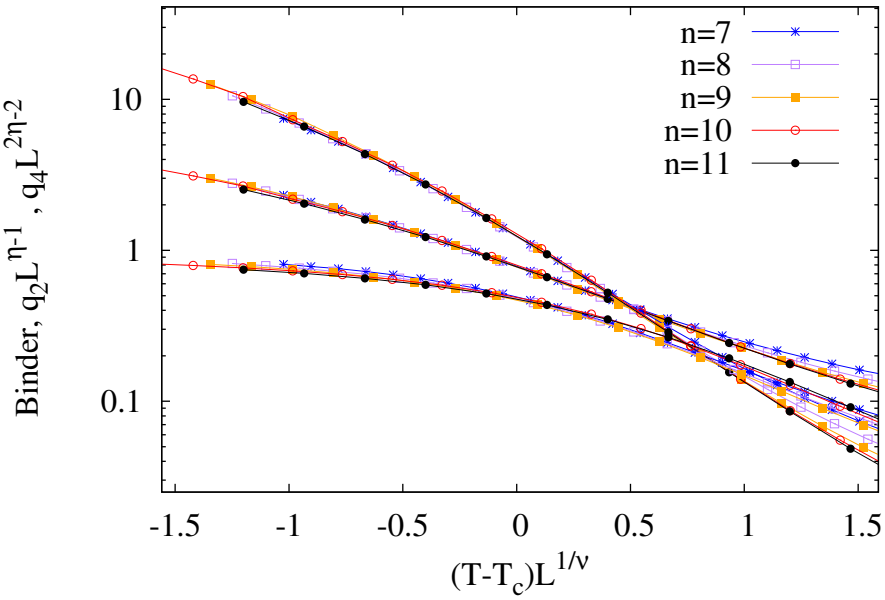

Figure 4.11. B, $q_2 L^{-1+\eta}$ and $q_4 L^{-2+2\eta}$ for different sizes as a function of $L^{1/\nu}(T - T_c)$. Curves at different sizes collapse quite well. The system has $\pm J$ interactions and $c = 2^{-\frac{5}{6}}$.

Part II

Relations between Short Range and Long Range models

Chapter 5

Basic concepts

5.1 Long-Range models

It is known for a long time that ferromagnetic systems of discrete spins with a finite range of interaction have a lower critical dimension $D = 1$. It means that a uni-dimensional chain of spins can not undergo a phase transition [60]. However one can also define long-range (LR) models [14] in d dimensions. They are fully connected models, with an Hamiltonian:

$$H = -\frac{1}{2}\sum_{i,j=1}^{N} J_{ij}\sigma_i\sigma_j. \tag{5.1}$$

The range of interactions is infinite and the intensity of the coupling J_{ij} decays as a power law with a certain distance of the spins: $J_{ij} \propto |r_{ij}|^{-(d+\sigma)}$. One can also define spin glasses on LR models, taking J_{ij} as independent identically distributed random variables, extracted from a distribution $P(J)$ (like for example a binary or Gaussian distribution), requiring that the variance of $P(J)$ decays as a power law: $\overline{J_{ij}^2} \propto |r_{ij}|^{-(d+\sigma)}$ [61]. These models can have a transition at dimensions smaller than the lower critical one for usual short range (SR) models. Indeed a ferromagnetic LR model can have a transition also in $d = 1$ as we have seen in Part I. Furthermore, varying σ, the behaviour of the system (such as for example the critical exponents) can vary from a mean field to a non mean field one until it reaches a certain value σ_L and the behaviour of the corresponding SR system is recovered. In fact one can write down a relation between σ and the effective dimension D of an equivalent SR model. At σ_L, the effective dimension D reduces to the real dimension d of the LR system. The behaviour in and out the range of validity of mean field approximation can thus be observed varying only a parameter, and this is very useful if one wants to simulate the system numerically because the complexity of the model does not change with the effective dimension. Different LR models have been introduced, and they have been studied by many people with many different methods. Moreover, more than one relation $\sigma - D$ exists. However, no-one has clarified the differences between various LR models, the exactness of the $\sigma - D$ relations and their limits. In Part I we have analyzed one particular LR model (the hierarchical model) and we have compared the results of our renormalization group method with SR models exponents. However we have not specified whether this operation was really justified. The purpose of this Part is to summarize the previous works on LR models, and to

answer some crucial questions on how good are LR models to simulate SR models, which is the best $\sigma - D$ relation, what is its range of validity and how similar are different LR models.

5.2 Algorithms: single spin flip versus cluster algorithms

The long range models are fully connected models, thus every spin interacts with all the others $N-1$ spins. If we want to simulate a LR model with a standard single spin flip Monte Carlo method, for every update of a single spin, we have to calculate its energy difference and it costs $O(N)$ operations. A single update of the whole system costs $O(N^2)$ operations.

However a version of the cluster algorithm proposed by Wolff in Ref. [91] has been generalized to FM fully connected models in Ref. [92], allowing to reduce the computational cost of a single Monte Carlo step to $O(N)$. The cluster methods are Monte Carlo algorithms that permit to overcome (or to reduce) the problem of the critical slowing down in ferromagnetic models around the critical temperature. In the following we will consider always Ising spins taking values $\sigma = \pm 1$. Firstly a spin σ_i is chosen randomly, then the cluster is expanding by adding the neighbors σ_j having the same sign, each with a probability

$$p_j = 1 - e^{-2\beta J_{ij}}. \tag{5.2}$$

The procedure is repeated trying to add in the cluster all the neighbors of the spins that are already in the cluster with the same rules as before. When no more spins can be added, the whole cluster is flipped. The choice of the probability in Eq. (5.2) assures that the detailed balance is satisfied with an acceptance rate of the flipping of the cluster that is always equal to 1. Near the critical temperature, when the correlation between spins grows, the size of the constructed cluster grows too, and this permits to reduce the critical slowing down. Unfortunately, when this algorithm is used in fully-connected models, it requires $O(N^2)$ steps, because every spin has N neighbors. In Ref. [92], the use of cumulative probability distribution for adding a neighbor at distance r from the spin in analysis allows to check all the neighbors of a given spin with the correct probability with $O(1)$ operations (as long as $T \neq 0$). The probability that the first spin to be included in the cluster is the j-th from the original one is:

$$P(j) = p_j(1 - p_{j-1})...(1 - p_1). \tag{5.3}$$

Now we define the *cumulative bond probability* as:

$$C(j) = \sum_{n=1}^{j} P(n). \tag{5.4}$$

At this point we extract a random number r uniformly in $[0, 1]$: if $C(j-1) < r \leq C(j)$, then the first spin included in the cluster is the j-th. The condition on the spin being parallel to those in the cluster is checked after the selection. If the selected spin is antiparallel to those in the cluster, it is not added. After the first step, we want to include in the cluster spins at distance $k > j$. Eq. (5.3) is generalized as

$$P_j(k) = p_k(1 - p_{k-1})...(1 - p_{j+1}) \tag{5.5}$$

and it leads to a cumulative bond probability:

$$C_j(k) = \sum_{n=j+1}^{k} P_j(n). \tag{5.6}$$

When Eq. (5.2) is inserted in the previous one, it simplifies to:

$$C_j(k) = 1 - \exp\left(\sum_{n=j+1}^{k} -2\beta J_n\right), \tag{5.7}$$

where J_n is the coupling between spins at distance n. A new random number is extracted and a new spin is selected. Spins are added in this way until the maximum distance $N/2$ is reached. Then we try to add neighbors starting from all the other spins already inserted in the cluster in the same way. Naturally in this procedure we have to take into account that there are more than one spin at distance k (especially in dimensions higher than 1), and we must ensure that every spin is counted with the right probability.

Given $C_j(k)$ two are the possibilities to calculate the distance k. The first one is to construct a look-up table. In fact the cumulative probability is calculated only at the beginning and it is the same for all the spins, because the system is homogeneous. Moreover only $C(j)$ has to be calculated. In fact $C_j(k)$ can be derived from it as:

$$C_j(k) = \frac{C(k) - C(j)}{1 - C(j)}.$$

Once the random number is extracted, we search in the look-up table to determine k. This operation has a cost $O(\log(N))$. However the advantage of this method is that it is exact.

The second possibility is to approximate the interaction $J_{ij} = |i-j|^{-(\sigma+d)}$ into a continuous form:

$$J_{ij} = \int_{|i-j|-\frac{1}{2}}^{|i-j|+\frac{1}{2}} x^{-(d+\sigma)} dx. \tag{5.8}$$

With this definition, Eq. (5.7) becomes:

$$C_j(k) = 1 - \exp\left(-2\beta \int_{j-\frac{1}{2}}^{k+\frac{1}{2}} x^{-(d+\sigma)} dx\right). \tag{5.9}$$

The integral is exactly soluble, thus we can solve the equation $C_j(k) = r$, where r is the extracted random number and we can calculate k directly. This method is fast, and not expensive in terms of computational memory, however it is approximated. It differs from the original version by terms that are powers higher than $\sigma + d$. For this reason the choice of the approximated version should not imply changes in the universality class of the model. If the memory cost of the look-up table is too high, for example when large sizes in dimensions higher than 1 are studied, one can choose also to use the look-up tables at small distances and to approximate the couplings for distances greater than a cut-off, because the differences between the approximated and the original couplings decay very fast with the distance. With this cluster algorithm the computational cost is $O(N)$, and it allows to study larger sizes.

5.3 Dense versus sparse LR models

Unfortunately, the cluster algorithm can not be used when the system is not homogeneous, namely when $C_j(k)$ is not the same for all the spins. This includes the case in which the disorder is present. In fact we can not memorize a different look-up table for each spin, and if the couplings are random the integral in Eq. (5.9) is no more soluble. However the problem of the $O(N^2)$ time of simulations for SG LR models was overcome in Ref. [59] with the introduction of a diluted version of LR models.

In the new version the quenched random couplings J_{ij} are again independent and identically distributed random variables, but they take a non zero value with a probability decaying with the distance between spins σ_i and σ_j as $P(J_{ij} \neq 0) \propto |r_{ij}|^{-(d+\sigma)}$.

Non-zero couplings take values from a $P(J)$, that is for example a Gaussian with zero mean and unit variance. An average coordination number z is introduced. Authors of Ref. [59] use $z = 6$. The universality class depends on the value of the exponent σ, and for $\sigma > 0$ it turns out to be equal to the one of the fully connected version of the model previously introduced, where bonds are Gaussian-distributed with zero mean and a variance depending on the distance as $\overline{J_{ij}^2} \propto |r_{ij}|^{-(d+\sigma)}$. For $-d \leq \sigma < 0$ the model behaves like a SG on a Bethe lattice [62][63], that is perfectly recovered when $\sigma = -d$, at variance with the fully connected version that is ill-defined for any $\sigma < 0$ because the energy is no longer extensive.

The diluteness of the model permits to simulate larger sizes and to limit the strong finite size effects that are the strongest problem to the numerical analysis of LR SG models.

Even if in principle the diluted version can be applied to every LR model, it has been introduced only for models with quenched disorder. No one has used it for the FM LR model, because for homogeneous model there are ways to reduce the computational complexity without changing the model, like the algorithm explained in the previous section.

Chapter 6

Known results on LR models

6.1 Analytical and numerical results for ferromagnetic models

The simplest LR model that can undergo a paramagnetic/ferromagnetic phase transition is a one-dimensional chain of spins that has the Hamiltonian in Eq. 5.1 with $J_{ij} \propto \frac{1}{|i-j|^{1+\sigma}}$. For this model, Dyson demonstrated analytically that there is a standard second order phase transition if $0 < \sigma < 1$ [14]. For $\sigma \leq 0$ the energy is no longer an extensive quantity.

This model can be easily generalized to d dimensions, redefining the couplings as $J_{ij} \propto \frac{1}{|r_{ij}|^{d+\sigma}}$ where r_{ij} is the euclidean distance $r_{ij} = \sqrt{\sum_{x=1}^{d} |(r_x)_i - (r_x)_j|^2}$.

6.1.1 ϵ-expansion for LR models

The FM version of this model has been analyzed using a renormalization group approach in Ref. [45] and we review here the most important results of this work. The field theory in the momentum space (for n-dimensional spins) can be written as:

$$\int dx \mathcal{L}(\phi) = \sum_k u_2(k)\phi(k)\phi(-k) + u \sum_{k_1 k_2 k_3} \phi(k_1)\phi(k_2)\phi(k_3)\phi(-k_1 - k_2 - k_3) \tag{6.1}$$

where $u_2(k) = r + j_\sigma k^\sigma + j_2 k^2$, and the parameter r varies linearly with the temperature as usual. If $\sigma > 2$, the leading term in $u_2(k)$ is the k^2 one, then the usual short range behaviour in d dimensions is recovered.

When $\sigma < 2$, the leading term in $u_2(k)$ is the k^σ one, the k^2 term can be ignored and a new behaviour is present. In this latter case, supposing u to be small, in differential form the renormalization-group equations for r and u to leading order are

$$\frac{dr}{dl} = \sigma r + (n+2)\frac{u}{j+r} \qquad \frac{du}{dl} = \epsilon u - (n+8)\frac{u^2}{(j+r)^2}$$

where j depends on j_σ and we have defined the parameter $\epsilon = 2\sigma - d$.

The Gaussian fixed point $u^* = r^* = 0$ is stable if $\epsilon < 0$. The critical exponents are easily calculated, leading to $\nu = 1/\sigma$, $\eta = 2 - \sigma$, $\gamma = 1$. At $\epsilon = 0$, this fixed

point is marginally stable and logarithmic behaviour appears for the correlation length and susceptibility. This point corresponds to the upper critical exponent $\sigma_U = \frac{d}{2}$. For $\epsilon > 0$ the Gaussian fixed point is unstable with respect to u and a new fixed point $u^* = O(\epsilon)$ is found. The critical exponents can be obtained as a series expansion in ϵ:

$$\frac{1}{\gamma} = 1 - \frac{n+2}{n+8}\frac{\epsilon}{\sigma} + O(\epsilon^2)$$

The second order term has been calculated too [45]. η is found to be not renormalized up to third order in ϵ and it is commonly believed that it will have the mean-field value at all orders because under renormalization new $k^\sigma \phi(k)\phi(-k)$ terms are not generated. This has been also verified numerically with good accuracy in Ref. [64].

6.1.2 Problems at the lower critical σ

The picture that emerges from the work of Ref. [45] is very simple and intuitive: for $0 < \sigma < \sigma_U = \frac{d}{2}$ the system is in a mean-field region, for $\frac{d}{2} = \sigma_U < \sigma < \sigma_L = 2$ the exponents are different from the mean field ones and change continuously with σ, for $\sigma > \sigma_L = 2$ the SR behaviour is recovered. However there are some debated points. For example from this ϵ expansion, the lower critical exponent is $\sigma_L = 2$, for all the dimensions [1]. However in $d = 1$, at $\sigma = 1$ the transition becomes of the Kosterlitz-Thouless (KT) type [66], characterized by a discontinuous jump of the order parameter at the critical temperature T_c and by a correlation length that diverges exponentially approaching T_c and remains infinite below T_c. The KT transition picture is supported by analytical [67] [68] evidences. This is a very curious thing: the one-dimensional LR model was the first model in which a KT transition was supposed, even if this kind of transition became famous only after that it was found in the two dimensional XY short range model. Numerical evidences of this kind of transition [69] were found only after decades, when the new cluster algorithm of Sec. 5.2 was developed.

In Ref. [65] the ϵ-expansion for the one-dimensional model has been performed around the lower critical exponent $\sigma_L = 1$. The lowest order expansion leads to

$$\nu = \frac{1}{\sqrt{2\,(1-\sigma)}} \tag{6.2}$$

for the Ising model that has $n = 1$. The behaviour is qualitatively different if $n > 1$. For $\sigma > 1$ the transition disappears.

The problem of the inconsistency of the results of [45] near $\sigma = 2$ is not related only to the one-dimensional case. In fact, according to the picture of Ref. [45], $\eta = 2 - \sigma$ for $\sigma < 2$ and $\eta = \eta_{SR}$, for $\sigma > 2$. This would imply a jump discontinuity in η at $\sigma = 2$, and a non-monotonic behaviour in σ. While this phenomenon is not forbidden by thermodynamic arguments (which only require $\eta \leq 2 + \sigma$), it has attracted considerable attention over the past decades, because it is quite singular.

[1] In SR systems the lower critical dimension is the dimension at which there exists no more a phase transition. In LR models, we call as lower critical exponent the value of σ for which the SR behaviour is recovered. If the SR model has a transition in d dimensions, thus there is a transition also for $\sigma > \sigma_L$, while if the SR model does not have a transition in d dimensions, there is no transition for $\sigma > \sigma_L$

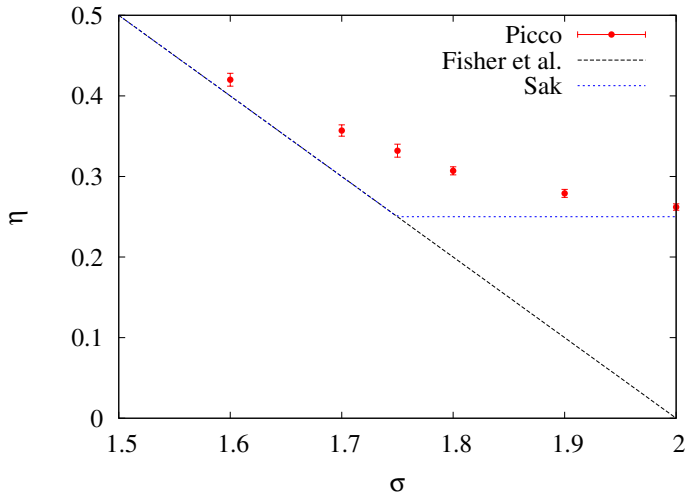

Figure 6.1. Behaviour of $\eta(\sigma)$ as proposed in different works: in the work of Fisher et al. of Ref. [45], $\eta = 2-\sigma$ up to $\sigma = 2$, in the work of Sak of Ref. [71] $\eta = \max(2-\sigma, \eta_{SR} = \frac{1}{4})$, in the data of Picco of Ref. [18] η seems to interpolate smoothly between $2-\sigma$ and $\eta_{SR} = \frac{1}{4}$.

In Ref. [71] a different scenario was proposed. In fact, if the term $j_2 k^2$ is not ignored in Eq. (6.1) when $\sigma < 2$, as done in Ref. [45], it can be seen that the non-trivial fixed point is characterized by $j_2^* = O(\epsilon^2) \neq 0$. Even if one starts with $j_2 = 0$, SR forces appear after the renormalization, determining the critical behaviour. As a consequence, for $d < 4$ the boundary between the intermediate and the SR regime was found to shift from $\sigma_L = 2$ to $\sigma_L = 2 - \eta_{SR}$. In particular, for $\sigma < 2 - \eta_{SR}$, the introduction of $j_2 \neq 0$ does not change the critical exponents, that remain those of Ref. [45]. When $\sigma > 2 - \eta_{SR}$, all the exponents become the SR ones, without discontinuity, and without loosing the monotonicity in σ. In fact in this regime the fixed point is characterized by $j_\sigma^* = 0$, and the field theory is the usual SR one.

In support to this picture, in a field-theoretic approach, Honkonen and Nalimov [72] proved, to all orders in perturbation theory, the stability of the SR fixed point for $\sigma > 2 - \eta_{SR}$ and of the LR one for $\sigma < 2 - \eta_{SR}$. Within this new scenario, the theory is also consistent with the exact results for the one-dimensional case. In fact, for $d = 1$, $\eta_{SR} = 1$. In this way the lower critical exponent is $\sigma = 1$, as expected. However, the analysis of [71] has also been the subject of criticism: in Ref. [73] the results for $n \geq 2$ are contested, in Ref. [74] the absence of the kink at $\sigma = 2 - \eta_{SR}$ is hypothesized, in Ref. [75] the picture of Ref. [45] is supported. All this works on the subject are related to the importance to understand how to treat systems in presence of different, competing fixed points.

There are also numerical studies. In Ref. [64] a Monte Carlo study of a LR model in $d = 2$, using cluster algorithms, supports the scenario of Ref. [71] where $\eta = \max(2-\sigma, \eta_{SR} = \frac{1}{4})$, excluding definitively the picture of Ref. [45]. In particular they affirm to find logarithmic corrections to scaling at $\sigma = 1.75$, clear indication of a crossover between different critical points. Very recently, in Ref. [18] the same study has been improved. In fact, the measurement of η for a LR system in $d = 2$ has been repeated, close to the region where its behavior is changing, i.e. for

$\sigma \simeq 2 - \eta_{SR}$, obtaining more precise results. The author confirms that there is no discontinuity but a clear deviation from the behavior predicted by Sak in Ref. [71] is measured. In particular in the intermediate regime up to $\sigma \simeq 1.5$ the results are in agreement with the prediction $\eta = \eta_{LR} = 2 - \sigma$. For $\sigma > 2$, η is in perfect agreement with the value for a SR model. In the remaining part for $1.6 \leq \sigma \leq 2$ the results do not agree with the prediction of the RG analysis [45][71]. On the contrary, η seems to interpolate smoothly between these two behaviors. Moreover logarithmic corrections are not found in this region. The results in Ref. [64] are compatible with those in Ref. [18], due to the larger error bars. Concluding, the scenario at lower critical exponent is far to be clear. The three proposed behaviours are summarized in Fig. 6.1.

6.1.3 Comparison between Hierarchical and Long Range models

The hierarchical model [14] (see [15] for a review) is a particular one-dimensional LR model, in which the Hamiltonian of 2^n spins can be constructed iteratively, as explained in Sec. 3.3.1. The intensity of the interactions decreases with the level by a factor $c = 2^{-(\sigma+1)}$. One expects the model to behave like the usual LR one, with the same exponent σ, because the decaying at large scales of the coupling intensity is the same. Indeed the model undergoes a standard second order phase transition if $2^{-1} > c > 2^{-2}$ [14] (i.e. $0 < \sigma < 1$). For $2^{-1} > c > c_U = 2^{-3/2}$ (i.e. $0 < \sigma < \sigma_U = 1/2$), the Gaussian solution of the field theory associated to this model is the stable one and the critical exponents are the mean-field ones as for usual LR systems. Again, for $2^{-3/2} > c > c_L = 2^{-2}$ (i.e. $1/2 < \sigma < \sigma_L = 1$) the exponents differ from the classical ones, but nobody has checked if and how much they differ from the LR ones. The first order term in the ϵ-expansion of the two models is the same, while the second order one differs slightly, the coefficients being 4.445 for the HM and 4.368 for the LR model [88].

One crucial difference between the two models is that for the borderline case $\sigma_L = 1$ there is no KT phase-transition for the HM. Indeed in the HM all the interactions are weaker than in the usual LR model. For this reason if the HM has a transition, it implies that the LR model has a transition too, but the vice-versa is not necessarily true. However there is a KT phase transition in the HM for $\sigma = 1$ if interactions at level n, $J_n = 2^{-2n}$, are made slightly stronger: $J_n = 2^{-2n}\log(n)$ [70].

6.2 Analytical and numerical results for SG models

In this section, we review the most important works on disordered SG LR models, following the previous line of FM LR models.

6.2.1 ϵ-expansion for LR SG models

The SG LR model is a d dimensional model that has the Hamiltonian (5.1) with couplings extracted from a probability distribution with zero mean and variance $\overline{J_{ij}^2} \propto |r_{ij}|^{-(d+\sigma)}$. It has been introduced and analyzed using a renormalization group approach in Ref. [61]. The field theory in the momentum space (for n-dimensional spins) can be written as:

$$\int dx\mathcal{L}(\phi) = \sum_k u_2(k)Q^{ab}(k)Q^{ab}(-k) + u\sum_{k_1k_2}\sum_{abc} Q^{ab}(k_1)Q^{bc}(k_2)Q^{ca}(-k_1-k_2) \tag{6.3}$$

where Q is the replica field, a, b, c, are replica indices, $u_2(k) = r + j_\sigma k^\sigma + j_2 k^2$, and the parameter r varies linearly with the temperature as usual. If $\sigma > \sigma_L = 2$, one can think naively that the leading term for $u_2(k)$ is the k^2 one, then the usual short range behaviour in d dimensions is recovered. However, as for the FM case, this is not really true, see next Section. When $\sigma < \sigma_L$, the leading term for $u_2(k)$ is the k^σ one, the k^2 term can be ignored and a new behaviour is present.

Supposing u to be small, the renormalization-group equations for r and u can be written. Defining the parameter $\epsilon = 3\sigma - d$, the Gaussian fixed point $u^* = r^* = 0$ is found to be stable if $\epsilon < 0$. This defines the upper critical exponent as $\sigma_U = \frac{d}{3}$. The mean field critical exponents are easily calculated, leading to $\nu = 1/\sigma$, $\eta = 2 - \sigma$ in the region $0 < \sigma < \sigma_U = \frac{d}{3}$. For $\epsilon > 0$ the Gaussian fixed point is unstable with respect to u and a new fixed point $u^* = O(\epsilon)$ is found. The critical exponents can be obtained as a series expansion in ϵ: $\nu = \frac{3}{d-2\epsilon}$. As in the FM case, η is found to be not renormalized. This has been verified numerically with good accuracy in Ref. [59] using the diluted version of LR models introduced in Sec. 5.3. Because of strong finite size effects, this check failed in previous works [76].

6.2.2 Problems at the lower critical σ

While ferromagnetic models have an exponent $\eta_{SR} > 0$, models described by a cubic field theory, like SG, have in general $\eta_{SR} < 0$. For these systems, some works [77] [78] predict that the LR fixed point is the important one as long as $\sigma < 2$. When $\sigma = 2$, the SR behaviour is restored, inducing a discontinuous jump in the exponent η to its SR value. At difference with FM models, this scenario preserve the monotonicity with σ. However, as in FM case, this scenario is not the correct one in the one-dimensional case, where for $\sigma > 1$ there is no transition. For $\sigma = 1$ in Ref. [61] a KT transition is supposed, as in the FM version. Alternatively a simple $T = 0$ transition can be present. However there are no numerical studies in support of one of this pictures. Like in the FM case, more recent papers [79][80] show that also in the case $\eta_{SR} < 0$ the long-range interaction dominates as long as $2 - \sigma = \eta_{LR} > \eta_{SR}$. At $\eta_{LR} = \eta_{SR}$ the exponents change continuously to their SR values that hold everywhere for $\sigma > \sigma_L = 2 - \eta_{SR}$. In the SG case there are no numerical simulation to confirm predictions due to the fact that one should simulate a LR SG system in $d = 3$ (the lower critical dimension is $d \simeq 2.5$), with a quite big computational effort.

6.3 $\sigma - D$ relations

6.3.1 The different relations

Comparing the field theory of a LR model in one dimension with that of a SR model above its upper critical dimension ($D > D_U$), the relation

$$\sigma = \frac{2}{D} \tag{6.4}$$

can be obtained, in the same way of Sec. 3.3.2. The upper critical dimension for the FM SR model, $D_U = 4$, thus corresponds to the upper critical exponent for the FM LR model $\sigma_U = 1/2$. In the same way, the upper critical dimension for the SG SR model, $D_U = 6$, corresponds to the upper critical exponent for the SG LR model $\sigma_U = 1/3$. Moreover $\sigma = 0$ corresponds to $D = \infty$, as one can expect. However, this relation has a problem. In fact, the exponent for which there is no more a phase transition, $\sigma_L = 1$, will correspond to a lower critical dimension in SR models $D_L = 2$. But we know that the lower critical dimension for a SR model (with discrete degrees of freedom) is $D_L = 1$. This problem can be overcome modifying slightly the matching relation [16]:

$$\sigma = \frac{2 - \eta_{SR}(D)}{D} \tag{6.5}$$

Eq. (6.4) and (6.5) coincide in the mean-field region where $\eta_{SR} = 0$ but differ in the non classical region. In Eq. (6.5) $\sigma = 1$ corresponds to $D_L = 1$, as required. If Eq. (6.5) holds, then one expects that $\gamma_{SR}(D) = \gamma_{LR}(\frac{2-\eta_{SR}(D)}{D})$ if a perfect matching holds between a $d = 1$ LR model with $\sigma = \frac{2-\eta_{SR}(D)}{D}$ and a SR model in D dimensions. As a consequence of Eq. (6.5), using the scaling relation $\nu = \gamma/(2 - \eta)$ and the known value of $\eta_{LR} = 2 - \sigma$ in the region $\sigma < 2 - \eta_{SR}$, the relation for the ν exponent of the correlation length will be:

$$\nu_{SR}(D) = \frac{\gamma_{SR}(D)}{2 - \eta_{SR}(D)} = \frac{1}{D\sigma}\gamma_{LR}(\frac{2 - \eta_{SR}(D)}{D}) = \frac{1}{D}\nu_{LR}(\frac{2 - \eta_{SR}(D)}{D}). \tag{6.6}$$

Another $\sigma - D$ matching formula can be constructed [17] directly imposing that

$$D\nu_{SR}(D) = \nu_{LR}(\sigma) \tag{6.7}$$

One may ask if Eq. (6.5) and (6.7) are equivalent. They are equivalent in the mean-field region, at the lower critical dimension and in the first order of the ϵ-expansion around σ^U.

6.3.2 A more general formulation

Eq. (6.5) and (6.7) can be justified both in a more general formulation [81]. As said in Sec. 2.2.4, the singular part of the free energy density for a system in D dimensions has the scaling form:

$$f_s = \frac{1}{L^D}\Phi(L^{y_t}t, L^{y_h}h, L^{y_u}u),$$

where u is the irrelevant operator that gives the leading corrections to scaling and $y_u = -\omega$. If we suppose that there is a connection between a LR model in one-dimension and a SR model in D dimensions, we can equate the singular part of their free energy densities:

$$\frac{1}{L^D}\Phi_{SR}(L^{y_t^{SR}}t, L^{y_h^{SR}}h, L^{y_u^{SR}}u) = \frac{1}{L}\Phi_{LR}(L^{y_t^{LR}}t, L^{y_h^{LR}}h, L^{y_u^{LR}}u). \tag{6.8}$$

In order to compare the exponents, we want to eliminate the different prefactors, and we can obtain this result writing everything in terms of the total number of spins N, where $N = L^D$ in the SR model and $N = L$ in the LR one. We obtain

$$\frac{1}{N}\Phi_{SR}(N^{y_t^{SR}/D}t, N^{y_h^{SR}/D}h, N^{y_u^{SR}/D}u) = \frac{1}{N}\Phi_{LR}(N^{y_t^{LR}}t, N^{y_h^{LR}}h, N^{y_u^{LR}}u).$$

Thus the connection between the exponents is

$$y^{LR}(\sigma) = \frac{y^{SR}(D)}{D}.$$

If we recall the relations with the critical exponents of Eqs 2.9 and 2.10, the previous equation becomes:

$$\begin{aligned} &\nu_{LR}(\sigma) = D\nu_{SR}(D); \quad 2 - \eta_{LR}(\sigma) = \sigma = \frac{2 - \eta_{SR}(D)}{D}; \\ &\gamma_{LR}(\sigma) = \gamma_{SR}(D); \quad \omega_{LR}(\sigma) = \frac{\omega_{SR}(D)}{D}. \end{aligned} \tag{6.9}$$

The first relation is Eq. (6.7), while, knowing the value for η in LR systems, and substituting it in the second relation leads directly to Eq. (6.5). Thus each relation among the four in Eq. (6.9) defines a $\sigma - D$ correspondence. If Eq. (6.8) holds, then all the four correspondence in Eq. (6.9) are equivalent. If they are not equivalent, it means that the free energy of SR and LR models are not exactly the same.

Please note that the useful aspect of our definitions of the models is that all the $\sigma - D$ relations of this Section are valid both for the FM and the SG versions of the models.

6.3.3 Numerical tests of the σ-D relations

If one want to test the exactness of the equivalence between a D-dimensional SR model and a one-dimensional LR model, one has to simulate a LR system at a value of σ that corresponds to D following for example Eq. (6.5), and verify if there is the correspondence between all the exponents as in Eq. (6.9). For the FM there is not a systematic study of the correspondence, while, only during the writing of this Thesis, this has been analyzed for SG in Ref. [81] for $D = 3$ and $D = 4$, using the diluted LR version. In $D = 4$ the authors measure $\eta_{SR}(4) = -0.320(13)$ that corresponds to $\sigma = 0.58$. For this value $\nu_{LR}(0.58) = 4.41(19)$ is measured, to be compared with $4{\cdot}\nu_{SR}(4) = 4.272(20)$ and $\omega_{LR}(0.58) = 0.277(8)$ to be compared with $\omega_{SR}(4)/4 = 0.26(4)$. In $D = 3$ the value $\eta_{SR}(3) = -0.375(10)$ has been measured in Ref. [82]. It leads to $\sigma = 0.792$. For this value they measure $\nu_{LR}(0.792) = 8.7(1.9)$ to be compared with $3 \cdot \nu_{SR}(3) = 7.35(45)$ but they can not measure ω, because of the small finite size corrections. In summary, for $D = 4$ the matching between LR and SR model seems very good. For $D = 3$ the data are evenly compatible, however errors are bigger and the answer is not definite. Anyhow it is reasonable that the correspondence between SR and LR models becomes weaker approaching the lower critical dimension. Indeed at the upper critical dimension the field theory is exactly the same, while at the lower critical dimension for the FM model we know that SR and LR models have even qualitatively different behaviours. In fact the SR model has a $T = 0$ transition, while the LR model has a KT transition.

Chapter 7

New results on the connection between LR and SR models

In this Chapter we report our new results on the relation between LR and SR models. We have focused on FM models, where many things are still unclear. The same work on SG systems is left as a very interesting future generalization.

7.1 The one dimensional LR model

We were not able to find estimates of the critical exponents in $d = 1$ for values of σ corresponding to $D = 2$ and $D = 3$ following Eq. (6.5) neither for the power law LR models nor for the HM. For this reason we have done Monte Carlo simulations at these values of σ. Indeed Eq. (6.5) was introduced recently studying SG models, and was never applied to FM, for which the relation (6.4) was often used. Moreover we want to see how similar is the HM with respect to the power law LR model because to our knowledge there is not a systematic study of the differences between these two models.

7.1.1 Details of the simulations

We have simulated the $d = 1$ LR model using the cluster algorithm proposed in Ref. [92] in the version with the look-up table for the cumulative bond probability of a spin to be inserted in the cluster, as explained in Sec. 5.2. We have put periodic boundary conditions, in this way two spins i and j interact with a single coupling that depends on the minimum distance between them: $r_{ij} = \min(|i-j|, L-|i-j|)$, where L is the size of the system. We have performed a Monte Carlo simulation with a number of cluster flips going from $N = 10^6$ for the largest sizes up to $N = 10^7$ for the smallest ones. We have checked the equilibration dividing the first measurements into bins with a logarithmically growing size, and we have assumed that the system has reached the equilibrium when the average of the magnetization of two neighbouring bins is the same within the error. We have found that the equilibration time is $\tau \simeq 10^5$ cluster MC steps for the largest sizes. We want to compute the susceptibility and the Binder parameter, thus we need the second and fourth moments of the magnetization. We have obtained two different estimates of

this quantity. The first is the usual one:

$$m^2 = \langle \left(\frac{1}{N} \sum_i \sigma_i \right)^2 \rangle, \quad m^4 = \langle \left(\frac{1}{N} \sum_i \sigma_i \right)^4 \rangle.$$

The second one uses the *improved estimators* that can be defined when cluster algorithms are used [83]. We can think to the cluster algorithm proposed by Wolff, and here used, in a slightly different way. We try to construct clusters, with the rules explained before, until each spin is in a cluster, like in the Swedsen-Wang algorithm [84]. The number of clusters will be N_C. Then we choose a spin randomly and we flip the cluster of the chosen spin. The probability to choose a certain cluster will be proportional to its size $|C|$: $P_C = \frac{|C|}{N}$. The average size of the cluster flipped in the Wolff algorithm is thus $\langle |C| \rangle = \langle \sum_{x=1}^{N_C} \frac{|C_x|}{N} |C_x| \rangle$. Using this relation we can write the squared magnetization as:

$$m^2 = \frac{1}{N^2} \langle \sum_{i,j} \sigma_i \sigma_j \rangle = \frac{1}{N^2} \langle \sum_{i,j} \sum_{x=1}^{N_C} \delta_{i,j}(C_x) \rangle = \frac{1}{N} \langle \sum_{x=1}^{N_C} \frac{|C_x|}{N} |C_x| \rangle = \frac{1}{N} \langle |C| \rangle \tag{7.1}$$

The function $\delta_{i,j}(C)$ is 1 if the two spins σ_i and σ_j are in the same cluster C, otherwise it is 0. The first passage is justified by the fact that in a cluster algorithm, two spins are correlated only if they are in the same cluster.

In an analogous way we can derive the relation between the fourth moment and the cluster sizes:

$$\begin{aligned} m^4 =& \frac{1}{N^4} \langle \sum_{i,j,k,l} \sigma_i \sigma_j \sigma_k \sigma_l \rangle = \frac{1}{N^4} \langle \sum_{i,j,k,l} \left(\sum_{x=1}^{N_C} \delta_{i,j,k,l}(C_x) + 3 \sum_{\substack{x,y=1 \\ x \neq y}}^{N_C} \delta_{i,j}(C_x) \delta_{k,l}(C_y) \right) \rangle = \\ =& \frac{1}{N^4} \langle \sum_{i,j,k,l} \left(3 \sum_{x,y=1}^{N_C} \delta_{i,j}(C_x) \delta_{k,l}(C_y) - 2 \sum_{x=1}^{N_C} \delta_{i,j,k,l}(C_x) \right) \rangle = \\ =& \langle \frac{3}{N^2} \sum_{x,y=1}^{N_C} \frac{|C_x|^2 |C_y|^2}{N^2} - \frac{2}{N^3} \sum_{x=1}^{N_C} \frac{|C_x|^4}{N} \rangle = \frac{3}{N^2} \langle |C||C'| \rangle - \frac{2}{N^3} \langle |C|^3 \rangle. \end{aligned} \tag{7.2}$$

Operatively, we compute $\langle |C||C'| \rangle$ in the following way: we choose randomly a spin and, starting from it, we construct a cluster. We call $|C|$ the number of spins of this first cluster. Then we choose a second spin randomly. If it is in the constructed cluster, we put $|C'| = |C|$. If it is not in the cluster, we construct a new cluster starting from it, and we call the new cluster size $|C'|$. C and C' are disjoint (i.e. non overlapping). Please note that we can not compute the average $\langle |C||C'| \rangle$ simply as $\langle |C|^2 \rangle$ because in this way we do not take into account the condition $|C| + |C'| \leq N$.

Eq. (7.1) has been already introduced [83], while we believe Eq. (7.2) is new.

The improved estimators have been introduced because they have a reduced variance with respect to the usual estimators. In fact the average is performed using the observable $\delta_{i,j}(C)$ that takes values 0 or 1, at difference with the usual method that uses the observable $\sigma_i \sigma_j$, that assumes values -1 and 1. However, the measure of $\delta_{i,j}(C)$ can be more correlated with respect to the measure of $\sigma_i \sigma_j$.

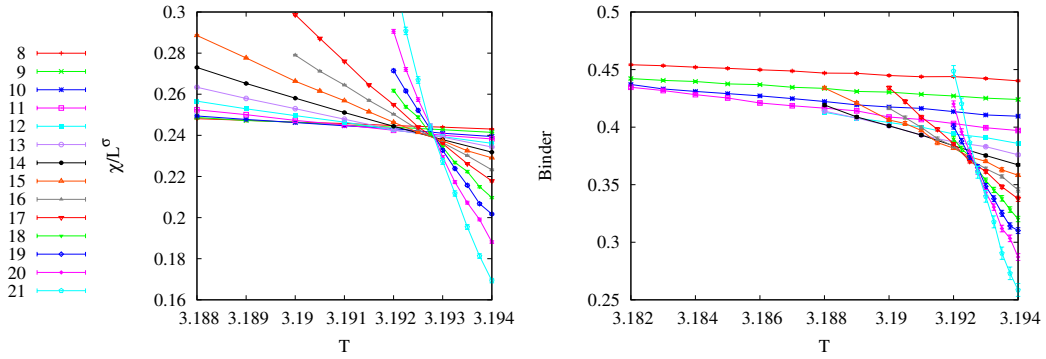

Figure 7.1. Scale invariant observable χ_L/L^σ (left) and Binder cumulant (right), computed at different $n = \log_2 L$, as a function of the temperature T, at $\sigma = 0.654533$. The curves at different sizes should cross at a temperature that approaches T_c when L grows.

For this reason, it is not obvious that the final error is smaller for the improved estimators, especially when bigger clusters are present [85]. This can be the case of the LR model, where we expect clusters to be bigger with respect to the usual SR one.

We have computed the susceptibility and the Binder parameter and their error with the jackknife method separately for the two methods. The error for the cluster method is slightly bigger than that for the usual spin method. At the end we have taken the weighted average between the two values. In this way we are conscious that we are underestimating a little the error because the two measures are correlated but we assume them to be uncorrelated when we perform the weighted average.

7.1.2 Determination of the critical exponents

We have used this method to simulate a one-dimensional LR model with values of σ corresponding to $D = 2$ and $D = 3$. In $D = 2$ we know exactly the exponent $\eta = \frac{1}{4}$ and it corresponds to $\sigma = \frac{2-1/4}{2} = 0.875$. In $D = 3$, $\eta = 0.0364(5)$ as found in Ref. [87] and it corresponds to $\sigma = \frac{2-0.0364}{3} = 0.65453$. We have computed the critical exponents ν and ω using the Finite Size Scaling (FSS) analysis explained in Appendix A. Here we look in detail at the case with $\sigma = 0.65453$, but the analysis is the same for all the other systems (except for some special ones that will be mentioned specifically).

A great advantage of LR models is that the η exponent is not renormalized in the non-classical region as explained before. Thus we know its analytical expression: $\eta = 2 - \sigma$. For this reason we can compute the susceptibility $\chi = \frac{N}{T}\langle m^2 \rangle$ and we can construct a scale-invariant quantity just dividing it by its dimension: χ_L/L^σ. Another quantity that we look at is the dimensionless Binder parameter: $B = \frac{1}{2}[3 - \frac{\langle m^4 \rangle}{\langle m^2 \rangle^2}]$. Both observables should cross at T_c for large sizes.

In Fig. 7.1 the two observables χ_L/L^σ and B_L are plotted as a function of the temperature, around the critical temperature T_c, for different sizes $L = 2^n$ of the systems. We have extracted the temperatures T_L^* of the crossing of χ_L/L^σ for sizes

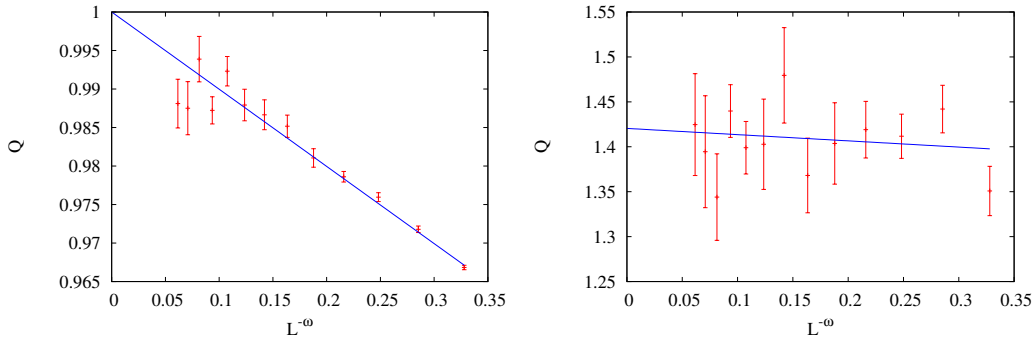

Figure 7.2. Left: quotient of the Binder parameter for L and $2L$ at T_L^*, computed at the crossing temperature of χ_L/L^σ. The straight line is the best fit using Eq. (A.6) with ω left as a free parameter. Right: quotient of the derivative of the Binder parameter at T_L^*. The straight line is the best fit as a function of $L^{-\omega}$ using Eq. (A.7), with ω determined from the previous fit and the intercept $2^{1/\nu}$ left as a free parameter.

$L = 2^n$ and $L' = 2L = 2^{n+1}$. They should approach the critical point following Eq. (A.4). We have computed the values of the Binder parameter $B(L, T_L^*)$ and the quotient $Q = \frac{B(2L,T_L^*)}{B(L,T_L^*)}$ at the previously extracted temperatures T_L^*. Q should behave as in Eq. (A.6). Thus we have performed a log-log linear fit with ω left as a free parameter. The results are shown in the left side of Fig. 7.2. Once we have determined ω, we extract the derivative of the Binder parameter at T_L^*, $B'(L, T_L^*)$, as the angular coefficient of the straight line passing through the data. We compute the quotient $Q = \frac{B'(2L,T_L^*)}{B'(L,T_L^*)}$ that should follow Eq. (A.7), with $s^{x_D/\nu}$ that in this case is simply $2^{1/\nu}$. Thus, using the value of ω previously determined and performing a linear fit as a function of $L^{-\omega}$, we extract the value of ν from the intercept. The results are shown in the right panel of Fig. 7.2. At this point, fitting with a line the values of T_L^* as a function of $L^{-\omega-1/\nu}$, with the previously determined ω and ν, we can extract T_c as the intercept, using Eq. (A.4), as shown in Fig. 7.3.

7.1.3 Results for the 1d LR models

The results in $d = 1$ for $\sigma = 0.875$ corresponding to $D = 2$ and $\sigma = 0.654533$ corresponding to $D = 3$ are the following:

$$\frac{1}{\nu_{LR}(0.875)} = 0.4124(13), \quad T_c(1.875) = 2.10589(1)$$

$$\frac{1}{\nu_{LR}(0.65453)} = 0.506(14), \quad \omega_{LR}(0.65453) = 0.201(11), \quad T_c(0.65453) = 3.19289(2).$$

For $\sigma = 0.875$ it is quite impossible to determine ω because we see very little evolution of T_L^* with L and the quotient of the Binder parameter is nearly independent of the size.

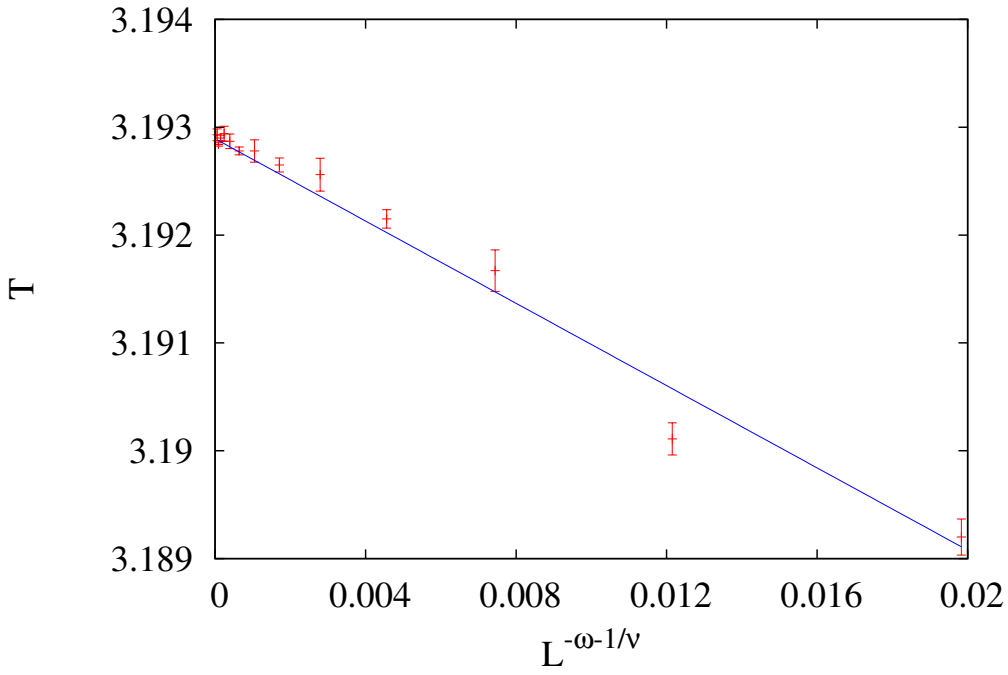

Figure 7.3. T_L^* determined as the crossing temperature of χ_L/L^σ for L and $2L$ as a function of $L^{-\omega-1/\nu}$, where ω and ν have been determined as in Fig. 7.2. The straight line is the best fit using Eq. (A.4), leaving the intercept T_c as a free parameter.

For the hierarchical model, we performed the same analysis. The only difference is that we computed the Binder parameter and the susceptibility exactly using Eq. (3.3.1). The results are:

$$\frac{1}{\nu_{HM}(0.875)} = 0.3841 \pm 0.0009, \quad \omega_{HM}(0.875) = 0.462 \pm 0.003$$
$$\frac{1}{\nu_{HM}(0.65453)} = 0.5186 \pm 0.0072, \quad \omega_{HM}(0.65453) = 0.212 \pm 0.005.$$

Naturally for the HM, many other methods can be used to obtain more precise results. However, for the exponent ω only an estimate is available [94]

$$\omega_{HM}(2/3) = 0.2185787,$$

consistent with our results. The values for the ω exponents of LR and HM for $\sigma = 0.65453$ are in perfect agreement. If we compare them with the SR values [87]

$$\omega_{SR}(D = 3) = 0.84(4), \quad \omega_{SR}(D = 2) = 2$$

and remembering the supposed relation between them, $\omega_{SR}(D) = D\omega_{LR}(\sigma)$, it seems that LR models have bigger finite size effects (smaller ω) than SR models. Thus, looking at the ω exponent, Eq. (6.9) in not satisfied, especially for $D = 2$.

In Fig. 7.4 $1/\nu$ is plotted as a function of the parameter σ in the non mean-field region, for the HM model as found in Ref. [88], and for the LR one-dimensional

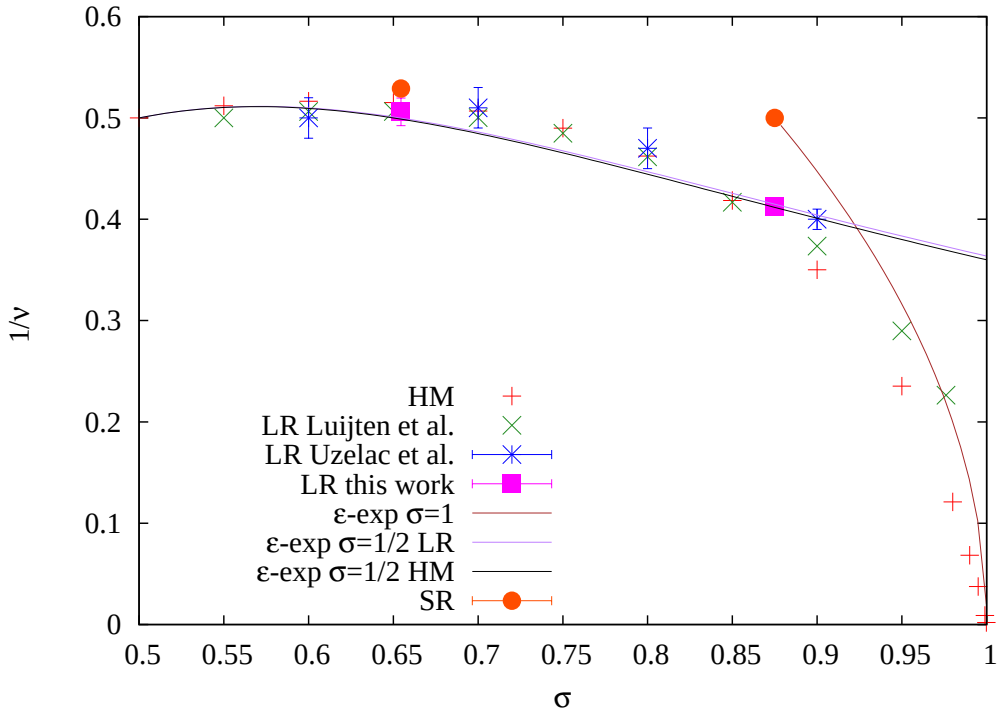

Figure 7.4. $1/\nu$ as a function of the exponent σ as found in various works and in this work for the HM and LR model in $d = 1$. The SR values follow the matching formula 6.5.

model, from Ref. [89] and [90]. For the LR model, our results for $D = 2$ and $D = 3$ are reported too. From Fig. 7.4 it is clear that the two analyzed one-dimensional models (HM and the LR one) are not in the same universality class. While their critical exponents are quite similar near to the upper critical $\sigma_U = 1/2$, the differences grow approaching the lower critical $\sigma_L = 1$. This is reasonable, because we know that the two models have very different behaviours at $\sigma_L = 1$. We have reported also the ϵ-expansion at the second order around $\sigma_U = 1/2$ of the two models. They are indeed very similar. Moreover we have added the ϵ expansion of the LR model around $\sigma_L = 1$ as in Eq. (6.2).

To verify the exactness of Eq. (6.6), in Fig. 7.4 the values of the exponent of the SR model are placed at the correspondent value of σ as in Eq. (6.5): in $D = 2$, $\nu_{SR}(2) = 1$ is placed at the correspondent $\sigma = 0.875$, for $D = 3$ the point at $\nu_{SR}(3) = 0.6301(4)$ [87] corresponds to $\sigma = 0.65453$. Eq. (6.6) is a good approximation near to the upper critical dimension (it is good for $D = 3$) but it is no more good for $D = 2$. Remembering also the results for the ω exponent, we can assert that it is not possible to find a single value of σ that verifies the equivalence for all the critical exponents as in Eq. (6.9).

7.2 In more than one dimension

7.2.1 Generalization of the $\sigma - D$ relations

How can we generalize the $\sigma - D$ relations of Sec. 6.3 if the LR model is defined in more than one dimension? Let us first remark the notation: d is the real dimension of the LR model while D is the dimension of an equivalent SR model. If we use the same arguments of the one-dimensional case in Sec. 6.3.2 for the scaling form of the free energy, the relation

$$\frac{\sigma}{d} = \frac{2 - \eta_{SR}(D)}{D} \tag{7.3}$$

is obtained.

However Eq. (7.3) can be also obtained from another way. In fact one can think that an approximate super-universality exists. The conjecture is that the exponent $\gamma_{LR}(d, \sigma)$ and other quantities are approximately functions only of $\hat{\sigma} = \sigma/d$. This conjecture is exact in all the mean-field region. In fact, $\gamma_{LR} = 1$ in the same region $0 < \hat{\sigma} < \frac{1}{2}$, independently on d. The SR model is recovered when $\sigma = \sigma_L(d) = 2 - \eta_{SR}(D = d)$ [64] [71]. If now we use this information, we obtain that $\gamma_{SR}(D) = \gamma_{LR}(\hat{\sigma} = \frac{2-\eta_{SR}}{D}) = \gamma_{LR}(\frac{\sigma}{d})$. Thus the new relation between a LR model in d dimensions and an effective SR model in D dimensions is Eq. (7.3). In this way we have connected two problems: the determination of the $\sigma - D$ relation and the threshold σ_L where the SR behaviour is recovered. These problems are often viewed as disconnected, however we think that they are closely connected.

Please note that the value of σ_L is not universal: $\sigma_L(1) = 1, \sigma_L(2) = \frac{7}{4}$ [86], $\sigma_L(3) = 2 - 0.0364 = 1.9636$ [87], $\sigma_L(4) = 2$. In the same way, $\hat{\sigma} = \hat{\sigma}_L$ is not universal: $\hat{\sigma}_L(1) = 1$, $\hat{\sigma}_L(2) = 0.875$, $\hat{\sigma}_L(3) = 0.65453$, $\hat{\sigma}_L(4) = 0.5$. For the exponent of the correlation length, using the scaling relation $\nu = \gamma/(2 - \eta)$, the known value of $\eta = 2 - \sigma$ in the LR region and Eq. (7.3), one obtains:

$$\nu_{SR}(D) = \frac{\gamma_{SR}(D)}{2 - \eta_{SR}(D)} = \frac{d}{D\sigma}\gamma_{LR}(\frac{2 - \eta_{SR}(D)}{D}) = \frac{d}{D}\nu_{LR}(\frac{2 - \eta_{SR}(D)}{D}) \tag{7.4}$$

In analogy with Eq. (6.9), one can thus suppose that there exists a value of σ that satisfies all the following relations for the critical exponents:

$$\begin{aligned} &\nu_{LR}(\sigma) = \frac{D}{d}\nu_{SR}(D); \quad 2 - \eta_{LR}(\sigma) = \frac{d}{D}\left(2 - \eta_{SR}(D)\right); \\ &\gamma_{LR}(\sigma) = \gamma_{SR}(D); \quad \omega_{LR}(\sigma) = \frac{d}{D}\omega_{SR}(D). \end{aligned} \tag{7.5}$$

Please note that the two dimensions enter only with their ratio.

7.2.2 Simulations in $d = 2$

Unfortunately there were not previous estimates for the ν exponent for the LR model in more than one dimension, only during the writing of this Thesis in Ref. [18] the value $\nu_{LR} = 0.96(2)$ for $\sigma = 1.6$ in $d = 2$ was reported, extracted from a Monte Carlo simulation. For this reason we have also done simulations in $d = 2$ to extract the exponents at values of $\sigma = 1.20, 1.60$ and in particular at $\sigma = 1.30906$ that corresponds to $D = 3$ and $\sigma = 1.75$ where the SR behaviour in $D = 2$ should be

recovered. For $\sigma = 1.2$ and $\sigma = 1.30906$, the simulations have been performed with the same cluster algorithm and the same analysis method as for $d = 1$, described in Sec. 7.1.1 and 7.1.2. The obtained values for the $\nu_{LR}(\sigma)$ and $\omega_{LR}(\sigma)$ exponents and for the critical temperatures are:

$$\frac{1}{\nu_{LR}(1.2)} = 1.024(34), \quad \omega_{LR}(1.2) = 0.480(25), \quad T_c(1.2) = 6.83427(1),$$

$$\frac{1}{\nu_{LR}(1.30906)} = 1.014(33), \quad \omega_{LR}(1.30906) = 0.32(15), \quad T_c(1.30906) = 6.32546(4).$$

The value of ν_{LR} at $\sigma = 1.30906$ is compatible with the one for the $D = 3$ SR model $\nu_{SR} = 0.6301(4)$ [87] following Eq. (7.5). The value of ω_{LR} at $\sigma = 1.30906$ is very difficult to extrapolate because there are strange non-monotonic finite size effects.

For $\sigma = 1.6$ and $\sigma = 1.75$ the finite size effects seem too strong. In fact the "apparent" critical temperature at which the Binder at different sizes cross changes very quickly, and it is not possible to extract the critical Binder value $B(\infty, T_c)$. For this reason we choose to use a slightly different model, that does not consider only the minimum image but also all the others:

$$J_{ij} = \sum_{x=-\infty}^{\infty} \sum_{y=-\infty}^{\infty} \left((x_i - x_j + Lx)^2 + (y_i - y_j + Ly)^2 \right)^{-(d+\sigma)/2}$$

as done in Ref. [64]. In the thermodynamic limit the two models are the same. In Ref. [64] they can compute the contribution of all the images exactly because they use the couplings defined with the integral of Eq. (5.8). Instead we use the exact definition of the couplings, thus in principle it is not possible to include all the images exactly. To overcome this problem, we estimate the error that we commit including only the first $4a$ images in the coupling between two points at distance 0:

$$\int_{\substack{|x|>a \\ |y|>a}} \mathrm{d}x\mathrm{d}y \left((Lx)^2 + (Ly)^2 \right)^{-(2+\sigma)/2} < 2\pi L^{-(2+\sigma)} \int_a^{\infty} \mathrm{d}r r^{-(1+\sigma)},$$

and we impose that it is smaller than 10^{-9}, in this way we obtain a. At this point we compute the new coupling between two spins as the sum of the couplings between the $4a$ images. We have replaced the sum over the images with an integral, and we have changed the integration bound from a square to a circle. This is not a problem because we simply overestimate the computed error. Due to the large values of σ, the number of images considered is always small. If it results to be smaller than 10, we put always $a = 10$. Adding the images, the observables show a reduced dependence from the size, and the analysis is easier.

We have not used the dimensionless quantity $\chi_L/L^{2-\eta}$ because there is not agreement on the values of η in this region. For this reason we have performed the following analysis. We have looked at the temperatures T_L^* at which the Binder parameters for L and $2L$ cross each other. They scale again with Eq. (A.4). Then we have fitted the values of $B(L; T_L^*)$ with a power law function of the type in Eq. (A.5), determining ω. For $\sigma = 1.75$, assuming that the Binder parameter at the critical point should recover the SR value, we have used the value of the Binder parameter $B_\infty(T_c) = 0.91588...$ [97] in the fit to reduce the uncertainty in the determination of ω. At this point we have computed the quotient of the derivative

of the Binder parameter at T_L^* and extracted the exponent ν. Knowing ν and ω, we have extracted T_c.

The obtained results are the following:

$$\frac{1}{\nu_{LR}(1.6)} = 0.996(33), \quad \omega_{LR}(1.6) = 0.130(45), \quad T_c(1.6) = 5.29321(4),$$

$$\frac{1}{\nu_{LR}(1.75)} = 0.98(10), \quad \omega_{LR}(1.75) = 0.213(8), \quad T_c(1.75) = 4.89455(17).$$

We do not see logarithmic corrections, as said in Ref. [64]. The value of ω_{LR} at $\sigma = 1.75$ is much smaller than that for a SR model in $D = 2$, an explanation will be given in the next section. The value for $\nu_{LR}(1.75)$ is compatible with the SR one.

7.2.3 Near to the lower critical σ

In addition to the verification of the $\sigma - D$ relations, we have concentrated our attention to the problems arising when approaching the value of σ where the SR behaviour is recovered. In particular we want to verify if the scenario of Ref. [71] holds, with $\eta = \max(2 - \sigma, \eta_{SR} = \frac{1}{4})$, or if, for $1.6 \leq \sigma \leq 2$, η interpolates smoothly between $2 - \sigma$ and η_{SR} as stated in Ref. [18]. Firstly we want to stress that if the second scenario holds, the superuniversality conjecture can not be verified in the region near to $\sigma_L(d)$ where the η exponent interpolates smoothly between the two behaviours. Instead superuniversality is compatible with the first scenario.

We have tried to measure η in $d = 2$ approaching $\sigma = 1.75$. We have performed a MC simulation in $\sigma = 1.6$ and $\sigma = 1.75$, on systems with a single image. We have looked at the two points correlation at the critical point that decays as $G(x) = \langle\sigma(0)\sigma(x)\rangle = |x|^{-(d-2+\eta)} = |x|^{-\eta}$. If we identify the spin variables with the two indices i and j of the positions in the x and y direction, we have measured

$$G(x) = \frac{1}{N^2} \sum_{i,j} \left(\langle \sigma_{i,j}\sigma_{i+x,j} \rangle + \langle \sigma_{i,j}\sigma_{i,j+x} \rangle \right).$$

In Fig. 7.5 we have plotted the spin-spin correlation function for different sizes. As it can be seen, $G(x)$ seems to decay as the sum of two different powers. It decays faster at small distances and slower at large distances. The same feature is not present at smaller σ, near to the upper critical $\sigma = 1$, nor in the SR model in $D = 2$. This is not a finite-size effect because it persists at large sizes.

Despite the large sizes simulated (up to $L = 1536$, $N = 2359296$), it seems that the correlations have still not reached the asymptotic behaviour. This effect makes the extraction of the critical exponent η from the correlation function very difficult in this regime. We have focused the analysis on the larger size in the region where it coincides with the second largest one, that is the region not effected from finite-size effects. We have performed a fit with a function of the type $f(x) = ax^{-\eta} + bx^{-\eta'}$, where $\eta = 2-\sigma$ and a fit with a function $g(x) = ax^{-\eta_P} + bx^{-\eta'}$, where η_P is the value reported by Picco in Ref. [18], $\eta_P(1.6) = 0.42$, $\eta_P(1.75) = 0.332$. η' is left as a free parameter. The results are shown in Fig. 7.6. Both the scenarios are compatible with the data and much larger sizes are needed to exclude one of the two. The values of η' obtained from the fit are $\eta'(1.6) = 0.839(1)$, $\eta'(1.75) = 0.628(1)$ using $f(x)$ and $\eta'(1.6) = 0.932(3)$, $\eta'(1.75) = 0.846(3)$ using $g(x)$.

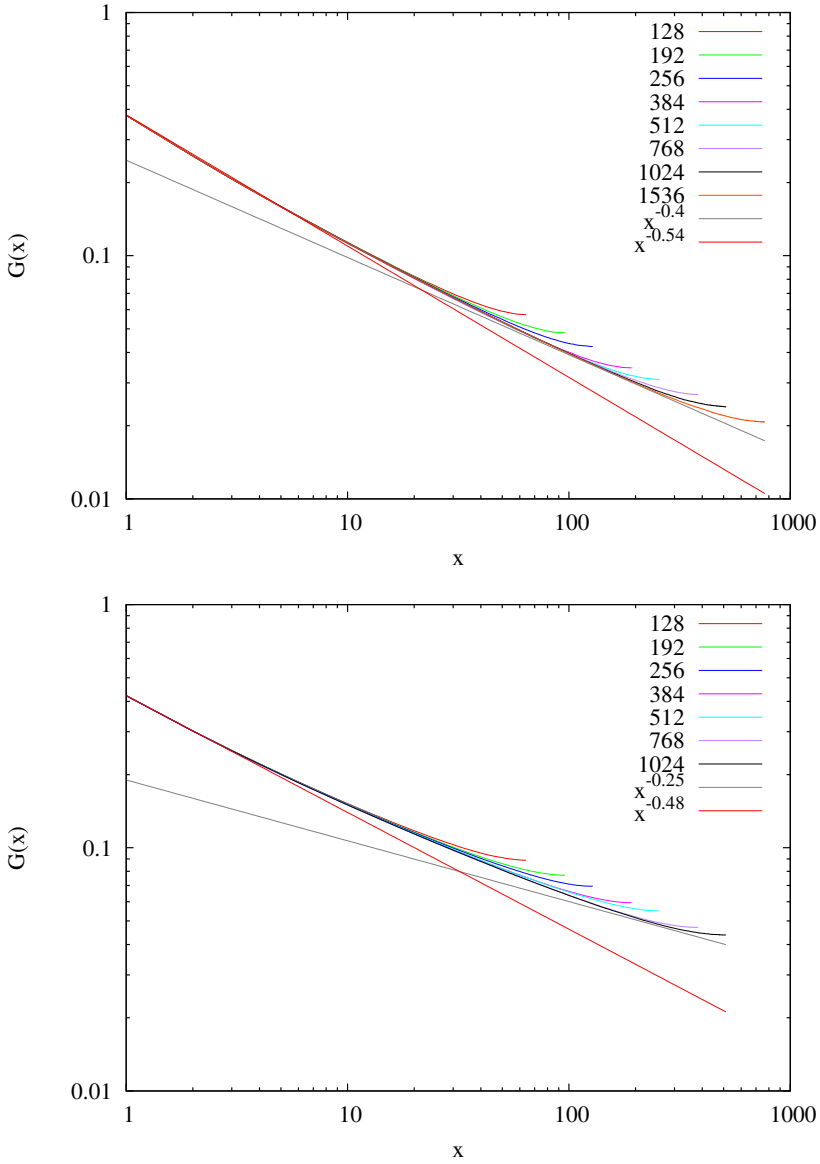

Figure 7.5. Log-log plot of the spin-spin correlation function for different sizes, at $\sigma = 1.6$ (top) and $\sigma = 1.75$ (bottom), $d = 2$. The gray line is the expected behaviour $x^{2-\sigma}$, that can be recovered only at large distance, while the red one is the fit for the short distance behaviour with a different power.

The effect of the two power-laws in $G(x)$ is reflected also in the measure of the η exponent from the susceptibility. Indeed the susceptibility is the integral over x of $G(x)$. This means that if we measure χ as a function of the size of the system, it will not follow the usual scaling form of Eq. (A.2) with $x_D/\nu = 2 - \eta$. Instead, it will be of the form:

$$\langle \chi(L,t) \rangle = \left(aL^{2-\eta} + bL^{2-\eta'} \right) \left[F_\chi(L^{1/\nu} t) + L^{-\omega} G_\chi(L^{1/\nu} t) + \dots \right]. \tag{7.6}$$

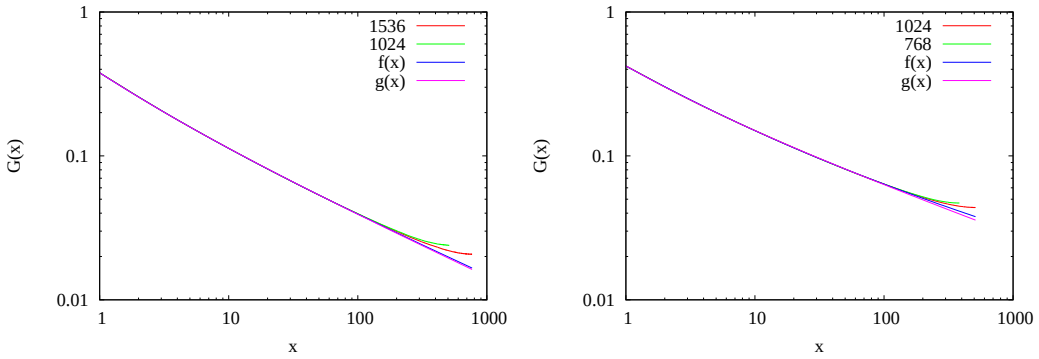

Figure 7.6. Log-log plot of the spin-spin correlation function for the two larger sizes, at $\sigma = 1.6$ (left) and $\sigma = 1.75$ (right), $d = 2$. Two fits with $f(x) = ax^{-\eta} + bx^{-\eta'}$ and with $g(x) = ax^{-\eta_P} + bx^{-\eta'}$ are performed. Both are compatible with the data and we can not determine η.

The contribution of the $L^{2-\eta'}$ term is a new correction to the asymptotic behaviour. Moreover it is much bigger than the correction that comes from the usual $L^{-\omega}$ term. In fact, the correction to scaling term takes into account the fact that the correlation function saturates at large distances as can be seen in Fig. 7.5, while the $L^{2-\eta'}$ term estimates the area between the correlation function and the asymptotic regime $L^{2-\eta}$. The latter area is much bigger than the former, as shown in Fig. 7.5.

If this new correction term is not considered properly, η can be overestimated. This can be the reason of the fact that in Ref. [18] the exponent η is found to be bigger than the one predicted by the RG analysis. The presence of this new correction term can be the cause of the small ω exponent found in the analysis of the previous Section, that is not in agreement with the large value of the SR model. Actually, we think that we are measuring $\eta' - \eta$ instead of ω.

We have measured the connected susceptibility at the maximum, that is at the apparent critical temperature for different sizes of the system. Analogously to what done for the correlation function, we have performed a fit of the susceptibility as a function of the size, with a function of the type $f(x) = aL^{2-\eta} + bL^{2-\eta'}$, where $\eta = 2 - \sigma$ and a fit with a function $g(x) = aL^{2-\eta_P} + bL^{2-\eta'}$, where η_P is the value reported by Picco in Ref. [18]. η' is left as a free parameter. We have ignored the corrections term $L^{-\omega}$ because, as seen, it is much smaller than the one considered. The results are shown in Fig. 7.7. The values of η' obtained from the fit are $\eta'(1.6) = 0.760(7)$, $\eta'(1.75) = 0.661(8)$ using $f(x)$ and $\eta'(1.6) = 0.788(8)$, $\eta'(1.75) = 0.763(8)$ using $g(x)$. The values are similar to the ones obtained from the correlation function. Again, both scenarios are compatible with the data and much larger sizes are needed to exclude one of the two.

The simulations of this Section have been performed on systems with periodic boundary conditions and minimum image convention. The use of the images is not useful in this case because it changes the intensity of the couplings when L is varied. Consequently $G(x)$ varies with L even at small distances. In particular correlations in small systems is bigger than that in bigger systems, and the curves are no more overlapping at small distances for different sizes. For this reason it is difficult to

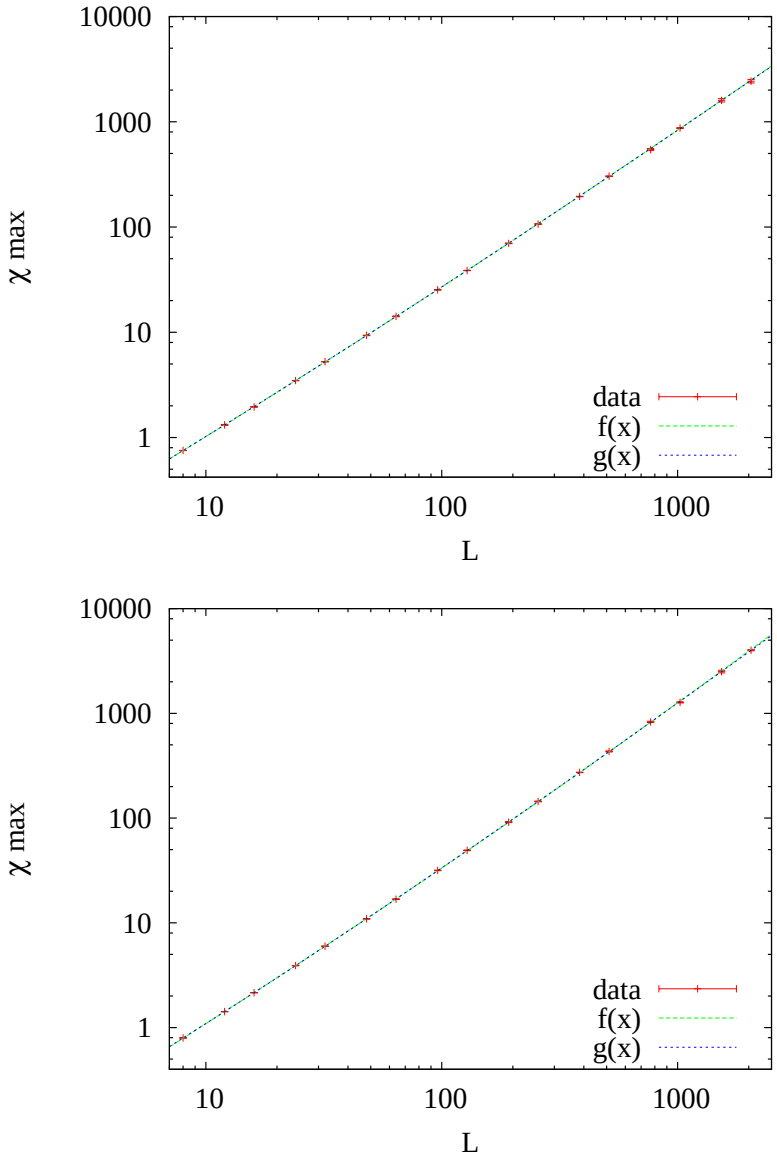

Figure 7.7. Log-log plot of the susceptibility at the maximum as a function of the size, at $\sigma = 1.6$ (top) and $\sigma = 1.75$ (bottom), $d = 2$. Two fits with $f(x) = aL^{2-\eta} + bL^{2-\eta'}$ and $g(x) = aL^{2-\eta_P} + bL^{2-\eta'}$ are performed. Both are compatible with the data and we can not determine η.

identify the region where there are not finite size effects.

The two powers behaviour is a very strange feature of the correlation length, because it is not present in the usual SR models and in the LR ones far from the lower critical σ. For this reason it should be the object of a future work to understand the physical origin of this phenomenon and to have an analytical description of it.

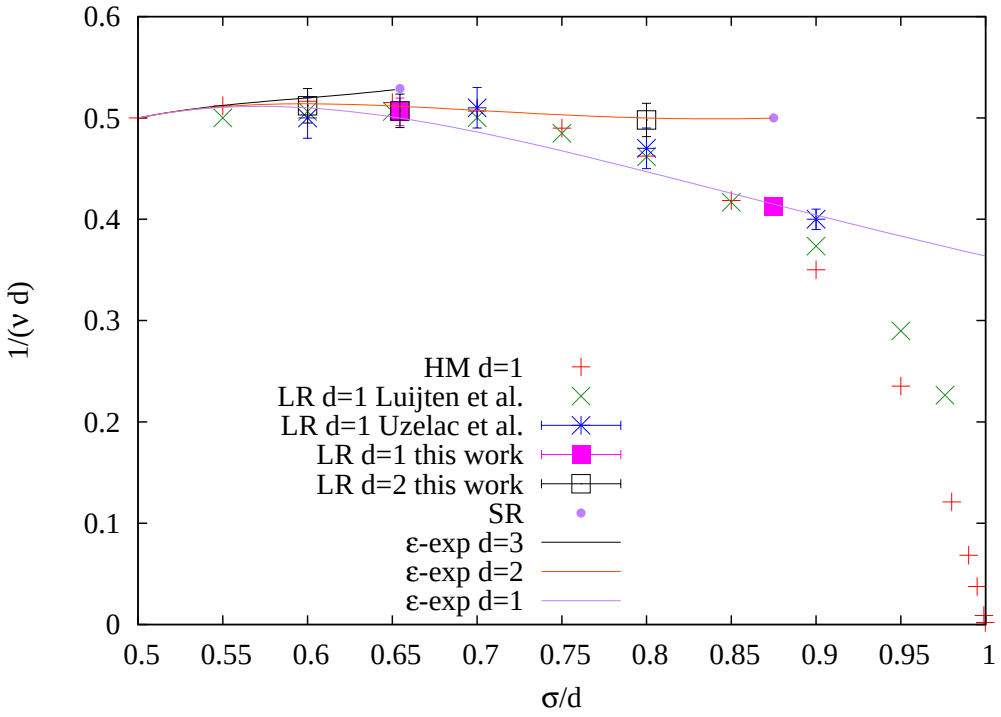

Figure 7.8. $1/(\nu d)$ as a function of the exponent $\hat{\sigma}$ as found in various works and in this work. The SR values follow the matching formula 7.3.

7.3 Check of the superuniversality conjecture

At this point we want to verify the superuniversality conjecture or, equivalently, Eq. (7.3) and (7.4). For this reason we summarize the results for the critical exponents in the literature.

In Fig. 7.8 $1/(d\nu)$ is plotted as a function of the parameter $\hat{\sigma}$ in the non mean-field region, for the HM model as found in Ref. [88], and for the LR one-dimensional model, from Ref. [89] and [90]. For the LR $d = 1$ and $d = 2$ model, our results are reported too. To verify the exactness of Eq. (7.4), in Fig. 7.8 the values of the exponent of the SR model as found in Ref. [87] are placed at the corresponding value of $\hat{\sigma}$ as in Eq. (7.3): $D = 2$ corresponds to $\hat{\sigma} = 0.875$, $D = 3$ corresponds to $\hat{\sigma} = 0.65453$. Eq. (7.4) is a good approximation near to the upper critical dimension (it is good for $D = 3$) but it is no more good for $D = 2$. This means that it is not possible to find a single value of σ that verify the equivalence for all the critical exponents as in Eq. (7.5). The lines are the third order ϵ-expansion for $d = 2$ and $d = 3$ as found in Ref. [45], where the third order has been fixed imposing that the curves recover the SR value at $\hat{\sigma}_L(d)$, and the second order ϵ-expansion for $d = 1$. For $d = 1$ we have not fixed the third order because at $\sigma_L(1) = 1$ there is not a second order phase transition. For this reason the curve for $1/\nu$ as a function of σ does not approach the point $\sigma_L(1) = 1$ continuously, but with a divergent derivative. Our data for $d = 2$ are in agreement with the ϵ-expansion.

In Fig. 7.9 $1/\gamma$ is plotted as a function of $\hat{\sigma}$ in the non mean-field region. The super-universality conjecture is not exact but it is a good approximation near σ_U.

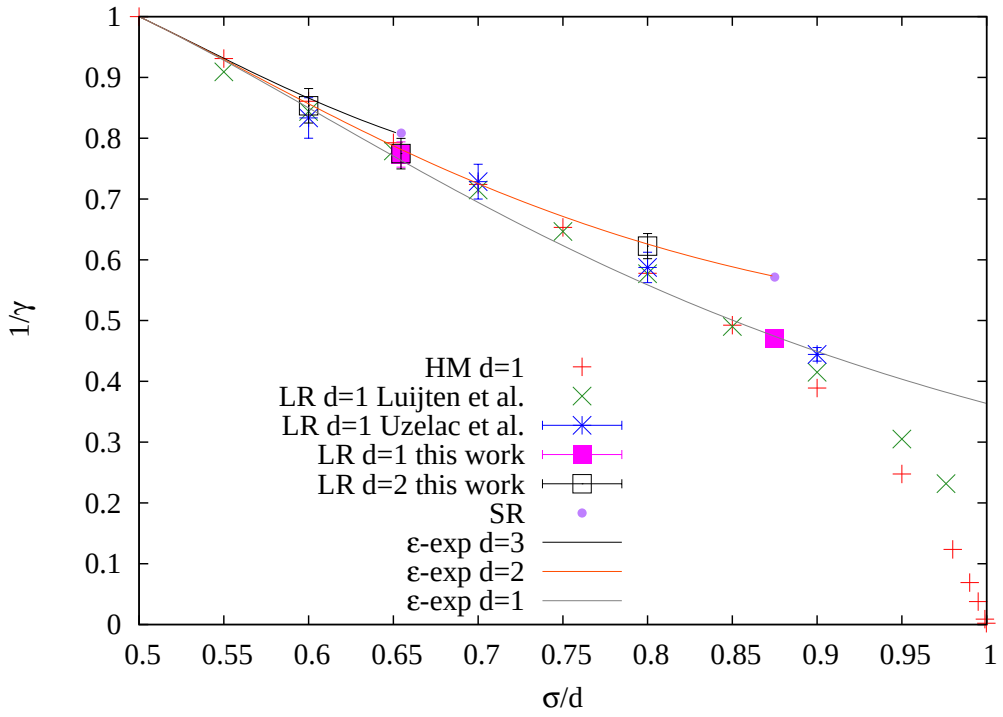

Figure 7.9. $1/\gamma$ as a function of the exponent σ in the non mean-field region as found in various works and in this work.

In fact $1/\gamma$ for $d = 1$ and $d = 2$ is nearly independent from d and the two curves are near when plotted versus $\hat{\sigma}$. The values for the SR model should be the end point of the line for $\gamma(\hat{\sigma})$ with $d = 2$ and $d = 3$, placed at $\hat{\sigma}_L(2), \hat{\sigma}_L(3)$. The straight lines are the third order epsilon-expansion as found in Ref. [45], where the third order has been fixed (as previously) imposing that the curve recover the SR value at $\hat{\sigma}_L(d)$.

Chapter 8

Conclusions

In Part I of the present Thesis, we have developed a semi-analytical real space RG method that can be generalized in a straightforward way to disordered systems considering it as a RG transformation between ensembles. This new RG scheme improves over previously available RG transformations for disordered systems essentially because:

- it is a real space one, thus it s very intuitive and the physics beyond it is clear,
- it considers averages over the disorder as the important physical observables, because we know that sample to sample fluctuations are stronger than thermal ones,
- it is predictive, in fact we can extract critical temperatures and critical exponents.

The method has been applied to the LR hierarchical model and in particular to its ferromagnetic, diluted and spin-glass versions. The reliability of the method has been tested comparing the values of critical temperatures and critical exponents with those obtained from MC simulations and the agreement is satisfactory for all the versions we have studied.

The HM can emulate a SR model in D dimensions changing the exponent σ that controls the power-law decay of the couplings with the distance. For the SG version, we have succeeded in identifying the critical temperature and the critical exponents, both in the mean-field and in the non-classical region at values of the parameter σ that correspond to effective dimensions $D = 3, 4, 5$.

In particular we have found that the critical exponent ν has a non monotonic behaviour passing from the mean-field to the non mean field region, confirming the results of the ϵ-expansion [45], in contrast with another real space RG approach recently proposed in Ref. [51]. This result confirms the importance to consider RG transformation between ensemble rather than between single samples for disordered models.

In Part II of this work, we have analyzed the connection between LR and SR systems. For simplicity we have considered the ferromagnetic version of the models, given that the connection we are interested in is still not well understood even in this simple case. First of all we have analyzed the $d = 1$ LR ferromagnetic model, for which the couplings have a power-law decaying with exponent σ, and we have

compared it with a SR system in D dimensions. We have reviewed all the $\sigma - D$ relations proposed in the literature and we have analyzed their accuracy performing Monte Carlo simulations to measure the exponents of the LR model through finite size scaling. We have compared them with the exponents of SR systems available in the literature. We have found that near to the upper critical dimension a reliable $\sigma - D$ relation exists: it means that, for example, for $D = 3$ a value of σ exists for which all the exponents of the LR and SR models are comparable, while near to the lower critical dimension, for example for $D = 2$, it is not possible to find a value of σ for which all the exponents of the LR model corresponds to those of the SR one.

Then we have generalized the $\sigma - D$ relation for LR systems in d dimensions showing that the dimensions D of the SR system and d of the LR one enter only through their ratio. The $\sigma - D$ relation can be deduced also from a superuniversality conjecture. It asserts that LR models properties depend only on $\hat{\sigma} = \sigma/d$. It means that for example the curves of the critical exponents as a function of σ for LR models in different dimensions collapse when plotted versus the parameter $\hat{\sigma}$. We have verified this property performing Monte Carlo simulations at various values of σ for $d = 2$ to measure the critical exponents. The superuniversality conjecture is a good approximation near to the upper critical dimension and becomes worst going towards the lower critical one.

We have then analyzed the region near to the lower critical dimension $\sigma = 1.75$ for the $d = 2$ LR model, because we want to verify if the scenario of Ref. [71] holds, with $\eta = \max(2 - \sigma, \eta_{SR} = \frac{1}{4})$, or if, for $1.6 \leq \sigma \leq 2$, η interpolates smoothly between $2 - \sigma$ and η_{SR} as stated in Ref. [18]. We have discovered that in this region the correlation function has a very strange behaviour, characterized by two decaying power-laws . This makes difficult to measure with high precision the critical exponents and the lower critical dimension. We think that this phenomenon can lead to overestimate η if a proper fit with a double power-law is not performed, as can be the case of Ref. [18]. It is very difficult to identify the right value of the η exponent, and thus to identify the lower critical σ numerically, thus we think that it is important to better understand the causes of the double power-law phenomenon from a theoretical point of view.

Appendix A

MC Finite Size Scaling analysis

The measure of the critical exponents in a Monte Carlo simulation is based on the Finite Size Scaling (FSS) ansatz, that is the application of the RG ideas to systems of finite size L. Let $\langle O(L,T)\rangle$ be the thermal average of the operator O, measured for a lattice of size L, and at temperature T. The observable is a dimensionless one if it remains finite at the critical point in the thermodynamic limit and if it is also universal, it means that it is invariant under the RG transformation. For these observables the FSS ansatz says that

$$\langle O(L,t)\rangle = F_O(L^{1/\nu}t) + L^{-\omega}G_O(L^{1/\nu}t) + \dots . \tag{A.1}$$

The dots stand for higher order scaling corrections. One example of these observables is the Binder parameter: $B = \frac{1}{2}\left[3 - \frac{\langle m^4\rangle}{\langle m^2\rangle^2}\right]$ [93] for a FM and $B = \frac{1}{2}\left[3 - \frac{\overline{\langle q^4\rangle}}{\overline{\langle q^2\rangle}^2}\right]$ for the SG.

If the observable diverges at the critical point in the thermodynamic limit with dimension x_D, $D(\infty,t) = t^{-x_D}$, where $t = \frac{|T-T_c|}{T}$, it is a dimensionfull observable, and Eq. (A.1) becomes:

$$\langle D(L,t)\rangle = L^{x_D/\nu}\left[F_D(L^{1/\nu}t) + L^{-\omega}G_D(L^{1/\nu}t) + \dots\right]. \tag{A.2}$$

Thus, when the size of the systems is finite, there are no thermodynamic singularities. For example the susceptibility will have a rounded off peak, that diverges with the size of the system as $L^{\gamma/\nu}$. To calculate the critical exponents we can apply the quotient method [95], following the scheme of Ref. [81]. For small t and large L, Eq. (A.1) can be rewritten as:

$$\langle O(L,t)\rangle \simeq F_O(0) + L^{1/\nu}tF'_O(0) + L^{-\omega}G_O(0). \tag{A.3}$$

Now we can determine the *finite size critical temperature* T^*_L where the observable takes the same value for size L and sL. s is a scale factor that can be freely chosen. It follows the law:

$$T^*_L = T^*_\infty(1 + A_{s,O}L^{-\omega-\frac{1}{\nu}}) \tag{A.4}$$

where $A_{s,O} = \frac{(1-s^{-\omega})G_O(0)}{(s^{1/\nu}-1)F'_O(0)}$. If now we compute a second dimensionless quantity P at $t^*_L = \frac{|T^*_L-T_c|}{T_c}$, obtained from the previous observable, we have:

$$P(L,t^*_L) \simeq F_P(0) + A_{s,O,P}L^{-\omega}, \tag{A.5}$$

with $A_{s,O,P} = A_{s,O}F'_P(0) + G_P(0)$. If we take again the quotient between the result for sizes L and sL we obtain:

$$Q_P = \frac{P(sL, t_L^*)}{P(L, t_L^*)} = 1 + B_{s,O,P}L^{-\omega}. \tag{A.6}$$

In this way we can determine ω with a log-log linear fit.

To determine the other exponents, e.g. ν or η we need dimensionfull observables D that scale as in Eq. (A.2).

Calculating the quotient of the chosen observable at the intersection temperatures t_L^* of the dimensionless observable O defined previously, we obtain:

$$Q_D = \frac{D(sL, t_L^*)}{D(L, t_L^*)} = s^{x_D/\nu} + B_{s,O,D}L^{-\omega}. \tag{A.7}$$

Knowing ω we are able to compute x_D through a new linear fit with variable $L^{-\omega}$.

Once the ν and ω exponents are computed, the critical temperature can be extracted from Eq. (A.4) through a linear fit with variable $L^{-\omega-1/\nu}$.

For the LR model that we have studied, we have extracted t_L^* as the crosses of the scale-invariant quantity $\frac{\chi}{L^\sigma}$. In this way we have divided a divergent quantity by its dimension $x_\chi = 2 - \eta = \sigma$, and the result remains finite at the critical temperature. We can do this for the LR model because we know exactly the value of η. To determine ν we have used as observable the derivative of the Binder parameter, which scales as $L^{\frac{1}{\nu}}$. We can not do the opposite, namely we can not use the derivative of $\frac{\chi}{L^\sigma}$ to extract ν because it is not a dimensionless quantity [96], it does not remain constant under the renormalization group. Thus for this kind of observable the scaling form is not the one in Eq. (A.1), and, while Eq. (A.4) remains the same, Eq. (A.7) changes.

There are many ways to do FSS analysis. The one explained here is a good method because the exponents are extracted not from the same observable. In this way the estimates are less correlated. Moreover exponents and critical temperature can be extracted only via linear fits.

Appendix B

An approximate description of HM using correlations

In this chapter we try to exploit the hierarchical structure of the HM to obtain an approximate description of the system. One of the advantages of the HM is that couplings at higher level have a smaller intensity than the previous ones, so one can try to do a high temperature expansion in these new couplings.

Indeed the partition function of the model with $n+1$ levels can be written as a function of the probability of the left and right block at level n, ($P_n(\{\sigma_L\})$ and $P_n(\{\sigma_R\})$) as

$$\mathcal{Z}_{n+1} = \sum_{\{\sigma\}} P_{n+1}(\{\sigma\}) = \sum_{\{\sigma\}} P_n(\{\sigma_L\}) P_n(\{\sigma_R\}) \prod_{i\in L, j\in R} e^{\beta c^{n+1} J_{ij}\sigma_i\sigma_j} =$$
$$= \sum_{\{\sigma\}} P_n(\{\sigma_L\}) P_n(\{\sigma_R\}) \prod_{i\in L, j\in R} \left[\cosh\left(\beta c^{n+1} J_{ij}\right)\left(1+\sigma_i\sigma_j \tanh\left(\beta c^{n+1} J_{ij}\right)\right)\right]$$

Now, if $\tanh(\beta c^{n+1} J_{ij}) \equiv t_{ij}$ is small, that is in high temperature, one can expand the product in the last term, keeping only the first orders:

$$\mathcal{Z}_{n+1} = \sum_{\{\sigma\}} P_n(\{\sigma_L\}) P_n(\{\sigma_R\}) \left(\prod_{i\in L, j\in R} \cosh(\beta c^{n+1} J_{ij})\right) \cdot$$
$$\cdot \left(1 + \sum_{i\in L, j\in R} \sigma_i\sigma_j t_{ij} + \sum_{\substack{i,k\in L, j,l\in R \\ (i,j)\neq(k,l)}} \sigma_i\sigma_j t_{ij}\sigma_k\sigma_l t_{kl} + O(t^3)\right)$$

At this point the thermal average can be performed separately for the observables in the right and left blocks that are uncorrelated before the level $n+1$, leading to:

$$\mathcal{Z}_{n+1} = \left(\prod_{i\in L, j\in R} \cosh(\beta c^{n+1} J_{ij})\right) \cdot$$
$$\cdot \left(1 + \sum_{i\in L, j\in R} \langle\sigma_i\rangle\langle\sigma_j\rangle t_{ij} + \sum_{\substack{i,k\in L, j,l\in R \\ (i,j)\neq(k,l)}} \langle\sigma_k\sigma_i\rangle t_{ij} \langle\sigma_j\sigma_l\rangle t_{lk} + O(t^3)\right)$$

Now we can introduce the vectors of the magnetizations inside each block $M_n^L = \{\langle\sigma_{i\in L}\rangle\}$ and $M_n^R = \{\langle\sigma_{j\in R}\rangle\}$ and the matrices of the correlations $C_n^L = \{\langle\sigma_{i\in L}\sigma_{k\in L}\rangle\}$ and $C_n^R = \{\langle\sigma_{j\in R}\sigma_{l\in R}\rangle\}$ and of the couplings $t = \{t_{ij}\}$ In terms of these matrices the previous equation becomes:

$$\mathcal{Z}_{n+1} = \left(\prod_{i\in L, j\in R} \cosh(\beta c^{n+1} J_{ij})\right) \cdot \left(1 + M_n^L t M_n^R + \mathrm{Tr}\left(C_n^L t C_n^R t - t^2\right)/2 + O(t^3)\right)$$

where the $-t^2$ in the second order term takes into account the fact that $(i,j) \neq (k,l)$, considering that $(C_n^L)_{ii} = (C_n^R)_{jj} = 1$ and the factor 2 removes the degeneracy $(i,j),(k,l) \leftrightarrow (k,l),(i,j)$. Similarly one can express correlations and magnetizations at level $n+1$ calculating the correction to correlations and magnetizations at level n in the left and right block due to the new couplings, stopping in the expansion at first orders.

For example the magnetization of a spin σ_i in the left block will change after the introduction of the couplings at level $n+1$ following the equation:

$$(M_{n+1}^L)_i = \frac{1}{Z}\left[(M_n^L)_i + (C_n^L t M_n^R)_i + \mathrm{Tr}\left((C_3^i)_n^L t C_n^R t - (M_n^L)_i t^2\right)/2 + O(t^3)\right].$$

We have introduced the matrix of the three point correlations $(C_3^i)_n^L = \{\langle\sigma_i\sigma_j\sigma_k\rangle_n\}$, where σ_j and σ_k are in the left block. Analogously, for the magnetization of the right block it is sufficient to change the index L with R.

In the same way we can write the equation for the correlation between two spins i and j that are both in the left block:

$$(C_{n+1}^{LL})_{ij} = \frac{1}{Z}\left[(C_n^L)_{ij} + (C_3^{ij})_n^L t M_n^R + \mathrm{Tr}\left((C_4^{ij})_n^L t C_n^R t - (C_n^L)_{ij} t^2\right)/2 + O(t^3)\right]$$

We have introduced the vector of the three point correlations $(C_3^{ij})_n^L = \{\langle\sigma_i\sigma_j\sigma_k\rangle_n\}$, where σ_k is in the left block and the matrix of the four point correlations $(C_4^{ij})_n^L = \{\langle\sigma_i\sigma_j\sigma_k\sigma_l\rangle_n\}$, where σ_k and σ_l are again in the left block. The correlation for two spins i and j that are in different blocks is:

$$(C_{n+1}^{LR})_{ij} =$$
$$\frac{1}{Z}\left[(M_n^L)_i (M_n^R)_j + (C_n^L t C_n^R)_{ij} + \mathrm{Tr}\left((C_3^i)_n^L t (C_3^j)_n^R t - (M_n^L)_i (M_n^R)_j t^2\right)/2 + O(t^3)\right]$$

Thus the whole matrix of the correlations at level $n+1$ will be composed of 4 submatrices: C^{LL}, C^{LR}, C^{RL}, C^{RR}.

In this way, one can approximate correlations and magnetizations (in principle at each order in t) in a time polynomial in N instead of calculate them exhaustively in a time exponential in N. This is particularly important for SGs in which equilibrium properties are very difficult to obtain.

Please note that with this method the self-correlation C_{ii} is always 1, as expected, because the numerator is exactly canceled by the denominator. This property is generally not verified by other approximations.

In the previous equations there are three and four point correlations that are in principle not known in our approximate description that considers only magnetizations and two point correlations. However in some specific cases 3 and 4 point

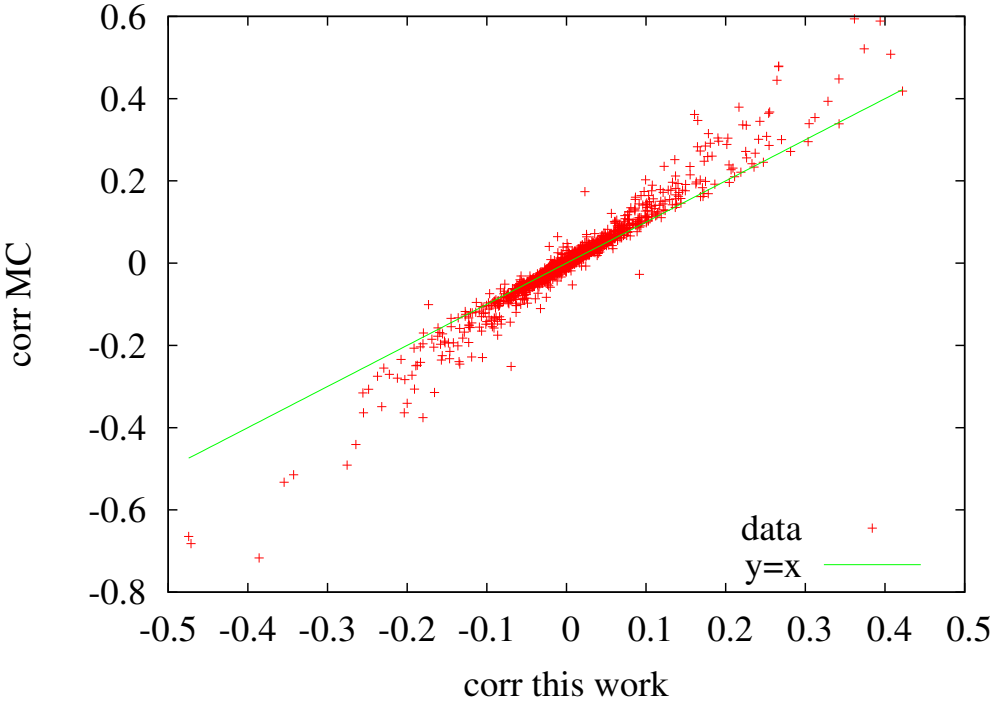

Figure B.1. Correlations obtained from our method plotted versus correlations obtained from a Monte Carlo simulation. The system is a $n = 6$ $c = 2^{-5/6}$ SG HM at $T = 1.6$.

correlations can be expressed in terms of two point correlations and magnetizations. For example in the mean field approximation connected correlations are null. This fact permits to obtain the following relations when the field is null:

$$\langle\sigma_i\sigma_j\sigma_k\sigma_l\rangle = \langle\sigma_i\sigma_j\rangle\langle\sigma_k\sigma_l\rangle + \langle\sigma_i\sigma_k\rangle\langle\sigma_j\sigma_l\rangle + \langle\sigma_i\sigma_l\rangle\langle\sigma_j\sigma_k\rangle \tag{B.1}$$

In a tree instead the correlations can be computed exactly as:

$$\langle\sigma_i\sigma_j\sigma_k\sigma_l\rangle = \max\left(\langle\sigma_i\sigma_j\rangle\langle\sigma_k\sigma_l\rangle, \langle\sigma_i\sigma_k\rangle\langle\sigma_j\sigma_l\rangle, \langle\sigma_i\sigma_l\rangle\langle\sigma_j\sigma_k\rangle\right) \tag{B.2}$$

We can choose to use both of them and to verify a posteriori which is the best approximation comparing the results with the exact ones (or with the ones obtained from MC simulations).

B.1 Comparison with Monte Carlo simulations

Operatively, if we want to calculate the magnetizations and correlations of a system with n levels, we start to analyze 2^{n-1} uncorrelated blocks of 2 spins considering only the couplings at level 1. For them we can write correlations and magnetizations exactly. Then we add the couplings at level 2 between pairs of near blocks and we compute the correlations and magnetizations for the 2^{n-2} blocks of 4 spins following the previous equations. We repeat this procedure until we reach the n-th level.

We have compared our results with the ones obtained from a Monte Carlo simulation. In Fig B.1 we have plotted the correlations obtained from the approximate

description as a function of the correlations obtained from the Monte Carlo simulations for a SG HM system with Gaussian couplings, no external field, $n = 6$ and $c = 2^{-5/6}$, at $T = 1.6$ ($T_c \simeq 0.54$ for this model). One can notice that the approximate description underestimates the correlations. This fact is not present in high temperature, but things get worse approaching the critical temperature when the correlations grow. It could be useful to see if this phenomenon is reduced when the third order in the expansion in t is added.

There are no significant differences if one uses the MF approximation in Eq. (B.1) or the tree approximation in Eq. (B.2) to approximate 4 points correlations. We have seen that the better results are obtained if the correlations are the mean over the terms:

$$\langle \sigma_i \sigma_j \sigma_k \sigma_l \rangle = \frac{1}{3} \left(\langle \sigma_i \sigma_j \rangle \langle \sigma_k \sigma_l \rangle + \langle \sigma_i \sigma_k \rangle \langle \sigma_j \sigma_l \rangle + \langle \sigma_i \sigma_l \rangle \langle \sigma_j \sigma_k \rangle \right) \tag{B.3}$$

although we have no explanation for this choice.

B.2 Comparison with mean-field approximations

We can compare our method with the other approximations present in the literature. We report here the estimates for the connected correlations given by the naive Mean Field approximation (nMFA), the TAP and the Bethe approximation (BA) [53] in the case of null magnetizations:

$$\begin{aligned} \left(C^{-1}_{nMF} \right)_{ij} &= \delta_{ij} - J_{ij} \\ \left(C^{-1}_{TAP} \right)_{ij} &= \left[1 + \sum_k J^2_{ik} \right] \delta_{ij} - J_{ij} \\ \left(C^{-1}_{BA} \right)_{ij} &= \left[1 + \sum_k \frac{t^2_{ik}}{1 - t^2_{ik}} \right] \delta_{ij} - \frac{t_{ij}}{1 - t^2_{ij}} \end{aligned} \tag{B.4}$$

We have compared the estimates for the correlations in a given sample obtained by this three method and by our method with the correlations obtained by a Monte Carlo simulation for the SG HM with Gaussian couplings without external field, and $c = 2^{-5/6}$. The results are shown in Fig. B.2. The nMFA is the worst approximation, as happens also for other models. The best ones are the TAP and the present approximation. This approximation has some divergences when approaching the critical temperature ($T_c \simeq 0.54$ for this model).

B.3 Future developments

The fact that the present approximation stops to give good results near to the critical temperature is expected because, near to the critical point, many different states with different magnetizations and correlations arise. Instead, our approximation considers that there is only one state characterized only by the averages M and C. However, at difference with the other mean-field approximations, the present approximation can easily be generalized to deal with many states. A future work can consider that different states can exist. In the region below the critical temperature,

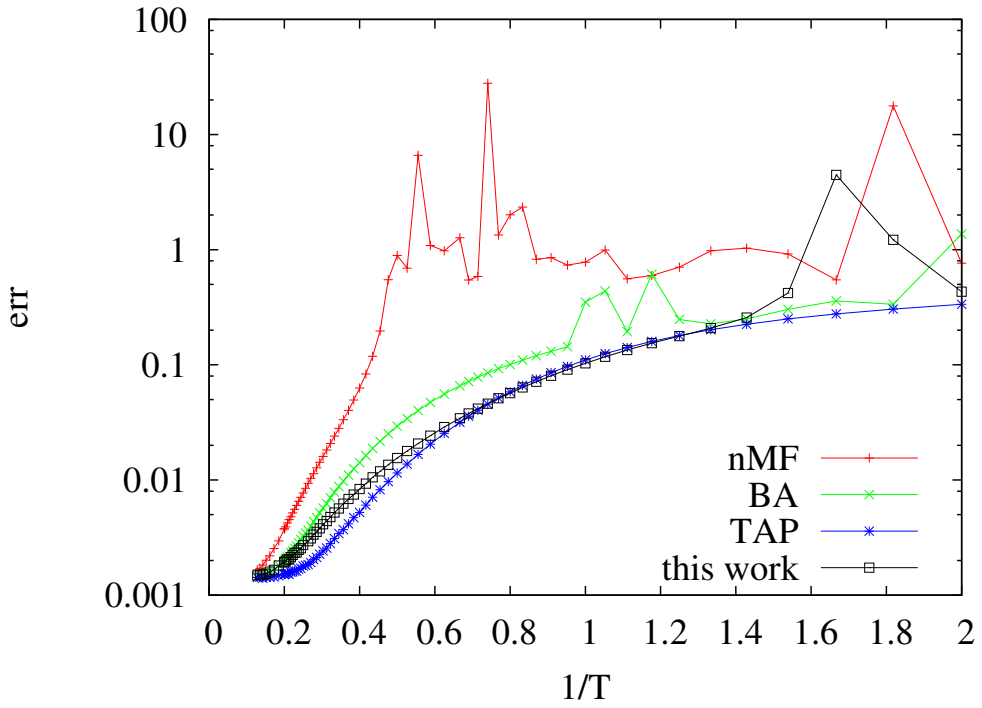

Figure B.2. Error made by three existing MF approximations and by the method proposed in this work, in estimating correlations given the couplings. The model is a $n = 7$ SG HM.

we do not know how many states there are, so one can try to count them. For each state a vector of magnetizations and a matrix of two points correlations can be defined. The magnetizations and three point correlations can be different from zero even if there is a null external field. In particular, three point correlations can be written exactly in the mean field approximation by:

$$\langle\sigma_i\sigma_j\sigma_k\rangle = \langle\sigma_i\rangle\langle\sigma_j\sigma_k\rangle + \langle\sigma_k\rangle\langle\sigma_i\sigma_j\rangle + \langle\sigma_j\rangle\langle\sigma_i\sigma_k\rangle - 2\langle\sigma_i\rangle\langle\sigma_j\rangle\langle\sigma_k\rangle$$

and Eq. B.1 is slightly modified to take into account terms with non null three point correlations. When a new level is added, one can take magnetizations and correlations of the two right and left blocks from an ensemble, and try to modify them with the new interactions. Some combinations of the states will generate other states, and some other will collapse in an existing one. In this way one can study the number of states and their properties. The transition below and above the critical dimension can be analyzed (just changing the scaling factor) and one can check if the spin glass phase is of the same type or of a different one.

Appendix C

Side projects

In this chapter two works are reproduced; their subjects are a bit disconnected from the main topic of this Thesis, however they have been included because they have been done during this Ph.D. The first work has been submitted to the 50th Annual Allerton Conference on Communication, Control, and Computing.

Compressed sensing with sparse, structured matrices

Maria Chiara Angelini
Dip. Fisica
Università La Sapienza
P.le Aldo Moro 5, 00185 Roma, Italy
Email: Maria.Chiara.Angelini@roma1.infn.it

Federico Ricci-Tersenghi
Dip. Fisica, CNR – IPCF, UOS Roma
INFN – Roma 1, Università La Sapienza
P.le Aldo Moro 5, 00185 Roma, Italy
Email: Federico.Ricci@roma1.infn.it

Yoshiyuki Kabashima
Dept. of Comput. Intell. & Syst. Sci.
Tokyo Institute of Technology
Yokohama 226-8502, Japan
Email: kaba@dis.titech.ac.jp

***Abstract*— In the context of the compressed sensing problem, we propose a new ensemble of sparse random matrices which allow one (i) to acquire and compress a ρ_0-sparse signal of length N in a time linear in N and (ii) to perfectly recover the original signal, compressed at a rate α, by using a message passing algorithm (Expectation Maximization Belief Propagation) that runs in a time linear in N. In the large N limit, the scheme proposed here closely approaches the theoretical bound $\rho_0 = \alpha$, and so it is both optimal and efficient (linear time complexity). More generally, we show that several ensembles of dense random matrices can be converted into ensembles of sparse random matrices, having the same thresholds, but much lower computational complexity.**

I. Introduction

Compressed sensing is a framework that enables an N-dimensional sparse signal $\boldsymbol{s} = (s_i)$ to be recovered from $M(< N)$ linear measurements of its elements, $\boldsymbol{y} = \boldsymbol{F}\boldsymbol{s}$, by exploiting the prior knowledge that $\boldsymbol{s}$ contains many zero elements [1]. A simple consideration guarantees that ℓ_0-recovery,

$$\hat{\boldsymbol{s}} = \underset{\boldsymbol{x}}{\operatorname{argmin}} ||\boldsymbol{x}||_0 \quad \text{subj. to} \quad \boldsymbol{y} = \boldsymbol{F}\boldsymbol{x}, \tag{1}$$

where $||\boldsymbol{x}||_0$ denotes the number of non-zero elements in $\boldsymbol{x}$, is theoretically optimal in terms of minimizing the number of measurements M necessary for perfectly recovering any original signal $\boldsymbol{s}$. However, carrying out ℓ_0-recovery for a general measurement matrix $\boldsymbol{F}$ is NP-hard. To avoid such computational difficulties, an alternative approach, ℓ_1-recovery

$$\hat{\boldsymbol{s}} = \underset{\boldsymbol{x}}{\operatorname{argmin}} ||\boldsymbol{x}||_1 \quad \text{subj. to} \quad \boldsymbol{y} = \boldsymbol{F}\boldsymbol{x}, \tag{2}$$

where $||\boldsymbol{x}||_1 = \sum_{i=1}^{N} |x_i|$, is widely employed, as (2) is generally converted into a linear programming problem, and therefore, signal recovery is mathematically guaranteed in an $O(N^3)$ computational time through the use of the interior point method. Nevertheless, the $O(N^3)$ cost of computation can still be unacceptably high in many practical situations, and much effort is being put into finding more computationally feasible and accurate recovery schemes [2]–[7].

Among such efforts, the recovery scheme recently proposed by Krzakala et al. [7] is worth special attention. Their scheme basically follows the Bayesian approach. Namely, the signal recovery problem is formulated as one of statistical inference from the posterior distribution,

$$P(\boldsymbol{x}|\boldsymbol{F},\boldsymbol{y}) = \frac{\delta(\boldsymbol{F}\boldsymbol{x}-\boldsymbol{y})P(\boldsymbol{x})}{Z(\boldsymbol{F},\boldsymbol{y})}, \tag{3}$$

where $Z(\boldsymbol{F},\boldsymbol{y})$ is a normalization factor imposing the condition $\int d\boldsymbol{x} P(\boldsymbol{x}|\boldsymbol{F},\boldsymbol{y}) = 1$ and a component-wise prior distribution $P(\boldsymbol{x}) = \prod_{i=1}^{N}[(1-\rho)\delta(x_i)+\rho\phi(x_i)]$ is assumed. ρ and $\phi(\boldsymbol{x})$ represent the density of the non-zero signal elements and a Gaussian distribution, respectively. Exactly inferring $\boldsymbol{s}$ from (3) is NP-hard, similarly to (1). However, by employing the belief propagation (BP) in conjunction with the expectation-maximization (EM) algorithm for estimating ρ and the parameters of $\phi(x)$, they developed an approximation algorithm, termed EM-BP, which has better recovery performance than (2) with a computational cost of only $O(N^2)$. Furthermore, they showed that, by employing a peculiar type of "seeded" matrix $\boldsymbol{F}$, the threshold of the compression rate $\alpha = M/N$ of EM-BP, above which the original signal is typically recovered successfully, can approach very close to that of ℓ_0-recovery, $\alpha_{s-EMBP} = \rho_0$, where ρ_0 is the actual signal density of $\boldsymbol{s}$ and $s-EMBP$ stands for 'seeded EM-BP'. The seeded matrix is composed of blocks along the diagonal densely filled with Gaussian random variables. It is important to remember that this result is achieved for the first time with an approach different from ℓ_0-recovery, being the threshold for ℓ_1-recovery that is much higher than the optimal one: $\alpha_{\ell_1} > \rho_0$. The optimality of the ℓ_0-recovery is guaranteed for EM-BP, which means that this scheme can practically achieve the theoretically optimal threshold of signal recovery with an $O(N^2)$ computational cost. This remarkable property was recently proved in a mathematically rigorous manner in the case that the matrix entries satisfy certain conditions concerning their statistics [8]. However, it is still unclear whether their scheme is optimal in terms of the computational complexity; there might be a certain design of the measurement matrix $\boldsymbol{F}$ that makes it possible to further reduce the computational cost while keeping the same signal recovery threshold.

The purpose of the present study is to explore such a possibility. For this, we focus on a class of matrices that are characterized by the following properties:

- **sparsity:** The matrix $\boldsymbol{F}$ has only $O(1)$ non-zero elements per row and column. This implies that the

measurements can be performed in a time linear in the signal length. This situation is highly preferred for the sake of practicality, given that such an operation typically needs to be done in real time, during data acquisition.

- **integer values:** The matrix elements are not real valued, but take on small integer values. This means that an optimized code for the measurements can work with bitwise operations, thus achieving much better performance without any loss of precision.
- **no block structure:** The block structure used in [7] may not be necessary for reaching the optimal threshold. As an alternative possibility, we study a structure made of a square matrix in the upper left corner (the seed) plus a stripe along the diagonal. This structure is much more amenable for analytic computations, since it corresponds to a one-dimensional model homogeneous in space.

The use of sparse matrices for compressed sensing has already been suggested in several earlier studies [9]–[13]. Our approach is particularly similar to that of [13] in the sense that both sides are based on the Bayesian framework and use integer-valued sparse measurement matrices. Nevertheless, these two approaches differ considerably in the following two points. Firstly, we adopt EM-BP, which updates only a few variables per node for the signal recovery, while the recovery algorithm of [13] involves functional updates and needs significantly more computational time than ours. Secondly, we thoroughly explored a simple design of $\boldsymbol{F}$ that achieves nearly optimal recovery performance. In contrast, the problem of the matrix design is not fully examined in [13]. By carrying out extensive numerical experiments in conjunction with an analysis based on density evolution [15], we show that a threshold close to the theoretical limit $\alpha = \rho_0$ can be achieved by using matrices with the above properties with an almost *linear* computational cost in the measurement and recovery stages.

This paper is organized as follows. In Section II, the EM-BP algorithm is briefly explained and the results for dense matrices are summarized. The algorithm is applied to homogeneously sparse matrices in Section III and to structured sparse block matrices in Section IV. A new type of "striped" sparse matrix without blocks is introduced in Section V. The last Section summarizes our work, focusing on its importance for practical use, and touches on future issues.

II. Expectation Maximization Belief Propagation

The new algorithm based on BP in conjunction with the EM proposed in Ref. [7] starts from Eq. (3). A similar idea was also proposed in Ref. [14]. In order to solve it with BP, $O(MN)$ messages for the probability distributions of the variables x_i are constructed in the following way:

$$m_{\mu\to i}(x_i) = \frac{1}{Z^{\mu\to i}} \int \prod_{j\neq i} dx_j m_{j\to\mu}(x_i) \delta\Big(y_\mu - \sum_k F_{\mu k} x_k\Big)$$

$$m_{i\to\mu}(x_i) = \frac{1}{Z^{i\to\mu}} \Big[(1-\rho)\delta(x_i) + \rho\phi(x_i)\Big] \prod_{\gamma\neq\mu} m_{\gamma\to i}(x_i)$$

where $Z^{i\to\mu}$ and $Z^{\mu\to i}$ are normalization factors. This EM-BP equations are very complicated because the messages are distribution functions. In order to make them simpler, the messages can be approximated by assuming that they are Gaussian, thus obtaining the equations for the mean $a_{i\to\mu}$ and the variance $v_{i\to\mu}$ of $m_{i\to\mu}(x_i)$. This approximation was introduced for sparse matrices in Refs. [16]–[19], and it becomes asymptotically exact if $\boldsymbol{F}$ is dense. In fact, it is derived from an expansion in small $F_{\mu i}$, and in the dense case $F_{\mu i} = O(1/\sqrt{N})$. Supposing that the elements of the original signal follow a Bernoulli-Gaussian distribution with parameters ρ_0, $\overline{x}_0$ and σ_0, the update rules for the messages are the following:

$$\begin{aligned}
a_{i\to\mu} &= f_a\left(\sum_{\gamma\neq\mu} A_{\gamma\to i}, \sum_{\gamma\neq\mu} B_{\gamma\to i}\right) \\
a_i &= f_a\left(\sum_{\gamma} A_{\gamma\to i}, \sum_{\gamma} B_{\gamma\to i}\right) \\
v_{i\to\mu} &= f_c\left(\sum_{\gamma\neq\mu} A_{\gamma\to i}, \sum_{\gamma\neq\mu} B_{\gamma\to i}\right) \\
v_i &= f_c\left(\sum_{\gamma} A_{\gamma\to i}, \sum_{\gamma} B_{\gamma\to i}\right) \\
A_{\mu\to i} &= \frac{F_{\mu i}^2}{\sum_{j\neq i} F_{\mu j}^2 v_{j\to\mu}} \\
B_{\mu\to i} &= \frac{F_{\mu i}\left(y_\mu - \sum_{j\neq i} F_{\mu j} a_{j\to\mu}\right)}{\sum_{j\neq i} F_{\mu j}^2 v_{j\to\mu}}
\end{aligned} \tag{4}$$

where f_a and f_c are some analytical functions depending on the parameters ρ, $\overline{x}$ and σ. For details, see Ref. [7].

In general, the original ρ_0, $\overline{x}_0$ and σ_0 are not known, but one can use EM to derive the update rules for them, using the property that the partition function

$$Z(\rho, \overline{x}, \sigma) = \int d\boldsymbol{x} P(\boldsymbol{x}) \delta(\boldsymbol{y} - \boldsymbol{F}\boldsymbol{x})$$

is the likelihood of the parameters $(\rho, \overline{x}, \sigma)$ and is maximized by the true parameters ρ_0, $\overline{x}_0$, and σ_0. Thus, after the update of all the messages, the inferred parameters of the original distribution are updated following these rules:

$$\overline{x} \leftarrow \frac{1}{\rho N}\sum_i a_i \ , \qquad \sigma^2 \leftarrow \frac{1}{\rho N}\sum_i (v_i + a_i^2) - \overline{x}^2 \ ,$$

$$\rho \leftarrow \frac{\sum_i \frac{1/\sigma^2 + U_i}{V_i + \overline{x}/\sigma^2} a_i}{\sum_i \left[1 - \rho + \frac{\rho}{\sigma(1/\sigma^2+U_i)^{\frac{1}{2}}} e^{\frac{(V_i+\overline{x}/\sigma^2)^2}{2(1/\sigma^2+U_i)} - \frac{\overline{x}^2}{2\sigma^2}}\right]^{-1}} \ ,$$

with $U_i = \sum_\gamma A_{\gamma\to i}$ and $V_i = \sum_\gamma B_{\gamma\to i}$. If the algorithm converges to the correct solution, $a_i = s_i$ and $v_i = 0$.

To reduce the number of messages from $O(NM)$ to $O(N)$, one can see that in the large N limit, the messages $a_{i\to\mu}$ and $v_{i\to\mu}$ are nearly independent of μ. Thus, we can derive the equations involving only a variable per each measurement node and a variable per signal node, if we are careful to keep the correcting Onsager reaction term as in the TAP equations of statistical physics [20]. This method was introduced in the context of compressed sensing in Ref. [6] and is called approximated message passing (AMP).

In general, the correct distribution of the original signal is unknown. However, in Ref. [7], it is demonstrated that if $\alpha > \rho_0$, the most probable configuration of $\boldsymbol{x}$ with respect to $P(\boldsymbol{x}) = \prod_{i=1}^{N}[(1-\rho)\delta(x_i) + \rho\phi(x_i)]$ with $\rho < 1$, restricted to the subspace $\boldsymbol{y} = \boldsymbol{F}\boldsymbol{x}$, is the original signal $\boldsymbol{s}$, even if the signal is not distributed according to $P(\boldsymbol{x})$. So our choice of a Gaussian distribution for $\phi(x)$ should be perfectly fine even if the original signal has a different distribution.

The free entropy $\Phi(D)$ at a fixed mean square error $D = (1/N)\sum_{i=1}^{N}(x_i - s_i)^2$ can be computed if a dense matrix is used. For $\alpha > \rho_0$, the global maximum of the function $\Phi(D)$ is at $D = 0$, that corresponds to the correct solution. However, below a certain threshold $\alpha < \alpha_{BP}$ that depends on the distribution $P(\boldsymbol{s})$, the free entropy develops a secondary, local maximum at $D \neq 0$. As a consequence, the EM-BP algorithm can not converge to the correct solution for $\rho_0 < \alpha < \alpha_{BP}$, because a dynamical transition occurs. Nonetheless, the threshold α_{BP} is lower than α_{ℓ_1}.

III. EM-BP WITH A SPARSE MATRIX

First of all, we want to verify if the use of a sparse matrix can reach the same results as the use of a dense one. For a sparse random matrix, the AMP equations can not be used; thus, we can use the update rules in Eq. (4) for inferring the original signal $\boldsymbol{s}$. In particular, we choose the matrix $\boldsymbol{F}$ to have only $K = O(1)$ elements different from zero in each row and $H = \alpha K = O(1)$ elements in each column, extracting them from the distribution,

$$P(F_{\mu i}) = \frac{1}{2}\delta(F_{\mu i} - J) + \frac{1}{2}\delta(F_{\mu i} + J) \tag{5}$$

with $J = 1$. The use of the messages $a_{i\to\mu}$ and $v_{i\to\mu}$ instead of the AMP equations does not involve an extra cost in memory, because the number of the messages is $O(N)$ from the sparsity of the matrix. In principle, the messages $m_{i\to\mu}(x)$ are not Gaussian if the matrix is sparse, so the use of only the two parameters $a_{i\to\mu}$ and $v_{i\to\mu}$ is not exact. However, the convolution of K messages (with $K = 20$ in a typical matrix we use) is not far from a Gaussian, and indeed, we can verify a posteriori that this approximation is valid, because it gives good results.

In all our numerical simulations, we use a Bernoulli-Gaussian distributed signal and a compression rate $\alpha = 0.5$.

Figure 1 (top) shows the probability of perfect recovery as a function of the sparsity of the signal ρ_0 for different sizes, by applying the EM-BP algorithm using a sparse matrix

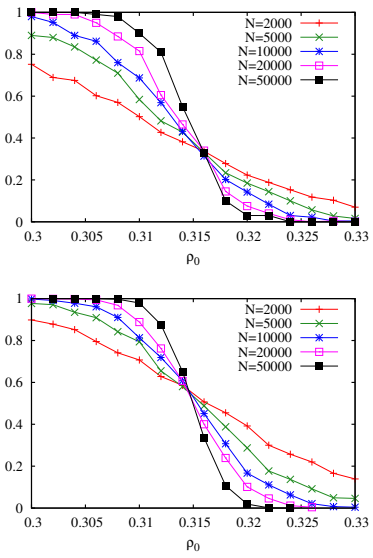

Fig. 1. Top: Probability of perfect recovery versus the signal sparsity ρ_0 using sparse matrices with $\alpha = 0.5$ and $K = 20$. The threshold is the same as with dense matrices. Bottom: Probability of perfect recovery computed with density evolution has the same threshold. Here, N is the population size.

with $K = 20$. The threshold for perfect recovery in the thermodynamic limit ($N \to \infty$) is $\rho_{BP} \simeq 0.315$, which is the same as the one obtained in Ref. [7] with a dense matrix. We can not analytically compute the free entropy $\Phi(D)$ as in [7], because we use sparse matrices and cannot use methods such as the saddle point one. However, we performed a numerical density evolution analysis, as shown in Fig. 1 (bottom), and found that the threshold is almost the same as the one computed with the matrices $\boldsymbol{F}$.

Next, we will verify that the correct solution is always the global maximum of $\Phi(D)$ and it is locally stable up to $\alpha \simeq \rho_0$ when using EM-BP with a sparse matrix. Since we can not analytically compute the free entropy, we must resort to a numerical method. We start EM-BP with an initial condition very close to the correct solution: $a^0_{i\to\mu} = s_i + \delta_{i\to\mu}$, with $\delta_{i\to\mu}$ a random number uniformly distributed in $[-\Delta, \Delta]$. In this way, we have verified (see Fig. 2) that if Δ is sufficiently small, the correct solution can be found up to $\alpha \simeq \rho_0$, as in the case of a dense matrix.

For the algorithms based on the ℓ_1 minimization, it is known that the threshold with a sparse matrix is lower than that with a dense one. However, these algorithms are not optimal, because the correct solution disappears below the threshold α_{ℓ_1}. In this sense, the EM-BP algorithm is optimal, because the global maximum of the free entropy is always on the correct solution. Thus, one can expect that, if the rank of the sparse matrix is the same as that of the dense one, a

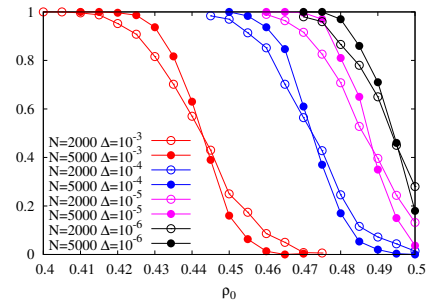

Fig. 2. Stability check of the solution determined by the EM-BP message passing algorithm. Starting the recovery process with a sparse matrix from an initial condition differing less than Δ from the correct solution, the latter is recovered as long as $\rho_0 < \alpha_{stab}(\Delta)$. In the limit $\Delta \to 0$, the stability limit $\alpha_{stab}(\Delta)$ tends to the theoretical bound α (which is 0.5).

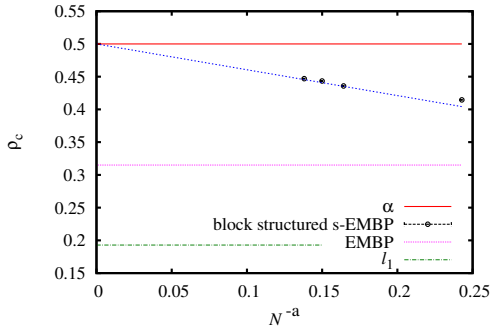

Fig. 3. $\rho_c(N)$ with a sparse, structured matrix with blocks, for different sizes N and values of L (see text). The thresholds for the ℓ_1-recovery and for EM-BP without any structure are also drawn. For comparison with the data in Fig. 5, we used the exponent $a \simeq 0.18$ best fitting those data.

similar threshold can be reached (as we have demonstrated numerically).

In summary, we can say that the EM-BP algorithm of Ref. [7] seems to reach the same threshold α_{BP}, either using a dense Gaussian matrix or a sparse binary one if the numbers of non-zero elements per row/column are $O(1)$ but sufficiently large. However, the use of a sparse matrix is computationally much faster than the use of a dense one. Moreover, the use of binary elements, instead of Gaussian real values, allows for better code optimization and eventually for hard-wired encoding of the compression process.

IV. Block-structured sparse matrices

To avoid the secondary maximum of the free entropy, in Ref. [7], the authors use a structured block matrix that helps to nucleate the correct solution. The idea is that the correct solution is found for the first variables, and then it propagates to the whole signal. This idea is similar to the so-called spatial coupling that is very useful for solving many different problems [21]. With this trick, the authors of Ref. [7] reach perfect recovery for almost any $\alpha > \rho_0$ in the large N limit while Ref. [22] reports that the gain is quite small when different recovery algorithms are used. Here, we try to use a matrix with the same block structure, but sparsely filled. We divide the N variables into L groups of size N/L and M measurements into L groups of size $M_p = \alpha_p N/L$ in such a way that $M = \sum_{p=1}^{L} M_p = \alpha N$ and $1/L \sum_{p=1}^{L} \alpha_p = \alpha$.

In this way, the matrix $\boldsymbol{F}$ is divided into L^2 blocks, labeled with indices (p, q). Each block is a sparse binary matrix with k elements different from zero for each row and $h_p = \alpha_p k$ elements for each column, distributed according to Eq. (5), with $J = J_{p,q}$. As in Ref. [7], we choose $J_{p,p-1} = J_1$, $J_{p,p} = 1$, $J_{p,p+1} = J_2$, and $J_{p,q} = 0$ otherwise. The important ingredient to nucleate the correct solution is that in the first block $\alpha_1 = (M_1/N)L > \alpha_{BP}$ holds. For simplicity, we can choose $\alpha_1 = 1$ and $\alpha_p = (L\alpha - 1)/(L - 1)$ for $p \neq 1$. The recovery strongly depends on the parameters J_1 and J_2, and the best results for $\alpha = 0.5$ are obtained around $J_1 = 4$ and $J_2 = 1$. Moreover, we used these two values in the experiments described below because we wanted to work with matrices with elements having small integer values.

Similarly to the dense case, the use of a sparse structured matrix with blocks allows to overcome the dynamical transition at α_{BP} and to nucleate the correct solution until α is very close to ρ_0. Figure 3 shows the mean critical threshold $\rho_c(N)$ for different signal lengths at a fixed compression rate $\alpha = 0.5$. The x axis uses the same scaling variable as in Fig. 5, and the best parameter a obtained from the fit of data in Fig. 5 also interpolates the data in Fig. 3 quite well. In the thermodynamic limit, ρ_c extrapolates to a value compatible with the optimal one, α, and it is certainly much higher than the thresholds for ℓ_1-recovery and for EM-BP without any structure. We have also done a density evolution analysis that confirms this result.

For each value of N and L, the mean critical threshold ρ_c is computed as follows. We randomly generate a block structured matrix $\boldsymbol{F}$ with the given N and L. We start with a sufficiently sparse original signal $\boldsymbol{s}$, which has been recovered by the algorithm; we then add non-zero entries to the signal and check whether the new signal can be recovered by the algorithm; we go on adding non-zero elements to the signal until a failure in a perfect recovery occurs. The previous to the last value for ρ_0 is the critical threshold for the matrix $\boldsymbol{F}$. The mean critical threshold is obtained by averaging over many different random matrices and signals, with the same values of N and L. The number of such random extractions goes from 10^3 for the largest N value up to 10^4 for the smallest N value.

The values of (N, L, k) used for the simulations shown in Fig. 3 are the following: $(2250, 10, 9)$, $(19000, 20, 19)$, $(31200, 40, 39)$, and $(49000, 50, 49)$. We need to increase both N and L if we want to obtain good results in the thermodynamic limit. However, if we change L, we must change k too. Indeed, in order to have the same number of

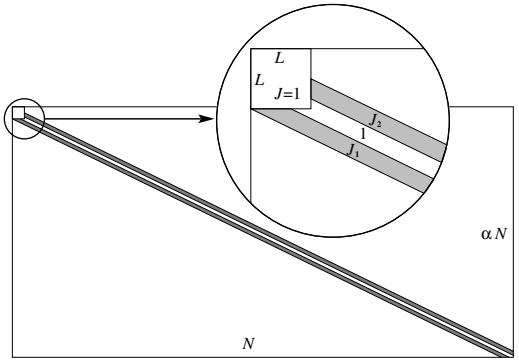

Fig. 4. A nearly one-dimensional sparse matrix with a square block of size $L \times L$ at the top left and non-zero elements in the stripes around the diagonal can achieve compression and perfect recovery close to the theoretical bound in linear time.

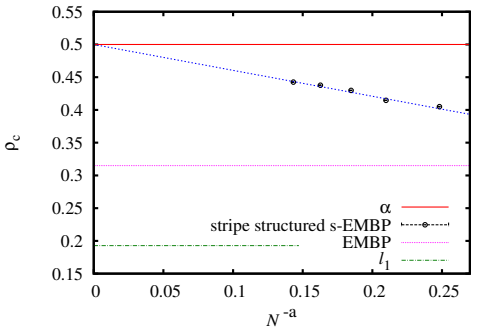

Fig. 5. $\rho_c(N)$ with a sparse, striped matrix, as described in Section V for different sizes (from $N = 2000$ to $N = 40000$). The thresholds for ℓ_1-recovery and for EM-BP without structure are drawn for comparison. The best fitting parameter is $a \simeq 0.18$, and it leads to an extrapolation of $\rho_c(N)$ in the thermodynamic limit compatible with α.

elements per row and column for each of the L^2 blocks, we must satisfy the conditions: $(N/L)/M_p = k/h_p$ with k and h_p integer valued. Here, we have used the smaller possible value for k, that is $k = L - 1$. The fact that it is impossible to keep k constant while increasing L implies that these kinds of block-structured matrices always become dense in the thermodynamic limit. This is a limitation of the block structure that we want to eliminate with the matrix proposed in the following Section.

V. And without blocks?

The matrix proposed in Ref. [7] is not the only one that allows the optimal threshold to be reached. Reference [23] analyzes the use of other good dense, block-structured matrices. However, the block-structure is not so simple to handle if one wants to do analytical calculations in the continuum limit. Moreover, in making these block-structured matrices sparse, one has to be careful to find the right values of $L, M, N, M_p, \alpha_p, k$. For these reasons, we want to know if the block structure is crucial, and, if not, we want to eliminate it.

We tried a different structured sparse matrix (see Fig. 4), that we called a striped matrix. It has one sparse square block of size L on the top left of the matrix with $K = O(1)$ elements for each row and column extracted from (5) with $J = 1$. This arrangement is fundamental for nucleating the correct solution. Apart from this first block, the residual compression rate is $\alpha' = \frac{M-L}{N-L}$. Then, we construct a one-dimensional structure around the diagonal of the remaining matrix. For each column $c > L$, we randomly place $2K\alpha'$ non-zero elements, again extracted from (5), in the interval of the width $2L\alpha'$ around the diagonal. One element with $J = 1$ is always placed on the diagonal (actually on the position closest to the diagonal). For the remaining elements, we use the following rules. If the element is at a distance $d \leq L\alpha'/3$ from the diagonal, we use $J = 1$. Otherwise, if its distance is $d > L\alpha'/3$, we use $J = J_1$ below the diagonal and $J = J_2$ above the diagonal. In this way, the number of elements per column is constant, while the number of elements per row is a truncated Poisson random variable with mean $2K$: indeed, there are no empty rows, thanks to the rule of placing the first element of each column closest to the diagonal. When constructing the matrix, we apply exactly the same rule to each column, but in the last L columns it may happen that a non-zero element has a row index larger than M: these elements are then moved below the first square matrix by changing the row and column indices as follows: $r \leftarrow r - (M - L)$ and $c \leftarrow c - (N - L)$.

In this way, we have some kind of continuous one-dimensional version of the block-structured matrix discussed in the previous Section. Within this striped matrix ensemble, the thermodynamic limit at a fixed matrix sparsity can be calculated without any problem, by sending $N, L \to \infty$ at a fixed L/N and fixed $K = O(1)$. In Fig. 5, we show the mean critical threshold reached by using striped matrices with a fixed ratio $L/N = 1/50$ (the same used in the plot of Fig. 4) and different signal lengths. Perfect decoding up to ρ_c is again achieved by using the EM-BP algorithm. We extrapolated the $\rho_c(N)$ data to the thermodynamic limit by assuming the following behavior in the large N limit:

$$\rho_c(N) = \rho_c(\infty) - bN^{-a} \tag{6}$$

The data in Fig. 5 are plotted with the best fitting parameter $a \simeq 0.18$, and the extrapolated value $\rho_c(\infty)$ is perfectly compatible with the theoretical bound α.

Hence, we can conclude that the important ingredient to reach optimality is not the block structure, but the nearly one-dimensional structure, associated with the initial block with $\alpha_1 > \alpha_{BP}$ to nucleate the correct solution.

It is worth noticing that the corresponding statistical mechanics model for these striped random matrices is a one-dimensional disordered model with an interaction range growing with the signal length, as in a Kac construction.

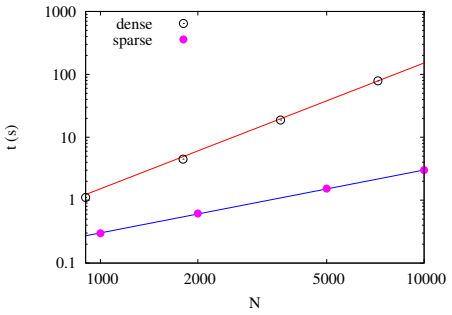

Fig. 6. Actual time (in seconds) for recovery of a signal with dense and sparse matrices for different data lengths N. The data are fitted respectively by a quadratic and a linear function.

Models of this kind are analytically solvable and have shown very interesting results [24].

The use of our striped sparse matrices allows for a great reduction in computational complexity. Indeed, the measurement and recovery times grow linearly with the size of the signal if sparse matrices are used, while they grow quadratically if dense matrices are used. Figure 6 shows the measurement and recovery times of a signal for different signal lengths N. For this test, we used dense block-structured matrices and sparse striped matrices. The number of EM-BP iterations to reach the solution is roughly constant for different N. A quadratic fit for the dense case and a linear fit for the sparse one perfectly interpolate the data.

VI. Conclusions and future development

We introduced an ensemble of sparse random matrices $\boldsymbol{F}$ that, thanks to their particular structure (see Figure 4), allow us to perform the following operations in linear time:
(i) measurement of a ρ_0-sparse vector $\boldsymbol{s}$ of length N by using a linear transformation, $\boldsymbol{y} = \boldsymbol{F}\boldsymbol{s}$, to a vector $\boldsymbol{y}$ of length αN
(ii) perfect recovery of the original vector $\boldsymbol{s}$ by using a message passing algorithm (Expectation Maximization Belief Propagation) for almost any parameter satisfying the theoretical bound $\rho_0 < \alpha$.

These striped sparse matrices that have such good performance because there is a 'seeding' sparse square matrix in the upper left corner that nucleates a seed for the right solution and the one-dimensional structure along the diagonal propagates the initial seed to the complete right solution. Both seeding and a one-dimensional structure have been used in the past [7], [21], but in our new ensemble, the matrices are sparse, and this permits us to perform all the operations in a time linear in the signal length.

We also checked that sparse matrices perform as well as dense ones in the case of block-structured matrices and for matrices with no structure at all.

Apart from the compressed sensing case, several other applications require a sparse matrix or equivalently linear time complexity [10]

In data streaming computing, one is typically interested in doing very quick measurements in constant time. For example, if the task is to measure the number of packets s_i with destination i passing through a network router, it is not possible to keep a vector $\boldsymbol{s}$ because it is generally too long. Instead, a much shorter sketch of it, $\boldsymbol{y} = \boldsymbol{F}\boldsymbol{s}$, is measured in such a way that a very sparse vector $\boldsymbol{s}$ can be recovered from $\boldsymbol{y}$. The matrix $\boldsymbol{F}$ must be sparse in order to be able to update the sketch $\boldsymbol{y}$ in a constant time for each new packet passing through the router.

Another interesting application is the problem of group testing, where a very sparse vector $\boldsymbol{s} \in \{0,1\}^N$ is given and one is interested in performing the fewest linear measurements, $\boldsymbol{y} = \boldsymbol{F}\boldsymbol{s}$, that allow for detection of the defective elements ($s_i = 1$). In this case, the experimental constraints require a sparse matrix $\boldsymbol{F}$: only if the tested compound $y_\mu = \sum_i F_{\mu i} s_i$ is made of a very few elements of $\boldsymbol{s}$, the linear response holds and non-linear effects can be ignored.

However, in the more general case, one does not directly observe the sparse signal $\boldsymbol{s}$ but rather a linear transformation of it, $\boldsymbol{x} = \boldsymbol{D}\boldsymbol{s}$, made with a dictionary matrix $\boldsymbol{D}$ (which is typically a Fourier or wavelet transformation, and thus is a dense matrix). In this more difficult case, one would like to design a sparse measurement matrix $\boldsymbol{A}$ such that the measurement/compression operation, $\boldsymbol{y} = \boldsymbol{A}\boldsymbol{x}$, is fast, and the resulting observed data $\boldsymbol{y}$ is short, thanks to the sparseness of $\boldsymbol{s}$. The conflicting requirement is to have a fast recovery scheme, because, now, to recover the original signal one should solve $\hat{\boldsymbol{s}} = \operatorname{argmin} ||\boldsymbol{s}||_0$ subject to $\boldsymbol{y} = (\boldsymbol{A}\boldsymbol{D})\boldsymbol{s}$, where $\boldsymbol{A}\boldsymbol{D}$ is typically dense (e.g. in case of Fourier and wavelet transformations). So a very interesting future development of the present approach is to extend it to this more complex case.

Acknowledgments

FR-T is grateful for his useful discussions with F. Krzakala, M. Mézard and L. Zdeborova and financial support from the Italian Research Minister through the FIRB Project No. RBFR086NN1 on "Inference and Optimization in Complex Systems: From the Thermodynamics of Spin Glasses to Message Passing Algorithms".

YK is supported by grants from the Japan Society for the Promotion of Science (KAKENHI No. 22300003) and the Mitsubishi foundation.

References

[1] E. J. Candès and M. B. Wakin, "An Introduction To Compressive Sampling," *IEEE Signal Processing Magazine*, vol. 25, pp. 21–30, 2008.
[2] M. A. T. Figueiredo, R. D. Nowak and S. J. Wright, "Gradient Projection for Sparse Reconstruction: Application to Compressed Sensing and Other Inverse Problems," *IEEE Journal of Selected Topics in Signal Processing* vol. 1, pp. 586–597, 2007.
[3] R. Cartrand and W. Yin, "Iteratively reweighted algorithms for compressive sensing," in *IEEE International Conference on Acoustics, Speech and Signal Processing, 2008*, pp. 3869–3872, 2008.
[4] W. Yin, S. Osher, D. Goldfarb and J. Darbon, "Bregman Iterative Algorithms for ℓ_1-Minimization with Applications to Compressed Sensing," *SIAM J. Imaging Sciences*, vol. 1, pp. 143–168, 2008.
[5] T. Blumensath and M. E. Davies, "Iterative hard thresholding for compressedsensing," *Applied and Computational Harmonic Analysis*, vol. 27, pp. 265–274, 2009.

[6] D. L. Donoho, A. Maleki and A. Montanari, "Message-passing algorithms for compressed sensing," *PNAS*, vol. 106, 18914–18919, 2009.
[7] F. Krzakala, M. Mézard, F. Sausset, Y. F. Sun and L. Zdeborova, "Statistical-physics-based reconstruction in compressed sensing," *Phys. Rev. X*, vol. 2, 021005 (18pages), 2012.
[8] D. L. Donoho, A. Javanmard and A. Montanari, "Information-Theoretically Optimal Compressed Sensing via Spatial Coupling and Approximate Message Passing," arXiv:1112.0708, 2008.
[9] R. Berinde and P. Indyk, "Sparse recovery using sparse random matrices," Preprint, 2008.
[10] A. Gilbert and P. Indyk, "Sparse Recovery Using Sparse Matrices," *Proceedings of the IEEE*, vol. 98, pp. 937–947, 2010.
[11] M. Akçakaya, J. Park and V. Tarokh, "A Coding Theory Approach to Noisy Compressive Sensing Using Low Density Frames," *IEEE Trans. on Signal Processing*, vol. 59, pp. 5369–5379, 2011.
[12] Y. Kabashima and T. Wadayama, " A signal recovery algorithm for sparse matrix based compressed sensing," arXiv:1102.3220, 2011.
[13] D. Baron, S. Sarvotham and R. G. Baranuik, "Bayesian Compressive Sensing via Belief Propagation," *IEEE Trans. on Signal Processing*, vol. 58, pp. 269–280, 2010.
[14] J. P. Vila and P. Schniter, "Expectation-Maximization Bernoulli-Gaussian Approximate Message Passing," in Proc. Asilomar Conf. on Signals, Systems, and Computers (Pacific Grove, CA), Nov. 2011.
[15] S.-Y. Chung, G. D. Forney Jr., T. J. Richardson and R. Urbanke, "On the Design of Low-Density Parity-Check Codes within 0.0045 dB of the Shannon Limit," *IEEE Comm. Lett.*, vol. 58 no.2, pp. 58-60, 2000.
[16] Y. Kabashima, "A CDMA multiuser detection algorithm on the basis of belief propagation," J. Phys. A, vol. 36, pp. 11111–11121, 2003.
[17] D. Guo and C. Wong, "Asymptotic Mean-Square Optimality of Belief Propagation for Sparse Linear Systems," in Proc. of Information Theory Workshop 2006, pp. 194–198, 2006.
[18] A. Montanari and D. Tse, "Analysis of Belief Propagation for Non-Linear Problems: The Example of CDMA (or: How to Prove Tanaka's Formula)," arXiv:cs/0602028, 2006.
[19] S. Rangan, "Estimation with random linear mixing, belief propagation and compressed sensing," *Proc. Conf. Inf. Sci. Syst.*, Princeton, NJ, pp. 1–6, 2010.
[20] D. J. Thouless, P. W. Anderson and R. G. Palmer, "Solution of 'Solvable model of a spin glass'," *Phil. Mag.*, vol. 35, pp. 593–601, 1977.
[21] S. H. Hassani, N. Macris and R. Urbanke, "Coupled graphical models and their thresholds," arXiv:1105.0785, 2011.
[22] S. Kudekar and H. D. Pfister, "The Effect of Spatial Coupling on Compressive Sensing," in Proc. the 48th Annual Allerton Conference on Communication, Control, and Computing, 2010.
[23] F. Krzakala, M. Mézard, F. Sausset, Y. Sun and L. Zdeborova, "Probabilistic Reconstruction in Compressed Sensing: Algorithms, Phase Diagrams, and Threshold Achieving Matrices," arXiv:1206.3953, 2012.
[24] S. Franz and A. Montanari, "Analytic determination of dynamical and mosaic length scales in a Kac glass model," J. Phys. A, vol. 40, pp. F251–F257, 2007.

Journal of Statistical Mechanics: Theory and Experiment
An IOP and SISSA journal

Entropic long range order in a 3D spin glass model

Maria Chiara Angelini[1] **and Federico Ricci-Tersenghi**[2]

[1] Dipartimento di Fisica, Università La Sapienza, Piazzale Aldo Moro 5, 00185 Roma, Italy
[2] Dipartimento di Fisica, INFN—Sezione di Roma 1 and CNR—IPCF, UOS di Roma, Università La Sapienza, Piazzale Aldo Moro 5, 00185 Roma, Italy
E-mail: Maria.Chiara.Angelini@roma1.infn.it and Federico.Ricci@roma1.infn.it

Received 24 November 2010
Accepted 3 January 2011
Published 1 February 2011

Online at stacks.iop.org/JSTAT/2011/P02002
doi:10.1088/1742-5468/2011/02/P02002

Abstract. We uncover a new kind of *entropic* long range order in finite dimensional spin glasses. We study the link-diluted version of the Edwards–Anderson spin glass model with bimodal couplings ($J = \pm 1$) on a 3D lattice. By using *exact* reduction algorithms, we prove that there exists a region of the phase diagram (at zero temperature and low enough link density), where spins are long range correlated, even if the ground state energy stiffness is null. In other words, in this region twisting the boundary conditions costs no energy, but spins are long range correlated by means of pure entropic effects.

Keywords: phase diagrams (theory), disordered systems (theory), spin glasses (theory)

ArXiv ePrint: 1007.1922

J. Stat. Mech. (2011) P02002

1742-5468/11/P02002+11$33.00

The low temperature phase of frustrated spin models is a very interesting and much debated subject [1]. Especially in models with discrete couplings, on lowering the temperature the frustration may produce surprising effects. For example, the classical 'order by disorder' effect discovered by Villain *et al* [2] shows up in 2D frustrated spin systems, where the ground states (GSs) have no magnetization, while a spontaneous magnetization is present at any positive temperature smaller than the critical one, $0<T<T_c$ (and this is a rather counterintuitive result!). In this case, the explanation is simple: due to the frustration, two subsets of GS exist, having ferromagnetic and antiferromagnetic long range order respectively; these GSs have exactly the same energy and so, at zero temperature ($T = 0$), they perfectly compensate each other, leading to null global magnetization; nonetheless, at positive temperatures, the energy of the ferromagnetic state is lower than the antiferromagnetic one and a long range (ferromagnetic) order is recovered. This example evidences the importance of exact cancelations at $T = 0$ in frustrated models.

Among frustrated models, spin glasses (SGs) [3] have a very complex low temperature phase. Entropy fluctuations in SGs with discrete couplings are known to play an important role and are most probably the main mechanism for making the free-energy spectrum gapless [4].

In this work we study 3D spin glasses with binary couplings ($J = \pm 1$) at $T = 0$, showing that frustration in SGs generates an effect even more impressive than the one found by Villain *et al*: a long range order only due to *entropic* effects. More precisely, in this entropically ordered SG phase, a typical SG sample has many GSs with exactly the same energy, such that, summing over all these GSs, no long range order is found in the system at $T = 0$. However, on a closer look, all these GSs are not really equivalent and taking into account also the entropic contribution to the $T = 0$ exact computation, we find that a subset of GSs is dominating the Gibbs measure and thus leads to long range order in the system.

In order to explain the entropic long range order more simply, we consider a pair of spins, σ_i and σ_j, at a very large distance, $|i - j| \simeq L$ (with L the system size) and try to estimate their thermodynamic correlation $\langle\sigma_i\sigma_j\rangle$ at $T = 0$ by computing the probabilities of being parallel or antiparallel, $\mathbb{P}[\sigma_i = \pm\sigma_j]$. The method that is typically employed computes the GS energy at fixed (relative) values of σ_i and σ_j: if the resulting GS energy difference $|E_{\rm GS}(\sigma_i = \sigma_j) - E_{\rm GS}(\sigma_i = -\sigma_j)|$ (the so-called energy stiffness) does not grow with L the system is believed to have no long range order. But this conclusion is wrong! Indeed, even if $E_{\rm GS}(\sigma_i = \sigma_j) = E_{\rm GS}(\sigma_i = -\sigma_j)$, the relative orientation of σ_i and σ_j still depends on the *number* of GSs, $\mathcal{N}_{\rm GS}$, with given values of σ_i and σ_j:

$$\mathbb{P}[\sigma_i = \pm\sigma_j] \propto \mathcal{N}_{\rm GS}(\sigma_i = \pm\sigma_j) \propto \exp[S_{\rm GS}(\sigma_i = \pm\sigma_j)],$$

where $S_{\rm GS}$ is the GS entropy. If the entropy difference $|S_{\rm GS}(\sigma_i = \sigma_j) - S_{\rm GS}(\sigma_i = -\sigma_j)|$ grows with L, then $|\langle\sigma_i\sigma_j\rangle| \to 1$ in the thermodynamical limit and the system shows an entropic long range order (the energy stiffness being null). Please note that the present entropic effect is taking place also at $T = 0$, while Villain's 'order by disorder' requires a positive temperature because it is due to an energy difference.

We are going to show, by exact reduction algorithms, that such an entropic long range order exists in SGs with discrete couplings on regular lattices in finite dimensions. We consider a link-diluted 3D Edwards–Anderson model defined by the Hamiltonian

doi:10.1088/1742-5468/2011/02/P02002

J. Stat. Mech. (2011) P02002

$H = -\sum_{<ij>} \sigma_i J_{ij} \sigma_j$, where the sum is over all the nearest neighbor pairs of a 3D simple cubic lattice of length L. The couplings J_{ij} are quenched, independent and identically distributed random variables extracted from the distribution

$$P_J(J) = (1-p)\delta(J) + \frac{p}{2}[\delta(J-1) + \delta(J+1)], \tag{1}$$

where $p \in [0,1]$ is the density of non-zero couplings.

This model has a critical line in the (p,T) plane that separates the paramagnetic phase from the SG phase. It was already shown by Bray and Feng [5] that, while in a model with a continuous coupling distribution this critical line ends for $T=0$ at the geometric link percolation threshold p_c [7], for discrete couplings the paramagnetic phase does extend beyond p_c, because of exact cancellations between positive and negative couplings. Let us call p_{SG} the critical value separating the paramagnetic from the SG phase at $T=0$. A tentative estimation of p_{SG} has been provided by Boettcher [6] by considering the 'defect' energy ΔE_{GS} between the GS energies obtained by swapping between periodic and anti-periodic boundary conditions along one direction. He found that for $p > p^* = 0.272(1)$ the variance of ΔE_{GS} grows with L (the mean being null by symmetry) thus leading to a SG long range order. After the work of Boettcher the threshold p^* has been identified with p_{SG}, but this is not generally true (as we are going to show now). In general only the inequality $p_{SG} \leq p^*$ holds. Recently in [8] the same model has been solved exactly on the hierarchical lattice, showing that $T=0$ computations can lead to misleading results. Indeed, while at $T=0$ the model shows a phase transition at p^*, the exact solution at positive temperatures predicts a critical line in the (p,T) plane ending in $(p_{SG},0)$, with $p_c < p_{SG} < p^*$ (strict inequalities hold). The right critical point p_{SG} is clearly sensitive to entropic effects, that are neglected in the computation of p^*. The determination of the p_{SG} value can be made by simply considering first order corrections in temperature to the $T=0$ computations. Thus, in the rest of the paper, we are going to work in this $T=0^+$ limit.

On a 3D cubic lattice the model cannot be solved exactly and Monte Carlo methods are very inefficient at low temperatures. To determine the right critical point p_{SG}, we are going to apply some exact decimation rules that reduce the system to a much smaller size, which can then be easily solved by numerical methods.

We consider periodic boundary conditions in the x and y directions, while spins in $z=0$ and $z=L-1$ are linked respectively to two different external spins, with quenched, independent and identically distributed random couplings extracted from the distribution in equation (1). The addition of these external spins does not modify the thermodynamic limit but it is very useful: to check for percolation it will be enough to find a path of non-zero couplings between these two external spins, while to check for the presence of long range order one can just measure the correlation between these two spins. So, in general, one will be satisfied with the computation of the effective coupling between the two external spins.

Given that the model is link diluted, we can eliminate recursively weakly connected spins, generalizing what was done in [6, 8]. In the original model the couplings are T-independent, but, by decimating spins, effective couplings are created whose intensity will depend on temperature. If we want to find entropic effects, the first order correcting term in T cannot be neglected, even when studying the system in the $T=0$ limit. For infinitesimal T, we can write the effective coupling as $J = \mathrm{sgn}(I)(|I| - TK)$ if $I \neq 0$ or

J. Stat. Mech. (2011) P02002

$J = TK$ if $I = 0$, where I and K are the energetic and entropic coupling respectively. The choice for the relative sign is dictated by the fact that thermal fluctuations decrease the coupling intensity. Spins and bonds are decimated using the following five rules.

(R1) A zero- or one-connected spin is eliminated.

(R2) A two-connected spin σ is eliminated and an effective coupling J_{12} is created between the two neighboring spins, σ_1 and σ_2, satisfying the equation

$$\sum_{\sigma=\pm1} \mathrm{e}^{(J_1\sigma\sigma_1+J_2\sigma\sigma_2)/T} \equiv A\mathrm{e}^{J_{12}\sigma_1\sigma_2/T},$$

for any choice of σ_1 and σ_2. Expanding at first order in T the two members, we have for the energetic component

$$I_{12} = \tfrac{1}{2}\Big(|I_1 + I_2| - |I_1 - I_2|\Big),$$

and for the entropic component

$$\begin{array}{ll} K_{12} = K_1 & \text{if } |I_1| < |I_2|, \\ \mathrm{e}^{2K_{12}} = \mathrm{e}^{2K_1} + \mathrm{e}^{2K_2} & \text{if } |I_1| = |I_2| \neq 0, \\ \tanh(K_{12}) = \tanh(K_1)\tanh(K_2) & \text{if } I_1 = I_2 = 0. \end{array}$$

(R3) Two bonds J^1_{ij} and J^2_{ij} between two spins i and j can be replaced by an effective coupling J_{ij} with components $I_{ij} = I^1_{ij} + I^2_{ij}$ and $K_{ij} = K^1_{ij} + K^2_{ij}$.

(R4) A three-connected spin σ is eliminated and effective couplings are created between the three neighboring spins σ_1, σ_2 and σ_3, satisfying the equation

$$\sum_{\sigma=\pm1} \mathrm{e}^{(J_1\sigma\sigma_1+J_2\sigma\sigma_2+J_3\sigma\sigma_3)/T} \equiv A\mathrm{e}^{(J_{12}\sigma_1\sigma_2+J_{23}\sigma_2\sigma_3+J_{31}\sigma_3\sigma_1)/T},$$

for any choice of σ_1, σ_2 and σ_3. Expanding at first order in T the two members, and introducing the couplings $\widetilde{J}_0 = J_1 + J_2 + J_3$ and $\widetilde{J}_k = \widetilde{J}_0 - 2J_k$ with $k = 1, 2, 3$, we get for the energetic components

$$I_{12} = \tfrac{1}{4}\Big(|\widetilde{I}_0| - |\widetilde{I}_1| - |\widetilde{I}_2| + |\widetilde{I}_3|\Big), \tag{2}$$

$$I_{13} = \tfrac{1}{4}\Big(|\widetilde{I}_0| - |\widetilde{I}_1| + |\widetilde{I}_2| - |\widetilde{I}_3|\Big), \tag{3}$$

$$I_{23} = \tfrac{1}{4}\Big(|\widetilde{I}_0| + |\widetilde{I}_1| - |\widetilde{I}_2| - |\widetilde{I}_3|\Big), \tag{4}$$

and for the entropic components

$$K_{12} = \tfrac{1}{4}\Big(f(\widetilde{J}_0) - f(\widetilde{J}_1) - f(\widetilde{J}_2) + f(\widetilde{J}_3)\Big), \tag{5}$$

$$K_{13} = \tfrac{1}{4}\Big(f(\widetilde{J}_0) - f(\widetilde{J}_1) + f(\widetilde{J}_2) + f(\widetilde{J}_3)\Big), \tag{6}$$

$$K_{23} = \tfrac{1}{4}\Big(f(\widetilde{J}_0) + f(\widetilde{J}_1) - f(\widetilde{J}_2) - f(\widetilde{J}_3)\Big), \tag{7}$$

where $f(J) = |K| + \ln(1 + \mathrm{e}^{-2|K|})$ if $I = 0$ and $f(J) = \mathrm{sign}(I)K$ if $I \neq 0$.

doi:10.1088/1742-5468/2011/02/P02002

J. Stat. Mech. (2011) P02002

(R5) A spin σ of any connectivity is eliminated if the number n_I of its couplings with a non-zero energetic component ($I \neq 0$) does not exceed three ($n_I \leq 3$). If $i, j = 1, \ldots, n_I$ index the spins connected to σ by couplings with $I \neq 0$, and if k indexes the other neighbors (for which $I_k = 0$), then the new couplings J_{ij} are computed following previous rules, while the new couplings $J_{ik} = \mathrm{sgn}(J_i)J_k$, i.e. $I_{ik} = 0$ and $K_{ik} = \mathrm{sgn}(I_i)K_k$.

We have applied recursively the above five rules in the order they are listed: i.e., at each decimation step, we try to use rule R1, and, only if it does not apply, we try to use rule R2, and if it does not apply, we try to use rule R3, and so on. The decimation process stops when it reaches a reduced graph where none of the above five rules can be applied. This reduced graph does depend on the order in which the above rules are applied (because rules R4 and R5 increase the degree of neighboring spins), and the order we have chosen is the one producing the smallest reduced graph.

If the couplings have a discrete spectrum then rule R3 may produce exact cancellations, thus leading to null effective couplings: this is the reason why $p_{\mathrm{SG}} > p_{\mathrm{c}}$ holds in general for models with discrete couplings. Applying the above rules recursively it is possible that, starting with only energetic couplings, the final effective coupling has only the entropic component (the energetic one being null). In this situation it is clear that entropic couplings are essential even in the $T = 0$ limit.

First of all we study percolation properties of the networks of I and K effective couplings that result from the recursive application of the above rules to all bonds and spins (except the external ones, that we want to keep). We are mainly interested in the percolation thresholds, p_{c}^I and p_{c}^K, for the energetic and the entropic components. These percolation thresholds do depend on the set of reduction rules and increase if more rules are used[3]. In figure 1 we show the percolation probabilities of the networks of I and K effective couplings for many different lattice sizes as a function of the link density p. By studying the crossing points p_{L_1,L_2} of these probabilities for sizes L_1 and $L_2 = rL_1$ with fixed r (we use $r = 3/4,\ 3/2,\ 2$) we have been able to estimate the percolation thresholds p_{c}^I and p_{c}^K through fits including the first scaling correction [9]: $p_{L,rL} = p_{\mathrm{c}} + A_r L^{-1/\nu-\omega}$, as shown in the inset of figure 1. The resulting values are $p_{\mathrm{c}}^I = 0.264\,75(10)$ and $p_{\mathrm{c}}^K = 0.251\,61(5)$. The value of p_{c}^I is correctly lower than $p^* = 0.272(1)$, the threshold value where a positive energy stiffness emerges: the fact that p_{c}^I and p^* in general differ can be easily understood by considering the 2D EA model, which is clearly percolating, but has negative energy stiffness. Moreover p_{c}^K is lower than p_{c}^I because the applied decimation rules leave the energetic component rational, while the entropic one may become real, thus leading to much less exact cancellations. Please note that p_{c}^K provides a lower bound to p_{SG} given that geometrical percolation of the effective couplings is a necessary, but not sufficient, condition to have SG long range order.

In the thermodynamic limit, for densities smaller than p_{c}^I, the energetic component I is not percolating and cannot induce any long range order. Therefore, in the link density region $p_{\mathrm{c}}^K < p < p_{\mathrm{c}}^I$ an eventual thermodynamic phase transition can be due solely to entropic effects.

[3] The five rules that we use are all those that keep the interactions pairwise. Indeed decimating a four-connected spin would produce a four-spins effective interaction.

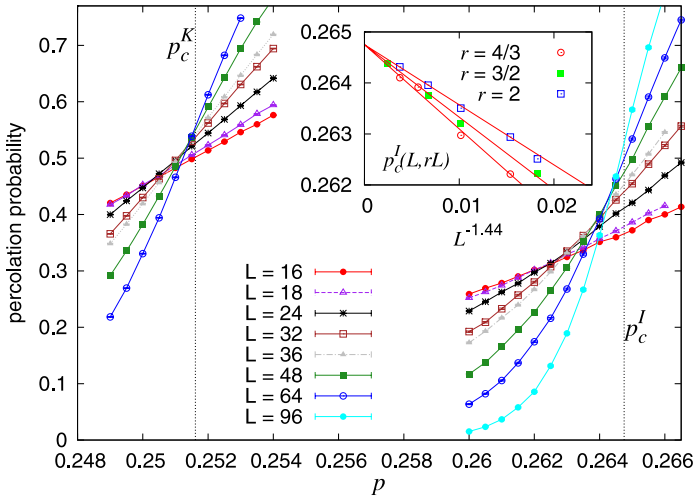

Figure 1. Percolation probability for different lattice sizes L as a function of the link density p for the energetic (right) and the entropic (left) part of the effective couplings. Inset: the infinite volume extrapolation for p_c^I.

To search for such an entropic phase transition, we further reduce the decimated graph. For $p_c^K < p < p_c^I$, with high probability in the large L limit, the decimated graph is percolating solely in K, while the I couplings form clusters of finite size (similarly to what happens in standard percolation below p_c). An example of the resulting graph after the decimation process is shown on the left side of figure 2, where full (respectively dashed) lines represent couplings with (respectively without) a non-null energetic component I. The two circles represent what we call I-clusters, that is groups of spins connected by couplings with a non-null energetic component I (note, however, that inside these I-clusters also couplings with only the entropic component K may exist, as in the rightmost circle in figure 2). The connections between any two different I-clusters have only entropic components.

Our idea is to map the original problem to a smaller and simpler one, where the variables are the I-clusters, that interact only through entropic couplings, as on the right side of figure 2.

Given that we are interested in the $T = 0$ limit, each I-cluster must be in a ground state (GS) configuration. So, for each I-cluster $\mathcal{C}$, we compute with an exact branch and bound algorithm all its $\mathcal{N}_\mathcal{C}$ GSs. We introduce then a Potts variable $\tau_\mathcal{C}$ for that I-cluster, taking values in $[1, \mathcal{N}_\mathcal{C}]$. We call $\{\sigma_i^\mathcal{C}(\tau_\mathcal{C})\}$ the GS configurations of the $\mathcal{C}$ cluster.

Working at $T = 0$, the GSs are calculated by taking into account solely the energetic component I of the couplings. Afterwards we consider also the entropic components K, that give rise to two different interacting terms. K bonds connecting two spins in the same I-cluster produce a self-interaction term

$$E^\mathcal{C}(\tau_\mathcal{C}) = \sum_{i,j\in\mathcal{C}} K_{ij}\sigma_i^\mathcal{C}(\tau_\mathcal{C})\sigma_j^\mathcal{C}(\tau_\mathcal{C}).$$

doi:10.1088/1742-5468/2011/02/P02002

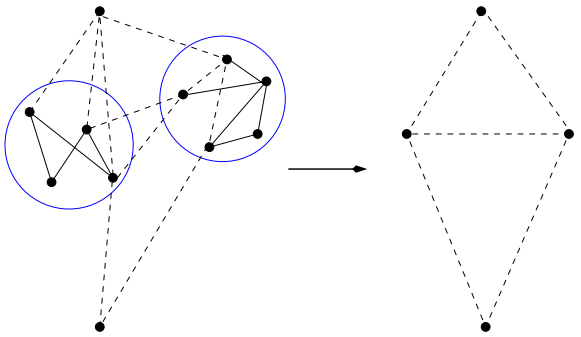

Figure 2. On the left we show an example of the system after the decimation. Full lines represent couplings with $I \neq 0$, while dashed lines represent couplings with $I = 0$. The two I-clusters are enclosed in circles and are connected only by purely entropic couplings. On the right, the system is mapped on a Potts model where each variable represents an I-cluster. These Potts variables are connected by effective entropic couplings taking into account all the interactions originally connecting the I-clusters. Please note that our decimation rules always produce a reduced system with degree not smaller than four, but here we have drawn fewer lines for the sake of figure readability.

This quantity may bias the choice among degenerate GSs even in the $T = 0$ limit. In the new Potts model, it can be interpreted like an external field acting on the Potts variable $\tau_{\mathcal{C}}$ that may bias its value.

K bonds connecting spins in different I-clusters generate the interaction between the Potts variables. This interaction depends on the configurations of both clusters, and so must be represented as a matrix

$$M^{\mathcal{C},\mathcal{C}'}(\tau_{\mathcal{C}}, \tau_{\mathcal{C}'}) = \sum_{i\in\mathcal{C}, j\in\mathcal{C}'} K_{ij}\sigma_i^{\mathcal{C}}(\tau_{\mathcal{C}})\sigma_j^{\mathcal{C}'}(\tau_{\mathcal{C}'}).$$

The Gibbs–Boltzmann measure for the reduced Potts model is then

$$\mu\Big(\{\tau_{\mathcal{C}}\}\Big) \propto \exp\Big[\sum_{\mathcal{C},\mathcal{C}'} M^{\mathcal{C},\mathcal{C}'}(\tau_{\mathcal{C}}, \tau_{\mathcal{C}'}) + \sum_{\mathcal{C}} E^{\mathcal{C}}(\tau_{\mathcal{C}})\Big]. \tag{8}$$

It is important to note that this measure does not depend on the temperature, because entropic couplings have a linear dependence on T that cancels the $1/T$ term in the Boltzmann factor. The Potts measure in equation (8) is an *exact* effective description of the original SG model at temperature $T = 0^+$, having many fewer variables and a smaller complexity with respect to the original model.

In order to locate a possible SG transition, we compute the correlation between the external spins under the measure μ in equation (8). If the effective Potts model has a linear topology, namely each variable has at most two neighbors, we solve it exactly by the transfer matrix method (the probability P to have these 'linear' systems is rather high: e.g., around the critical density p_{SG}, $P > 0.9$ for $L \leq 24$, $P \simeq 0.7$ for $L = 32$, $P \simeq 0.6$ for $L = 36$ and $P \simeq 0.2$ for $L = 48$). Otherwise we use a Metropolis Monte Carlo

J. Stat. Mech. (2011) P02002

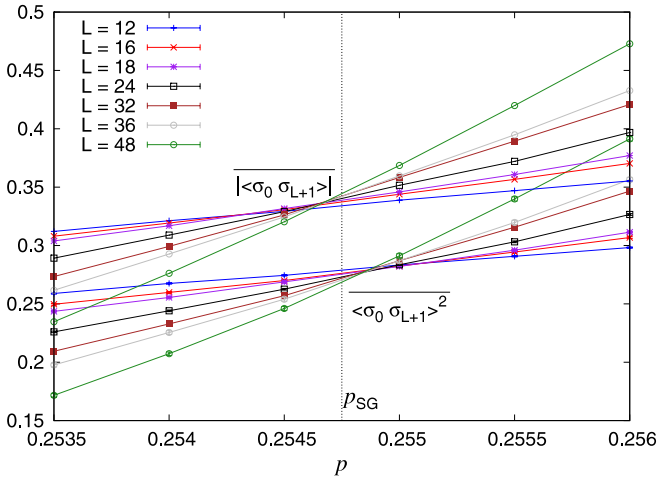

Figure 3. Average of square (below) and absolute value (above) of correlations at distance L, for different lattice sizes, as a function of link density p. The errors are not larger than the symbols.

method to sample the measure in equation (8), and the equilibration of the Markov chain is not an issue given the small number of variables. Since the Gibbs–Boltzmann measure in equation (8) does not depend on temperature, one can think of it as that of a Potts model at $\beta = 1$. Thus, for equilibrating the corresponding Markov chain, we perform a simulated annealing from $\beta = 0$ to 1, with steps $\Delta\beta = 0.1$ and different cooling rates (100, 300 and 1000 Monte Carlo steps per temperature). We checked that the average of the interesting quantities, like the correlations, does not depend on the cooling rate.

For the very few samples that show percolation in the energetic components, we assume a correlation between external spins equal to one. This approximation makes no error in the thermodynamical limit as long as $p < p_c^I$.

Being interested in a SG long range order, we show in figure 3 the average over the samples of the square and of the absolute value of the correlation between the external spins (which are at distance L in the original model) as a function of the link density p. This quantity should decrease with L in a paramagnetic phase, while it should grow with L if a SG long range order is present: thus the crossing point of the curves in figure 3 roughly identifies the critical density p_{SG}. Our best estimation for p_{SG} has been obtained by the finite size analysis of the crossing points of the correlations measured in systems of sizes L and sL, that should scale as

$$p_{cross}(L, sL) = p_{SG} + B_s L^{-1/\nu-\omega}.$$

In figure 4 we show the values of p_{cross} obtained with $s = 1.5$ and 2, together with the best fits. In the abscissa we have used the scaling variable L^{-2} that provides the best joint fit to all the data shown in the figure. However the uncertainty on this scaling exponent is large given the very small spread of p_{cross} around p_{SG} for the sizes we have studied. Our final estimation for the SG critical threshold is $p_{SG} = 0.254\,73(3)$.

doi:10.1088/1742-5468/2011/02/P02002

J. Stat. Mech. (2011) P02002

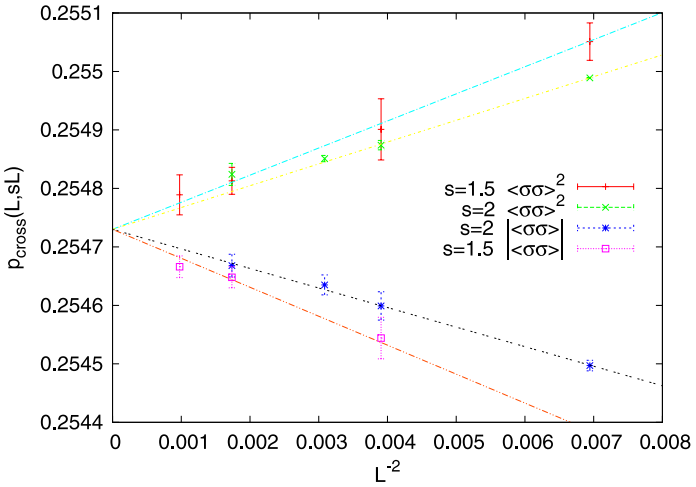

Figure 4. Crossing points of the data shown in figure 3 with sizes L and sL as a function of L^{-2}.

By studying the slopes of the data shown in figure 3 at the critical point $p_{\rm SG}$ as a function of the system size we have been able to obtain an estimation of the exponent ν controlling the shrinking of the critical region and we get $\nu = 0.9(1)$. This value for the ν exponent does not coincide with the one measured at criticality for the undiluted ($p = 1$) or weakly diluted ($p = 0.45$) EA model, which is $\nu_T = 2.2$ (the subscript T should remind us that this exponent is related to the shrinking of the critical region in temperature). However a simple argument gives the connection between the two exponents: if the critical line close to the $T = 0$ fixed point behaves like $T_{\rm SG}(p) \propto (p - p_{\rm SG})^{\phi}$, then $1/\nu_T = \phi/\nu$. Our results thus suggest a value $\phi \simeq 0.4$ for the shape of the critical line.

We have shown that in 3D spin glasses frustration and coupling discreteness may induce an entropic long range order: in this phase the energy stiffness is zero (i.e. boundary conditions can be changed at no energy cost), but the states with largest entropy dominate the Gibbs measure. This dramatic effect of entropic contributions to the Gibbs states has been extensively studied in mean-field models of spin glasses with finite connectivity at $T = 0$, especially in the context of random constraint satisfaction problems [10]–[12]. However in the present work we have proved the existence of such an entropic phase in a 3D spin glass model. Moreover this *entropy dominated SG phase* should persist also at positive temperatures as long as $p \lesssim p^*$ and the energy stiffness is null (see figure 5).

One may question why perfectly discrete couplings are difficult to find in Nature. Nonetheless if one considers a model with quasi-discrete couplings (e.g. integer values plus a small Gaussian term of variance $\sigma^2 \ll 1$) the critical line looks like the dotted curve in figure 5: it mainly follows the critical line of the corresponding model with discrete couplings and only for $T \lesssim \sigma$ moves towards $p_{\rm c}$. It is clear that the identification of such a critical line is based on the correct estimation of $p_{\rm SG}$ in the model with discrete couplings.

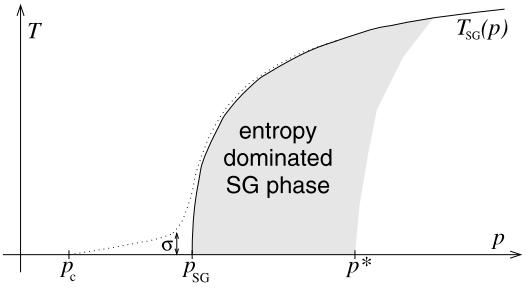

Figure 5. A schematic phase diagram in the (p, T) plane, showing that entropic long range order must exist also at positive temperatures. The dotted curve is the critical line of a model with quasi-discrete coupling.

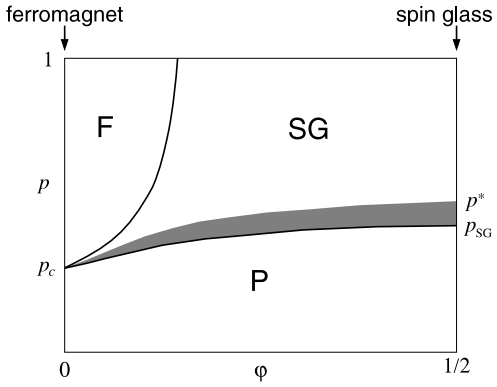

Figure 6. Conjectured phase diagram at $T = 0^+$ by varying the level of frustration φ in the model. The entropically long ranged phase should exist for any frustrated model, $\varphi > 0$, with discrete energy levels.

One more comment about the generality of our results regards what happens when couplings have a ferromagnetic bias. Indeed perfectly symmetric coupling (i.e. with a null mean, $\overline{J_{ij}} = 0$) are again difficult to find in Nature, and it is important to check whether the entropic long range order is stable with respect to the addition of a ferromagnetic bias in the couplings. The answer is contained in the pictorial phase diagram shown in figure 6, where the link density p is reported as a function of some degree of frustration φ. A quantitative measure for φ on a regular lattice can be, for example, the fraction of frustrated elementary plaquettes: for $\varphi = 0$ we have a pure ferromagnetic model, while for $\varphi = 1/2$ we have the spin glass model studied in this work. In this phase diagram, the addition of a ferromagnetic bias in the couplings corresponds to reducing the value of φ with respect to the value $\varphi = 1/2$ it takes in a spin glass model with symmetrically distributed couplings. The phase diagram shown pictorially in figure 6 contains, in general, three different phases: a paramagnetic one (P), a spin glass one (SG) and a ferromagnetic

one (F). Moreover, along the SG–F boundary a mixed phase can exist [13], containing a diverging number of states with a non-null magnetization (but here we do not want to enter the long-standing debate about the nature of the spin glass phase in 3D models). In figure 6 the gray region is our educated guess about the location of the entropically long range ordered phase: in other words we conjecture the presence of such a phase in any frustrated model ($\varphi > 0$) with discretized energy levels.

An important comment regards the implications of our results on the studies of the low temperature phase of SG models made by means of GS computations. In these numerical studies one or few GSs are usually computed per sample, under different boundary conditions, and only the GS energies are considered. Unfortunately this kind of study is not able to identify the entropic long range order. In the light of our results, this kind of numerical studies should be modified either by considering the first order correction in temperature when decimating the variables, or by computing many (or all) GS per sample, so as to identify the state which is entropically dominating. Some steps in this direction have been already taken in [14], where it has been recognized that a correct estimation of the GS clusters' entropy is necessary to extend predictions at positive temperatures.

Last, but not least, the present best estimation for the lower critical dimension in SGs, $d_L \simeq 2.5$, is based on GS energy stiffness computations [6], which ignore entropic effects. Most probably this result needs to be modified to a lower value due to the entropic long range order.

References

[1] Diep H T, 2005 *Frustrated Spin Systems* (Singapore: World Scientific)
[2] Villain J *et al*, 1980 *J. Physique* **41** 1263
[3] Fischer K H and Hertz J, 1993 *Spin Glasses* (Cambridge: Cambridge University Press)
Young A P, 1998 *Spin Glasses and Random Fields* (Singapore: World Scientific)
[4] Krzakala F and Martin O, 2001 *Europhys. Lett.* **53** 749
Jörg T *et al*, 2006 *Phys. Rev. Lett.* **96** 237205
[5] Bray A J and Feng S, 1987 *Phys. Rev.* B **36** 8456
[6] Boettcher S, 2004 *Europhys. Lett.* **67** 453
Boettcher S, 2004 *Eur. Phys. J.* B **38** 83
Boettcher S, 2005 *Phys. Rev. Lett.* **95** 197205
[7] Lorenz C D and Ziff R M, *On a cubic lattice, link percolation is* $p_c = 0.248\,8126(5)$, 1998 *Phys. Rev.* E **57** 230
[8] Jörg T and Ricci-Tersenghi F, 2008 *Phys. Rev. Lett.* **100** 177203
[9] Binder K, 1981 *Z. Phys.* B **43** 119
Ballesteros H G *et al*, 1997 *Nucl. Phys.* B **483** 707
[10] Krzakala F, Montanari A, Ricci-Tersenghi F, Semerjian G and Zdeborova L, 2007 *Proc. Nat. Acad. Sci.* **104** 10318
[11] Zdeborova L and Krzakala F, 2007 *Phys. Rev.* E **76** 031131
[12] Montanari A, Ricci-Tersenghi F and Semerjian G, 2008 *J. Stat. Mech.* P04004
[13] Castellani T, Krzakala F and Ricci-Tersenghi F, 2005 *Eur. Phys. J* B **47** 99
[14] Hartmann A and Ricci-Tersenghi F, 2002 *Phys. Rev.* B **66** 224419

J. Stat. Mech. (2011) P02002

Bibliography

[1] S.F. Edwards and P.W. Anderson, J. Phys. F **5**, 965 (1975).

[2] D. Sherringhton, S. Kirkpatrick, Phys. Rev. Lett. **35**, 1792 (1975).

[3] G. Parisi, J. Phys. A **13**, L115 (1980). G. Parisi J. Phys. A **13**, 1101 (1980). G. Parisi J. Phys. A **13**, 1887 (1980).

[4] D.J. Amit and V. Martin-Mayor, *Field theory, the renormalization group, and critical phenomena: graphs to computers* (World Scientific, 2005).

[5] J. Cardy, *Scaling and renormalization in statistical physics* (Cambridge University Press, 1996).

[6] A. N. Berker and S. Ostlund, J. Phys. C **12**, 4961 (1979).

[7] L.P. Kadanoff , Annals of Physics **100**, 359 (1976).

[8] T. Temesvari, C. De Dominicis, Phys. Rev. Lett. **89**, 097204 (2002). T. Temesvari, C. De Dominicis and I.R. Pimentel, Eur. Phys. J. B **25**, 361-372 (2002). Phys. Rev. B **65**, 224420 (2002).

[9] G. Parisi and T. Temesvari, arxiv:1111.3313v1.

[10] T. Temesvari, Phys. Rev. B **78**, 220401(R) (2008).

[11] T. Jorg, J. Lukic, E. Marinari e O. C. Martin, Phys. Rev. Lett. **96**, 237205 (2006).

[12] H. G. Katzgraber, M. Koerner, and A. P. Young, Phys. Rev. B **73**, 224432 (2006).

[13] T. Jörg, H. G. Katzgraber, Phys. Rev. B **77**, 214426 (2008).

[14] F. Dyson, Commun. Math. Phys. **12**, 91 (1969).

[15] Y. Meurice, J. Phys. A **40**, R39 (2007).

[16] H. G. Katzgraber, D. Larson, A. P. Young, Phys. Rev. Lett. **102**, 177205 (2009).

[17] D. Larson, H. G. Katzgraber, M. A. Moore, A. P. Young, Phys. Rev. B **81**, 064415 (2010).

[18] M. Picco, arXiv:1207.1018v1 [cond-mat.stat-mech].

[19] B. Widom, J. Chem. Phys. **43**, 3898 (1965).

[20] T. W. Burkhardt and J- M- J- von Leeuwen, *Real space renormalization* (Springer - Verlag, 1982).

[21] K. G. Wilson, Phys. Rev. B, **4**, 3174 (1971). K. G. Wilson, Phys. Rev. B, **4**, 3184 (1971).

[22] K. G. Wilson and M. E. Fisher, Phys. Rev. Lett, **28**, 240 (1972).

[23] M. Mezard, G. Parisi, M. Virasoro, *Spin glass theory and beyond* (World Scinetific, 1987).

[24] J.R.L. de Almeida, D.J. Thouless, J. Phys. A **11**, 983 (1978).

[25] G. Parisi, Phys. Rev. Lett. **50**, 1946 (1983).

[26] S. Boettcher, Phys. Rev. Lett. **95**, 197205 (2005).

[27] S. Franz, G. Parisi and M. A. Virasoro, J. Phys. France **4**, 1657 (1994).

[28] D.S. Fisher, D.A. Huse, Phys. Rev. B **38**, 386 (1988).

[29] E. Marinari, C. Naitza and F. Zuliani, J. Phys A **31**, 6355 (1998).

[30] F. Krzakala et al., Phys. Rev. Lett. **87**, 197204 (2001).

[31] L. Leuzzi, G. Parisi, F. Ricci-Tersenghi and J. J. Ruiz-Lorenzo, Phys. Rev. Lett. **103**, 267201 (2009).

[32] A.P. Young and H.G. Katzgraber, Phys. Rev. Lett. **93**, 207203 (2004).

[33] M. Sasaki et al., Phys. Rev. Lett. **99**, 137202 (2007).

[34] T. Jörg, H.G. Katzgraber and F. Krzakala, Phys. Rev. Lett. **100**, 197202 (2008).

[35] D. Petit, L. Fruchter and I.A. Campbell, Phys. Rev. Lett. **83**, 5130 (1999); *ibid* **88**, 207206 (2002).

[36] P.E. Jönsson et al., Phys. Rev. B **71**, 180412 (2005). P.E. Jönsson and H. Takayama, J. Phys. Soc. Jpn. **74**, 1131 (2005). P.E. Jönsson et al., J. Mag. Mag. Mat. **310**, 1494 (2007).

[37] A.J. Bray and S.A. Roberts, J. Phys. C **13**, 5405 (1980).

[38] L. P. Kadanoff, Phys. Rev. Lett. **34**, 1005 (1975).

[39] A. A. Migdal, Sov. Phys. JETP **42**, 743 (1976).

[40] F. D. Nobre, Phys. Rev. E **64**, 046108 (2001).

[41] M. Hinczewski and A. N. Berker, Phys. Rev. B **72**, 144402 (2005).

[42] M. Ohzeki, H. Nishimori, and A. N. Berker, Phys. Rev. E **77**, 061116 (2008).

[43] C. Cammarota, G. Biroli, M. Tarzia and G. Tarjus, Phys. Rev. Lett. **106**, 115705 (2011).

[44] E. Gardner, J. Physique **45**, 1755 (1984).

[45] M. E. Fisher, S. K. Ma, B. G. Nickel, Phys. Rev. Lett. **29**, 917 (1972).

[46] J. Godina, Y. Meurice, M. Oktay, Phys. Rev. D **59**, 096002 (1999).

[47] J. Godina, L. Li, Y. Meurice and M. Oktay, Phys. Rev. D **73**, 047701 (2006).

[48] P. Collet, J. P. Eckmann and B. Hirsbrunner Phys. Lett. B **71**, 385 (1977).

[49] S. Franz, T. Jörg and G. Parisi, J. Stat. P02002 (2009).

[50] M. Castellana, G. Parisi, Phys. Rev. E **82**, 040105(R) (2010), Phys. Rev. E **83**, 041134 (2011).

[51] M. Castellana, Europhys. Lett. **95**, 47014 (2011).

[52] G.Parisi, R. Petronzio and F. Rosati, Eur. Phys. J. B **21**, 605 (2001).

[53] F. Ricci-Tersenghi, J. Stat. Mech. P08015 (2012).

[54] A. B. Harris, J. Phys. C **7**, 1671 (1974).

[55] H. G. Ballesteros et al., Phys. Rev. B, **58**, 2740 (1998).

[56] M.C. Angelini *et al.*, in preparation.

[57] L. Klein, J. Adler, A. Aharony, A. B. Harris, Y. Meir, Phys. Rev. B **43**, 11249 (1991).

[58] R. H. Swendsen and J.-S. Wang. Phys. Rev. Lett., **57**, 2607 (1986).

[59] L. Leuzzi, G. Parisi, F. Ricci-Tersenghi and J. J. Ruiz-Lorenzo, Phys. Rev. Lett. **101**, 107203 (2008).

[60] G. S. Rushbrooke, H. D. Ursell, Math. Proc. Cambridge Phil. Soc. **44**, 263 (1948).

[61] G. Kotliar, P. W. Anderson, and D. L. Stein, Phys. Rev. B **27**, 602 (1983).

[62] L. Viana and A. J. Bray, J. Phys. C **18**, 3037 (1985).

[63] M. Mezard and G. Parisi, Eur. Phys. J. B **20**, 217 (2001).

[64] E. Luijten, W.J. Blöte Phys. Rev. Lett. **89**, 025703 (2002).

[65] J.M. Kosterlitz, Phys. Rev. Lett. **37** 1577 (1976).

[66] J. M. Kosterlitz and D. J. Thouless, J. Phys. C **6**, 1181 (1973); J. M. Kosterlitz, J. Phys. C **7**, 1046 (1974).

[67] J. Fröhlich and T. Spencer, Commun. Math. Phys. **84**, 87 (1982).

[68] P. W. Anderson and G. Yuval, J. Phys. C **4**, 607 (1971).

[69] E. Luijten, H. Meßingfeld, Phys. Rev. Lett. **86**, 5305 (2001).

[70] F. Dyson, Commun. Math. Phys. **21**, 269 (1971).

[71] J. Sak, Phys. Rev. B **8**, 281 (1973).

[72] J. Honkonen and M. Yu. Nalimov, J. Phys. A **22**, 751 (1989); J. Honkonen, J. Phys. A **23**, 825 (1990).

[73] A. C. D. van Enter, Phys. Rev. B 26, 1336 (1982).

[74] Y. Yamazaki, Phys. Lett. A **61**, 207 (1977); Physica A **92**, 446 (1978).

[75] M. A. Gusmao and W. K. Theumann, Phys. Rev. B **28**, 6545 (1983).

[76] H. G. Katzgraber and A. P. Young, Phys. Rev. B **67** 134410 (2003); **68** 224408 (2003).

[77] M.-c. Chang and J. Sak, Phys. Rev. B **29**, 2652 (1984).

[78] W. K. Theumann and M. A. Gusmao, Phys. Rev. B **31**, 379 (1985).

[79] Z Glumac and K Uzelac, J. Phys. A **24** 501, (1991).

[80] H. K. Janssen, Phys. Rev. E **58**, 2673, (1998).

[81] R. A. Baños, L. A. Fernandez, V. Martin-Mayor, A. P. Young, arXiv:1207.7014 [cond-mat.dis-nn].

[82] M. Hasenbusch, A. Pelissetto, and E. Vicari, Phys. Rev. B **78**, 214205 (2008).

[83] U. Wolff, Nucl. Phys. B (proc. Suppl.) **17**, 93 (1990).

[84] R. H. Swedsen and J. S. Wang, Phys. Rev. Lett. **58**, 86 (1987).

[85] F. Niedermayer, arXiv:hep-lat/9704009.

[86] L. Onsager, Phys. Rev. **65**, 117 (1944).

[87] A. Pelissetto, E. Vicari, Phys. Rep. **368** 549 (2002).

[88] D. Kim, C. J. Thompson, J. Phys. A: Math. Gen. **10** 1579 (1977).

[89] W.J. Blöte, E. Luijten, J.R. Heringa, Computer Phys. Comm. **147** (2002) 58.

[90] K. Uzelac, Z. Glumac, A. Anicic, Phys. Rev. E **63**, 037101 (2001).

[91] U. Wolff, Phys. Rev. Lett. **62**, 361 (1989).

[92] E. Luijten, W.J. Blöte, Int. J. Mod. Phys. C **6**, 359 (1995), Phys. Rev. B **56**, 8945 (1997).

[93] K. Binder, Z. Phys. B **43** (1981) 119.

[94] Y. Meurice, arXiv:0712.1190v3 [hep-lat].

[95] H. G. Ballesteros, L.A. Fernandez, V. Martin-Mayor, A. Munoz Sudupe, Nucl.Phys.B **483**, 707 (1997).

[96] M. Hasenbusch, A. Pelissetto, and E. Vicari, Phys. Rev. B **78**, 214205 (2008).

[97] J. Salas, A. D. Sokal, J. Stat. Phys. **98**, 551 (2000).